AD-A078 625 PURDUE UNIV LAFAYETTE IND PROJECT SQUID HEADQUARTERS F/G 21/2
THE STRUCTURE OF EDDIES IN TURBULENT FLAMES - I.(U)
MAR 79 N A CHIGIER , A J YULE N00014-75-C-1143
UNCLASSIFIED SQUID-US-1-PU NL

1 OF 2
AD
A078625

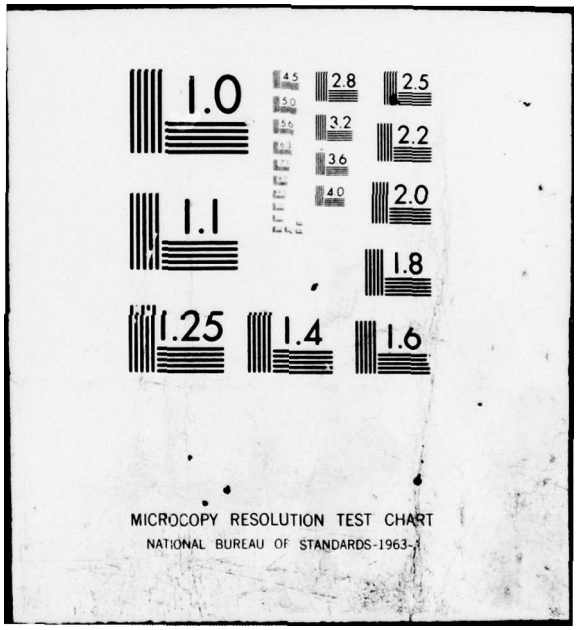
1.0
1.1
1.25
1.4
1.6
1.8
2.0
2.2
2.5
2.8
3.2
3.6
4.0
4.5
5.0
5.6
MICROCOPY RESOLUTION TEST CHART
NATIONAL BUREAU OF STANDARDS-1963-A

LEVEL II 6

SC

PROJECT SQUID

TECHNICAL REPORT US-1-PU

THE STRUCTURE OF EDDIES IN TURBULENT FLAMES - I

BY

NORMAN A. CHIGIER and ANDREW J. YULE
DEPARTMENT OF CHEMICAL ENGINEERING
AND FUEL TECHNOLOGY
UNIVERSITY OF SHEFFIELD
SHEFFIELD S1 3JD, ENGLAND

400 047

See 1473 in back

Project SQUID is a cooperative program of basic research relating to Jet Propulsion. It is sponsored by the Office of Naval Research and is assisted by Purdue University through Contract N00014-75-C-1143, NR-098-038.

Published for ONR by
School of Mechanical Engineering
Chaffee Hall
Purdue University
West Lafayette, Indiana 47907

MARCH 1979

Unclassified

SECURITY CLASSIFICATION OF THIS PAGE (When Data Entered)

REPORT DOCUMENTATION PAGE		READ INSTRUCTIONS BEFORE COMPLETING FORM
1. REPORT NUMBER US-1-PU	2. GOVT ACCESSION NO.	3. RECIPIENT'S CATALOG NUMBER
4. TITLE (and Subtitle) (6) THE STRUCTURE OF EDDIES IN TURBULENT FLAMES - I.		5. TYPE OF REPORT & PERIOD COVERED 6. PERFORMING ORG. REPORT NUMBER
7. AUTHOR(s) (10) Norman A. Chigier, Andrew J. Yule		8. CONTRACT OR GRANT NUMBER(s) (15) N00014-75-C-1143
9. PERFORMING ORGANIZATION NAME AND ADDRESS University of Sheffield Sheffield S1 3JD, England 321 650		10. PROGRAM ELEMENT, PROJECT, TASK AREA & WORK UNIT NUMBERS NR-098-038
11. CONTROLLING OFFICE NAME AND ADDRESS ONR-Power Program through Purdue University, West Lafayette, Indiana 47907		12. REPORT DATE (11) Mar[illegible]979 13. NUMBER OF PAGES 102
14. MONITORING AGENCY NAME & ADDRESS (if different from Controlling Office) Office of Naval Research, Power Program, Code 473 Dept. of the Navy 800 No. Quincy Street Arlington, VA 22217 (12) 104		15. SECURITY CLASS. (of this report) 15a. DECLASSIFICATION/DOWNGRADING SCHEDULE

16. DISTRIBUTION STATEMENT (of this Report)

This document has been approved for public release and sale; its distribution is unlimited.

17. DISTRIBUTION STATEMENT (of the abstract entered in Block 20, if different from Report)

(9) Technical Repts.

18. SUPPLEMENTARY NOTES

(14) SQUID-US-1-PU

19. KEY WORDS (Continue on reverse side if necessary and identify by block number)

Turbulent Flames
Reactive flows
Turbulent structure

20. ABSTRACT (Continue on reverse side if necessary and identify by block number)

This report includes a description of the objectives of the investigation, the experimental and data processing techniques and initial results. High frequency response measurement techniques are used with data processing and conditional sampling to measure large eddy structure and coherence in the transitional flow region of turbulent diffusion flames. Comparisons are made between nonburning and burning flow conditions; these show physical similarity for cold and burning flows in the transitional region. Flow visualization shows quasi-laminar interface layers which are distorted, stretched and

DD FORM 1 JAN 73 1473 EDITION OF 1 NOV 65 IS OBSOLETE
S/N 0102-LF-014-6601

Unclassified

SECURITY CLASSIFICATION OF THIS PAGE (When Data Entered)

403 627

convoluted by vortex interactions. Visualization by high-speed Schlieren colour movie shows axisymmetric wave and vortex ring formation. Velocity, temperature and ionization density measurements show that the transitional flow and the potential core of the jet are much longer in the flame than in the nonburning jet. A marked difference is found between the initial fundamental instability frequencies of the shear layers. The most amplified frequency predicted by stability theory for cold inviscid flow is found in the cold jet but not the flame. Increase in viscosity due to heat release causes delay and damping of the processes of vortex formation and coalescence; dilatation and buoyancy forces also contribute to differences between the flame and cold jet. Large eddies are shown to play an important role in the transitional region of turbulent jet flames.

Technical Report US-1-PU

(6)

PROJECT SQUID

A COOPERATIVE PROGRAM OF FUNDAMENTAL RESEARCH
AS RELATED TO JET PROPULSION
OFFICE OF NAVAL RESEARCH, DEPARTMENT OF THE NAVY

CONTRACT N00014-C-1143, NR-098-038

THE STRUCTURE OF EDDIES IN TURBULENT FLAMES - I

By

Norman A. Chigier and Andrew J. Yule
Department of Chemical Engineering
and Fuel Technology
University of Sheffield
Sheffield S1 3JD, England

Published for ONR by
School of Mechanical Engineering
Purdue University
West Lafayette, Indiana 47907

March 1979

THE STRUCTURE OF EDDIES IN TURBULENT FLAMES - I

Department of Chemical Engineering and Fuel Technology
University of Sheffield, Sheffield S1 3JD

Norman A. Chigier and Andrew J. Yule

Abstract

This report includes a description of the objectives of the investigation, the experimental and data processing techniques and initial results. High frequency response measurement techniques are used with data processing and conditional sampling to measure large eddy structure and coherence in the transitional flow region of turbulent diffusion flames. Comparisons are made between nonburning and burning flow conditions; these show physical similarity for cold and burning flows in the transitional region. Flow visualization shows quasi-laminar interface layers which are distorted, stretched and convoluted by vortex interactions. Visualization by high-speed Schlieren colour movies shows axisymmetric wave and vortex ring formation. Velocity, temperature and ionization density measurements show that the transitional flow and the potential core of the jet are much longer in the flame than in the nonburning jet. A marked difference is found between the initial fundamental instability frequencies of the shear layers; the most amplified frequency predicted by stability theory for cold inviscid flow is found in the cold jet but not the flame. Increase

in viscosity due to heat release causes delay and damping of the processes of vortex formation and coalescence; dilatation and buoyancy forces also contribute to differences between the flame and cold jet. Large eddies are shown to play an important role in the transitional region of turbulent jet flames.

Nomenclature

Figure 1 shows the coordinate system in the experimental investigation of an axisymmetric diffusion flame in a uniform secondary stream. The notation below covers the essential quantities arising in data acquisition and processing. Further quantities, occurring for example in various methods of conditional sampling, will be defined as they arise.

$b(x)$	mixing layer 'shear' thickness, $b = -(U_1-U_s)/(\partial U/\partial r)_{max}$
c_j	instantaneous local mass fraction of specie 'j'
D	diameter of burner nozzle
Fr	Froude number: $Fr = U_J^2/gD$
f	frequency (Hz)
f_v	vortex passing frequency in transition region
I	intermittency (with value 1, in turbulent fluid, and 0, in irrotational fluid)
I_{SAT}	instantaneous saturation ion current
M	momentum flux
$\dot{m}_j$	mass flow rate
n	number of samples in one time history
N	number of signal time histories
P	instantanious pressure

$p(\alpha_i)$ probability density function of α (PDF):

$$p(\alpha) = \left\{\frac{\text{Total time which signal is between } \alpha \text{ and } d\alpha}{T\, d\alpha}\right\}_{\left\{\begin{array}{l}\text{Limit as}\\ d\alpha \to 0\end{array}\right\}}$$

(p can be obtained by ensemble averaging N time histories)

$R_{i\ell}(\tau)$ cross correlation function (autocorrelation when $i = \ell$):

$$R_{i\ell}(\tau) = \lim_{T \to \infty} \frac{1}{T} \int_0^T \alpha_i(t)\alpha_\ell(t+\tau)\, dt$$

$\overline{R}_{i\ell}(\tau)$ cross correlation coefficient:

$$\overline{R}_{i\ell}(\tau) = R_{i\ell}(\tau) \,/\, (R_{ii}(0)\, R_{\ell\ell}(0))^{\frac{1}{2}}$$

Re_D Reynolds number: $Re_D = U_J D/\nu$

Re_δ Reynolds number: $Re_\delta = U_J \delta/\nu$

r radial distance from nozzle centreline

St_D Strouhal number based on spectrum peak or vortex passing frequency: $St_D = f_{PEAK}\, D/U_J$

St_δ Strouhal number: $St_\delta = f_{PEAK}\, \delta_J/U_J$

$S_{i\ell}(f)$ Cross (or Auto) power spectral density:

$$S_{i\ell}(f) = \int_{-\infty}^{\infty} R_{i\ell}\, e^{-i\, 2\pi f \tau}\, d\tau;$$ and, for large T:

$$S_{i\ell}(f) = \frac{1}{T}\, \overline{X_i^*\, X_\ell}$$

T length of signal time history

t time

t_e times of triggering events for conditional sampling

U,V,W instantaneous velocity components in x, y and z directions ($\overline{W} = 0$, and in general $\overline{U} >> \overline{V}$)

u, v, w components of fluctuating velocity: $u = U-\overline{U}$; $v = V-\overline{V}$ and $w = W$

$X_i(f)$ (Complex) Fourier transform of $\alpha_i(t)$

x,y,z coordinates based on nozzle lip (see Fig. 1)

x',y',z' coordinates based on arbitrary point P, e.g. trigger probe position

α_i	general notation for a dependent scalar or vector variable
β_i	a conserved scalar, e.g. β_J is the local concentration of fluid originating from the burner nozzle
$\gamma^2(f)$	coherence function: $\gamma^2 = (S_{i\ell})^2/S_i\, S_\ell$
δ_J	nozzle boundary layer shear thickness: $\delta_J = -U_J / (\partial U/\partial y)_{\substack{\max \\ x = 0}}$
δ_J^*, δ_J^{**}	nozzle boundary layer, displacement and momentum thickness
η	normalized radial coordinate for mixing layer: $\eta = y/x$
θ	temperature (K)
ν	kinematic viscosity
ρ	density
τ	probe time constant or time relative to t in correlations etc.

Subscripts

1	centre line value
c	convection velocity
D	based on jet diameter
F	fundamental frequency
i, ℓ, m	tensor components
I	irrotational flow value
j	"jth" species
J	primary (jet) flow value (at x = 0)
0	value at x = 0
S	secondary flow value
T	turbulent flow value

Superscripts

'	denotes a fluctuating component measured relative to a time mean
*	denotes complex conjugate

Averaging

$\langle \text{---} \rangle$ ensemble average, $\langle \alpha \rangle = \underset{n\to\infty}{Lt} \frac{1}{n} \sum_{1}^{n} \alpha$ or, in conditional sampling, $\langle \alpha(\tau) \rangle \equiv \underset{N\to\infty}{Lt} \frac{1}{N} \sum_{1}^{N} \alpha(\tau)$

$\overline{(\text{---})}$ time average $\overline{\alpha} \equiv \underset{T\to\infty}{Lt} \frac{1}{T} \int_{t_o}^{t_o+T} \alpha \, dt$

$\tilde{(\text{---})}$ Favre average, (not applicable to pressure),

$$\tilde{\alpha} \equiv \left(\underset{T\to\infty}{Lt} \frac{1}{T} \int_{t_o}^{t_o+T} \alpha\rho \, dt \right) / \overline{\rho}$$

1. Introduction

This report describes the experimental and data analysis approaches, both in use and under development by the authors, to study the roles of 'coherent structures' in axisymmetric turbulent gas diffusion flames. The experimental results from the first 17 months' work on the research project are described. These results concentrate on a description of the transitional flame structure near the burner nozzle and comparisons between the physical structures of cold and burning transitional flows.

In recent years, there has been considerable interest in the structures of large eddies in many types of turbulent flow; observations in jet-type free shear flows are of most interest here. The experiments in two-dimensional mixing layers by Roshko[1], Browand[2] and their coworkers yielded the dramatic results shown by their clear visualizations of repetitive, coherent eddies which appeared to dominate the flows. Observations have also been made in round jets, for example by Yule[3] and Browand and Laufer[4], which have indicated the repetitiveness, coherence and importance of the large eddies.

The philosophy behind the present investigation can be stated in its simplest form: Given that large eddies are such important features of nonreacting shear flows, are they also important in reacting flows when there is significant heat release and, if so, what are the structures of their eddies and how do they interact with combustion?

We have chosen to study the burning round jet configuration, which has been the subject of many previous investigations in its cold, nonreacting form. An axisymmetric, fuel rich gaseous jet mixes with surrounding, room temperature, air and burns as, essentially, a diffusion flame. The notation used is shown in Fig. 1. This burning flow will be referred to as the Jet Flame, and the nonburning flow will be termed the Cold Jet. In keeping with previous investigations of cold jet structure, great care is taken to ensure that the initial conditions at the nozzle are as laminar as is practically possible, with a uniform initial velocity profile. Rather surprisingly, there has been little attention paid in the past to the effects of initial and boundary conditions on the structure of turbulent combustion flow. Reacting turbulent flow is often implied to exist, *per se* , in some quasi-universal fully-developed turbulent form, generally referred to as a turbulent diffusion flame. There is a striking contrast with the many fundamental investigations of 'classical' cold turbulent shear flows in which initial and boundary conditions are controlled with great care, with the knowledge that these conditions can affect the turbulence, and its development, for some considerable distance downstream. Thus, the present objective, to obtain a fundamental understanding of turbulent flame structure, with emphasis on the roles of the large eddies, requires that the

jet flame is not disturbed significantly by, for example, pilot flames, swirl, free stream turbulence or recirculation regions used for the promotion of flame stabilization. In order to stabilize the flame, low velocities are required and, thus, the possibility arises of buoyancy forces becoming significant in certain regions of the flames. However, this is considered to be a small price to pay for the achievement of simple boundary conditions with the resulting simplification of analysis and data interpretation and the production of a 'classical' flow which can be readily repeated and reproduced.

It has been argued that the study of such a well controlled 'simple' flow is 'pathological' compared to most practical combustion flows which are more complex, with three-dimensionality, confinement, swirl and recirculation. The authors strongly criticize this point of view: Until we have achieved a fundamental physical understanding of certain basic turbulent reacting shear flows, with simple boundary conditions, we cannot hope to fully understand, and reliably model and predict, extremely complex situations. However, knowledge of the general structure of such complex flows is, of course, important in itself. It is undeniable that, at the present time, there is not a basic understanding of even 'simple' turbulent flame structure. This is obvious from the multifarious physical models and analytical approaches to the prediction of combustion flows, all of which have one common factor:- the lack of sufficient accurate, time resolved data in a form which allows conclusive validation of the assumed models and confirmation of modelling predictions.

It is argued here that one of the keys to the understanding of turbulent combustion lies in the recognition of the importance of

strong coherent large eddies. Such eddies are clearly present in many cold flows. Furthermore, examination of films of the internal flows in practical combustors, large and small, often gives indications of coherent burning regions moving for considerable distances through the flow. It is, thus, reasonable to attempt to examine a combustion flow from a quasi-Lagrangian viewpoint, following an eddy from its formation until it can no longer be recognized. In the process, experimental techniques must be used to measure how these eddies interact with each other and how they interact with the processes of combustion. For example, how do these eddies influence the entrainment and mixing of gases and does spatial and temporal coherence in such eddies result in 'flamelets', or coherent regions of reaction, which are recognizable for distances comparable with the total flame length? These aims require measurement and data processing techniques of the multiprobe conditional sampling type, which have been used successfully in cold flows[2,3]. Accurate, multipoint, time resolved measurements in flames require sophisticated diagnostic techniques, together with a considerable development effort, as is described in Section 2 of this report.

In the present experiments flame structure is investigated in a logical manner, by starting at the burner nozzle and extending the detailed measurements gradually downstream. The growth of large vortex-like eddies in the initial transitional, viscosity dominated, mixing layer-type flow is first examined. The interaction and breakdown of these initial eddies to form the turbulent flame, and the structures and convection of the eddies in the turbulent flame, are then studied. The techniques used must provide quantitative data on the structures and coherence of these eddies, and also on

the interactions between combustion and the eddies; for example, by comparing cold and burning flows of the same jets, and by detecting the regions of reaction associated with the eddies.

The Regions of a Jet

It is useful to outline current knowledge of the structure of cold, round turbulent jets developing from laminar nozzle boundary layers. As sketched in Fig. 1, the flow geometry for a free jet (i.e. $U_S = 0$) can be divided into three regions: (i) The *mixing layer*, or potential core, region, which extends up to $x/D = 5$ approximately. This is characterized by a central region of irrotational flow surrounded by the high shear, mixing layer; (ii) A *development region*, in which the mixing layer turbulence interacts and adjusts to produce the third, downstream region; (iii) the *fully developed region*, typically beyond $x/D = 15$, in which all mean and turbulence quantities have approximate (but never exact) self-preservation so that the mean velocity has the similarity form $U = x^{-1} (M_J/\rho)^{\frac{1}{2}} f(\frac{r}{x})$, where x is measured (in this region) from a virtual origin.

In addition, there is a very important division between the *transition region*, in which viscous forces are influential, and the *turbulent region*. The length of the transition region is dependent upon the initial conditions at the nozzle, and it has been suggested that $x_T \simeq 1000\ \delta_J^{**}$, although this has not been shown conclusively. Depending upon these conditions, the transition region can extend for a small distance along the mixing layer, $x_T/D < 0.25$, or it can extend beyond the end of the mixing layer region, $x_T/D > 5$. The initial part of the present investigation, which is described in this report, lays particular emphasis on understanding the transitional

region of the jet flame, and making comparisons between this region for cold and burning jets.

The Importance of Transitional Flow

There are three important reasons why the transitional flow structure is of importance when considering the structure of diffusion flames:

(i) Cold flow experiments show that the well organized vortical structures in transitional flow have basic similarities with the large eddies in the turbulent region of the same flow, further downstream. Indeed, experiments[3,4,5] indicate that turbulent eddies in the round jet evolve directly from the interactions, coalescing and breakdown of the transitional vortex rings formed near the nozzle.

(ii) Viscous forces increase by an order of magnitude due to heat release, so that transition distances in flames must be expected to extend much further than the distances for the equivalent nonburning flows.

(iii)It can be argued that, for cold nonreacting flows, the details of the initial conditions and the transitional flow are essentially 'forgotten' beyond some distance downstream, beyond which Reynolds number similarity applies. However, this argument cannot be used for burning flows: Heat release, mixing and product and pollutant formation in the transition region are integral to the whole flame and are not 'forgotten' by the turbulence structure after the end of the transition region. In qualitative terms, it is useful to think of the transitional flow structure as being determined by initial conditions at the burner nozzle, while the turbulent flow structure, in the flame, has a structure determined by conditions existing at the end of the transition region.

In addition, the well defined growth of orderly vortical structures expected in the transitional jet flame, and the quasi-laminar interface burning regions which should be associated with them, make the transitional flow an ideal environment for the application and development of the conditional sampling and flow visualization techniques used in this investigation.

The Physical Structure of the Round Jet

Yule[3] used flow visualization, time and frequency domain processing of velocity fluctuations and conditional sampling techniques to derive quantitative and qualitative knowledge of the mixing layer region of round jets at different Reynolds numbers. Figure 2 sketches the physical structure which was found at all Reynolds numbers investigated ($9000 \lesssim Re_D \lesssim 2 \times 10^5$).

Natural instability of the initial laminar shear layer, formed from the nozzle boundary layer, produces a periodic array of vortex-ring-like vorticity concentrations. The initial stages of this instability can be predicted satisfactorily. As these vortex rings move downstream, they generally coalesce with neighbouring rings, so that the scale and separation of the vortex rings increase with distance from the nozzle. Although point velocity measurements in this transitional flow exhibit periodic correlations and peaked spectra, there is considerable random variation in the strengths and movements of the coalescing vortices. Furthermore, the vortex rings lose their phase agreement across the jet as they move downstream. Fluctuations of the w velocity component increase with distance from the nozzle due to an almost linear growth of orderly wave deformations of the cores of the vortex rings. From one up to three regions of vortex coalescence have been observed in the

transition region depending upon the nozzle conditions, which also determine vortex passing frequencies and length of the transition region.

Yule[3] has argued that the last coalescence of vortices, prior to turbulent flow, involves rings which have core deformations larger than a critical size. The rings entangle, thus producing enhanced vorticity stretching and small scales of motion. The remains of these entangled vortices can be detected in the turbulent region, by conditional sampling, up to 5D downstream of transition, and, individually, they can be discerned visually for several diameters further than this, i.e. well downstream of the potential core. These modified vortex rings thus form large eddies in the turbulent region of the jet. It does not seem to be valid, in general, to consider that these rings completely break down or disintegrate into turbulent flow; rather, the large scale vorticity concentrations which they produce retain appreciable coherence beyond the end of the transition region. The details of the flows in the turbulent mixing layer and downstream jet regions are the subject of some controversy. There appears to be agreement that the large eddies are strong, coherent, and rather similar to vortex rings in cross-section when measurements are ensemble averaged for many consecutive eddies. Yule[3], however, proposed that it is not reasonable to describe these eddies, in the turbulent region, as vortex rings because of a lack of circumferential coherence and the smaller scales of motion within them. On the other hand, it has been proposed that the eddies of the turbulent region are, in fact, vortex rings but their circumferential coherence is concealed by 'phase scrambling' effects in multipoint measurements. The effects

of phase scrambling in the present investigation are discussed in Section 3. There is some visualization evidence, but no quantitative evidence, that the turbulent eddies coalesce, rather than disintegrate and reform, similar to the eddy coalescing observed in two-dimensional mixing layers[1,2]. Furthermore, the basic large eddy structure seems to be similar throughout the turbulent jet, from the mixing layer and into the fully developed region. These, and other points, await elucidation by carefully designed experiments.

We have not considered here the evidence of large eddy structure in two-dimensional mixing layers, much of it originating from work funded by Project SQUID. Although one can expect general similarities between the two-dimensional and round jet mixing layers, particularly near the nozzle, no presumptions are being made on similarities between two-dimensional and axisymmetric flows. Other factors, such as the effect of a secondary stream on the jet structure, will be discussed as they arise.

Diffusion Flame Structure

The existence of vortex rings, near the burner nozzle, in flames, has been recognized for many years. Consider, for instance, the studies of Tyndall[6] of the effect of sound on flames. Grant[7] has described some observations of these vortex rings and Ballantyne and Bray[8] have recognized the existence of such vortex structures in certain of the flames which they have studied. However, there is a lack of knowledge of the growth and interactions between these rings and combustion, and even such basic quantitative information as passing frequencies, coalescing positions, etc. Essentially, there is no systematic information on the interaction between combustion

and transition in the axisymmetric flame. For the downstream fully developed 'turbulent' flame (the assumption of local turbulent flow has been made implicitly in the past without proof) there are a number of investigations measuring various mean and rms quantities. Often these have indicated the importance of unmixedness, which is related to intermittency, probability density functions and, thus, to the large eddy structure. The work of Kent and Bilger[9] and their coworkers is perhaps the most thorough, and the most relevant to the present study. However, there is an almost complete absence of information on large eddy structure in turbulent diffusion flames in the published literature and no previous investigations have concentrated on the roles of eddy formation and coherence.

2 Experimental Facility and Techniques

2.1 *Introduction*

To meet the objectives described above requires high frequency measurement techniques with good spatial resolution. In order that conditional sampling and cross-correlation techniques can be applied, to educe eddy structures and their convective properties, facilities must be developed to acquire data simultaneously from several probes within the flame. The three major measurement techniques in this investigation have been chosen because of their relatively advanced stages of development, and relatively good reliability, resolution and accuracy. The design development and application of these techniques is described in Sections 2.3, 2.4 and 2.5 for measurements of velocity, temperature and ionization levels. Ultimately, to quantify the flame structure fully, a

technique for measurement of specie fluctuations is required. Laser Raman techniques may eventually fulfil this need, but versions of more conventional species concentration measurement techniques can provide useful data, as will be described in Section 2.6. It is well established, from cold flow studies, that flow visualization plays an essential part in any attempts to study the coherence and convective properties of structures in quasi-Lagrangian reference frames. The applications of flow visualization techniques in the present investigation is described in Section 2.7.

2.2 *Facility for Production of Axisymmetric Diffusion Flame*

Figure 3 shows a schematic diagram of the apparatus used for the production of an axisymmetric flame in a coflowing airstream. The main design requirements were that both the primary jet flow and the secondary flow had low turbulence levels with uniform velocity distributions. To enable accurate Laser Doppler Anemometer (LDA) measurements of velocity, it was essential that the flame was surrounded by a low velocity secondary stream, rather than by ambient air. This is because both the primary (fuel) jet and the entrained surrounding air, must be seeded equally with small particles so that biasing effects are minimized in the velocity measurements. All experiments reported here are conducted with U_s = 0.73 m/s, except for some results obtained with U_s = 0 (the free jet or free jet flame) for comparative tests. This uniform low velocity secondary flow also effectively protected the flame from small draughts in the laboratory, thus permitting an open flow with easy access by probes. The secondary flow was supplied by a fan via a plenum chamber containing sound-absorbing foam, to ensure that fan and pipe noise did not affect the flame. The primary jet is fed

via a mixing chamber, diffuser, settling chamber and a contoured nozzle with 16:1 area ratio. The mixing chamber has three inlets for the fuel gas (propane), diluting air containing LDA seeding particles and nitrogen. Nitrogen was used only for safety, to flush the system before and after runs; however, future studies of the effects of N_2 dilution are envisaged. All flows are measured and monitored by calibrated rotameters. The facility permits the production of flames ranging from 'pure' diffusion flames (no primary air) to fully premixed flames. Most of the initial experiments have used a propane/air primary flow with an equivalence ratio of 10 (Jet Flame I), which is sufficiently fuel-rich for burning to occur as a diffusion flame. This propane/air mixture has been used to achieve a reasonably high Reynolds number, $Re_D = 1.04 \times 10^4$, without an excessive drain from the propane bottles. Volume flow rates are relatively high in these experiments because of the large burner nozzle diameter used; D = 25.4 mm. The large diameter was selected to enable detailed, accurate measurements of initial conditions and in the transitional flow near the nozzle. The secondary flow convergence is square in cross-section and has an exit diameter of 0.4 m. Visible flame lengths from 1.5 m to 2 m are found and the initial experiments concentrate on the first metre of flow. The complete nozzle and secondary flow assembly can be traversed radially and vertically relative to the fixed LDA optics. The region $0 \leq x \leq 40$ D can be probed by the LDA. Other, intrusive, probes are carried by traversing apparatus mounted on vertical lathe beds outside the secondary flow.

A major design problem with the apparatus was the apparent incompatability of the required low initial turbulence levels with

the requirement that both jet and secondary flows were heavily seeded for the LDA. It was required to maximize the seeding of the flows to maximize the frequency range of velocity measurements. At the high particle densities used (of the order of 1 particle per mm^3) it was found that some agglomeration of the SiO_2 particles was inevitable. Thus, particles of the order of 2 μm in diameter were detected, although the nominal particle diameter was 0.1 μm. Consequently, any fine mesh screens, placed in either the jet or secondary flow supply systems, rapidly clogged with particles, causing unacceptable flow variations. After several different nozzle configurations were tried, the problem was overcome for the jet flow by omitting all smoothing screens, except for a honeycomb, after the mixing chamber and relying on long lengths of low velocity pipe flow to permit the decay of the turbulence created in the mixing chamber. The final design was successful, as shown by the 0.4% turbulence level measured at the nozzle exit. The secondary flow was seeded by injection of particles at low velocity from holes in a toroid surrounding the nozzle settling chamber, and downstream of the screens in the secondary flow settling chamber.

2.3 *Laser Doppler Anemometer*

The general arrangement of the LDA system is shown in Fig. 4. A one Watt Argon Ion Spectra Physics 164 laser is used, on the blue line, $\lambda = 0.488$ μm, with a TSI beam splitter and Bragg cell module. The EMI photomultiplier, with a narrow band interference filter, collects light in the forward direction and slightly off axis. The narrow vertical slit in front of the photomultiplier aperture is at the focus of the measurement control volume by the collecting lens. This results in a very short length of the control volume being

viewed by the photomultiplier. Characteristics of the LDA system are:

Beam intersection angle	=	4.8°
Measurement control volume i/e^2 width	=	310 μm
Length of measurement control volume seen by the photomultiplier	=	4.7 mm
Typical light collection angle	=	2°
Off-axis angle of collection optics	=	6.1°
Beam focusing less focal length	=	599 mm
Fringe spacing in measurement volume	=	5.87 μm
Typical particle arrival rate (at U ≃ 5 m/s)	=	1000 Hz
Accuracy of individual velocity measurement (U ≃ 5 m/s)	=	± 1%

The LDA operates in the single particle counting mode so that no more than one particle at a time is permitted in the region of the measurement volume viewed by the photomultiplier. A typical signal is sketched in Fig. 5. The LDA signal processing system has been designed at the University of Sheffield and developments have been made specifically to meet the requirements of the present investigations. Fringe counting logic circuits are used but various interchangeable circuit boards have been developed to meet different requirements, which are not always compatible, such as extremely high accuracy, fast data rates, or the uninterrupted acquirement of a large bulk of signals. Figure 6 shows the logic block diagram for the processor system used for the velocity measurements. In this processor, the squaring operations on fringe cycles and signal envelope, required to produce gating

signals for the operational amplifiers, are achieved by saturating amplifiers, rather than by Schmidt triggers as have been used previously.

The counting of signal fringe cycles commences when the signal envelope exceeds a threshold level, which can be preset to suit the prevailing signal quality and data rate requirements. The processor counts 6 cycles, and measures the count duration as the number of cycles T_6 of a 20 MHz clock. A count of 12 cycles is also made, with the duration T_{12} measured by a 10 MHz clock. These clock frequencies are chosen to match the flow velocities encountered; higher velocities can be measured by using faster clocks. The D.E.C. PDP11-03 minicomputer acquires T_6 and T_{12} for each signal and the machine code acquisition program accepts the data if T_6 and T_{12} are within 5% of each other. This comparison criterion value was derived from systematic experiments which showed that values less than 5% did not significantly improve data accuracy. There are two main sources of counting error. The first is due to the counting of either too few or too many fringe cycles, or false cycles, due to noise or signal quality variation (e.g. due to occasional large seeding particles). It is this possible error which is recognized and thus avoided by making a comparison test between the times for two numbers of fringes. The second general source of error arises when it is not possible to measure exact numbers of fringe cycle periods. There are several possible reasons for this; for example, fringe cycles do not all have the same amplitude so that counts can begin and end at different positions relative to cycles. The double fringe count comparison can remove some of the sources of error.

However, this type of error is minimized only by maximizing the fringe quality of signals and carefully tuning the electronics. It was necessary to acquire only the two clock counts, T_6 and T_{12}, to derive a particle velocity. A system developed earlier, also counted the actual numbers of fringes measured, because signals can always be found which are not long enough to satisfy the specified numbers. However, it was found that counts of say 6 and 13 cycles, rather than 6 and 12, are recognized by the comparison test and rejected. Despite the precautions taken, it is inevitable that small amounts of 'poor quality' data pass through the system and are stored by the computer, together with the accurate velocity measurements. These 'poor quality' measurements can be recognized and rejected by the high level program used to further process the date for determination of the velocity statistics. For each separate measurement location in the flow a file of velocity measurements is first presented as a probability density function (PDF) of velocity. Velocity measurements which are inaccurate enough to seriously affect the accuracy of velocity statistics are recognized by their occurrence in extended 'tails' at both ends of the PDF. Upper and lower cut-offs are applied to reject these measurements, which account for less than 3% of the total data. If this high level validation routine is not followed, errors of up to 50% can occur in measurements of $(\overline{u^2})^{\frac{1}{2}}$, although errors in $\overline{U}$ are insignificant. These 'tails' in LDA velocity PDFs are present in most LDA systems (including commercial systems) known to the authors. In general, their users are aware of the phenomenon, but it is worthwhile to stress that large errors can arise if due care is not taken with

data validation.

The signal processor also contains a 'Real Time' Clock, which times the occurrence of the beginning of each signal. This data is also acquired by the computer so that a file of velocity as a function of time is stored. Provided data rates are high, compared with the most energetic frequencies in the turbulence, accurate time averaged quantities can thus be derived, rather than simple ensemble averages of signals.

The present investigation requires a maximum error of no more than 1% in individual velocity readings, plus high frequency real time data acquisition, for detailed measurements of turbulence structure and to enable conditional sampling to be used. The LDA system was developed and checked by using fibres, attached to rotating disks, traversed at known velocities through the measurement volume, and also by directly comparing LDA measurements with hot wire measurements in the same flows.

2.4. *Fine Wire Thermocouples*

The types of thermocouple used in this investigation are shown in Fig. 7. Both 75 μm diameter, Pt-Pt/13%Rh and 25 μm diameter Pt/20%Rh-Pt/40%Rh, probes are used. The latter probes are fragile but offer a higher frequency regime. Unlike resistance probes which suffer from insurmountable drift problems in flames, the fine wire thermocouple has the advantage that the thermoelectric properties of the junction are well known and do not vary with time. When relatively thick wires are used, there is a thermal lag between the junction temperature and the local gas temperature in a fluctuating temperature field.

To the first order, the gas and wire temperatures are

usually assumed to be related by a time constant so that,

$$T_g = T_w + \tau \frac{\partial T_w}{\partial t} \quad (1)$$

The value of τ is a function of the local gas properties and velocity, as well as the geometry of the thermocouple. The authors[10] have developed a method of measuring τ with the thermocouple in the flame, without requiring assumptions to be made regarding the local gas characteristics or the wire geometry. As shown in Fig. 8, the time constant measurement system is controlled by a DEC PDP 11-03 computer, which can also be used subsequently to acquire a time history of the temperature T_w which is corrected by using Eq. (1). A square wave overheating current is applied to the thermocuple and a portion of the temperature decay curve of the thermocouple is measured after each overheating pulse. As shown in Fig. 9, these decay curves are ensemble averaged by summing, typically, 512 realizations. By this means, flame related temperature fluctuations are averaged out to give a smooth decay curve which describes the regime characteristics of the thermocouple (plus its electronics). The computer program matches this decay curve to the inverse exponential decay implied by Eq. (1), so that a local value for τ is derived. In addition[10], the precise shape of the measured decay curve provides information on the deviation of the regime characteristics from the first order assumption. In fact, the Fourier transform of the decay curve provides the true response characteristics of the probe. It was found[10] that the major source of deviations from the first order equation is the complex heat transfer characteristics when the thermocouple junction bead

is much larger than the wire diameter. For the 25 μm thermocouples used in this study, time constants of 10 ms are common, and accurate signal compensation up to 2 kHz is possible by using the first order compensation equation.

Figure 10 shows a length of time history before and after compensation. Compensation (i.e. signal correction) is applied digitally to the signal by high level program, rather than by specially designed analog circuitry as has been used in the past. This digital compensation procedure is convenient and flexible; the main requirement is that there is very little electronic noise introduced in the signal in the preamplifier and ADC electronics. Such noise would be amplified by applying Eq. (1) to the digitized signal. Low noise is achieved by the use of battery-driven electronics and shielded cables.

2.5. *Ionization Probes*

The ionization, or Langmuir, probes used in this investigation are based upon the designs used by Lockwood and Odidi[11]. As shown in Fig. 11, the probes are water-cooled and the materials and design are chosen to minimize leakage currents and flow interference. In hydrocarbon flames, the ion density near the reaction zone is several orders of magnitude higher than elsewhere. In the circuit, shown in Fig. 12, a negative voltage is applied to the platinum electrode, causing a current to flow which is dependent upon the attraction of the ions to the electrode (and the repulsion of electrons). Several theories[12] relate the instantaneous ion current to the ion density, flow velocity, probe geometry and biasing voltage. During the initial stages of the present investigation, the ionization probe is being used to measure the flame front fluctuations. Use is made of the high

frequency response (several kHz), good spatial resolution (< 0.5 mm^3) and high sensitivity of the probe to the local occurrence of reaction. As described in Section 3, these characteristics make ionization probes ideal for measurement of the topography of reaction zones and their convective properties. Further, when used in conjunction with probes measuring other quantities, they enable conditional sampling to be used to relate averaged local eddy structure to local burning characteristics. The signals are amplified by low noise, battery-driven, preamplifiers and a 16 bit ADC, and then fed to the DEC computer.

2.6. *Other Measurement Techniques*

In addition to the main techniques described above, DISA hot wires and constant temperature anemometers have been used to investigate the cold jets. Other techniques which are available, but which have not yet been applied to the flames, include streamlined microphones, for the measurement of near field pressure fluctuations, and standard quartz microprobe (sonic) sampling apparatus, for measurement of the local time mean species concentrations. Small modifications to the LDA system will permit the measurement of conserved scalar fluctuations, similar to the methods used by Bilger[9]. Preliminary LDA experiments have also been conducted in which only one of the gas streams is seeded. This provides 'weighted' velocity data which may be interpreted in broadly the same way as intermittency conditioned data in cold flows.

2.7. *Flow Visualization*

Flow visualization is considered to be the backbone of this investigation. Direct evidence is provided of 'structure' in the flow and important clues are provided to aid in the interpretation of quantitative measurements. The main flow visualization system is shown in Fig. 13. The large mirrors permit a 20 D length of flame to be filmed by using a Hadland 'Hyspeed' camera, which has a maximum framing rate of 20,000 frames/second. A Schlieren system is used, as interferometry would provide little advantage for complex three-dimensional turbulent flows. Colour Schlieren light stops are used to provide a clearer qualitative picture of the different density gradient regimes. Thus, for example, high temperature reacting interfaces can be identified by streaks of a certain colour (typically white). Kodak Eastman Ektachrome 7239 colour cine film is used.

No attempt has been made, at this stage, to interpret the films in terms of density, or temperature, variations. However, many different quantitative analyses can be applied to obtain important information on the development and interaction of coherent structures. The films can be analysed: (i) manually, using an 'editor'; (ii) by projection on a screen with subsequent semi-automated analysis by using an XY coordinate data-logger; or (iii) by using a Quantimet image analysis computer. Films are also taken directly of the flame, so that regions of luminous burning are seen most clearly. The differences between these films and the Schlieren films are striking, as will be discussed in Section 4. Signals, from probes in the flame, can be

recorded simultaneously on the cine films, to enable comparisons to be made between observed structures and the signals which they produce.

2.8. *Data Acquisition and Processing Facilities*

In general, all data is acquired, on-line, by DEC PDP 11-03 and PDP-8E computers via purpose built preamplifier, ADC and multiplexing interfaces. For the LDA, for example, up to 40,000 signals can be loaded on to the disk of the PDP-8E with the PDP 11-03 acting as a data buffer between the larger computer and the LDA processor/interface. Fortran, Basic and Machine Code programming are used for data processing. 16 bit or 12 bit words are used, depending on the accuracy required.

A spectroscope Model 5D335 Real Time Analyser is used to derive power spectra from continuous signals.

3 Data Analysis and Interpretation

3.1. *Laminar, Transitional, Turbulent and Buoyancy Influenced Regimes of Flames*

In the interpretation of quantitative measurements and flow visualizations, the local relative importance of various regimes of flow structure must be recognized. In fact, the relative importance of these various regimes can only be deduced from the measurements, and flow visualizations themselves. It is important to avoid an assumption of, say, local turbulent flow, without supporting data. The first flames to be studied are basically diffusion flames developing from relatively turbulence-free initial nozzle conditions. It is found that ignition and flame occur in an annulus within 2 mm of the nozzle lip. The initial flame is almost completely steady and laminar, both in

this region and also for several mm downstream. However, although the reacting region of the flow may be laminar, it does not necessarily follow that the complete width of the jet is laminar in the initial region. Indeed, it has been found that shear layer instabilities are already developing on the inner, high velocity, side of the mixing layer, although the outer 'sheath' of flame is completely laminar.

As sketched in Fig. 14, transitional flow develops after the laminar initial conditions. By definition, in the transitional flow viscous and inertial stresses are of the same order of magnitude, so that the flow is Reynolds number dependent. Transitional flow is complex, even in the cold case; however, certain repetitive physical stages can be identified[3]. An important feature is the development of three-dimensionality[3] from the initial axisymmetric conditions, although the dependence on these conditions is not yet fully understood. The damping influence of viscosity results in large orderly vortical structures, with little evidence of smaller eddy scales. The jet flame is even more complex, primarily because of:

(i) Increased viscosity due to heat release. The relative importance of this depends upon whether this viscosity increase is in a volume of fluid where viscous forces are important. This, in turn, depends upon a complex and, as yet, unknown dependence on all of the initial and boundary conditions of the flame.

(ii) Dilatation, or volumetric expansion, which must also influence the transitional flow in an unknown manner.

The initial series of experiments has concentrated on studying the interaction between combustion and the fluid

mechanics of the transitional flow with the objective of quantifying these effects.

Further downstream, the fully turbulent region is generally found, although for low velocity flames (or premixed flames) burning can be completed before turbulence has developed. Cold turbulent flows have been found[3] to have instantaneous three-dimensionality, large eddies, a wide range of wave numbers in fluctuations and Reynolds number similarity. It remains to be shown that all of these conditions are also a feature of the turbulent flame. As with the initial flow near the nozzle, it is important to bear in mind that, while most of the central core of the jet flame might have the characteristics of turbulent flow, this is not necessarily true for the outer low velocity region of the jet. One can envisage regimes in a diffusion flame where heat release occurs in relatively low velocity, outer regions so that significant reaction can occur in laminar or transitional flow conditions, while the bulk of the jet flame is turbulent.

The occurrence of significant buoyancy forces needs to be considered when interpreting flame data. All free diffusion flames contain regions where forces due to density differences are comparable with inertial or viscous forces.

Kennedy and Kent[13] and others have used the overall Froude number to indicate the importance of buoyancy forces. They showed that hydrogen diffusion flames, with $Fr_D = 7.5 \times 10^4$, were affected by buoyancy forces towards the end of the flame where 'flapping' was observed. The various independent parameters which determine flame structure are so numerous that one cannot

extend this observation simply to the present experiments, which use a larger nozzle and propane rather than hydrogen. Interest is being initially concentrated on the first 20 D of the transitional and turbulent flow, where buoyancy forces are of much less relative importance than at the end of the visible flame, at $x \simeq 80$ D. This flame, Jet Flame I, has $Re_D = 1.05 \times 10^4$, and $Fr_D = 1.63 \times 10^4$. The principal parameters for the jet flame are given in Table 1. The effects of buoyancy on specific regions of the flame will be examined by calculating the relative order of magnitude of inertial, viscous and buoyancy forces from measured data of velocity and temperature. Buoyancy forces will dominate in regions of high temperature and low velocity. Such conditions are found at the outer edge of the jet flame.

3.2. *Space, Time and Frequency Domain Analysis of Data*

An ultimate objective of this investigation is to measure coherent structures in flames in a quasi-Lagrangian reference frame, so that structures, and their interactions, are measured as they convect downstream. This objective requires specialized conditional analysis techniques of both multipoint data and flow visualization films. Conventional time average measurements also form an essential part of the investigation. The detailed information on coherent structures obtained by direct measurement requires to be related to structures determined by classical statistical averaging techniques. The various quantities to be measured in the flames (and cold jets) are listed and defined in the Notation. The single point time histories of velocity, temperature and ionization density are processed digitally for

selected regions of the flows. Power spectra and autocorrelations are derived using fast Fourier transform techniques. In addition, more detailed mapping of each flow, including the initial conditions, is made in which point measurements are processed to give time mean and rms fluctuating components of the various quantities, together with probability density functions. The data derived from the simultaneous multiprobe measurements (currently under development for conditional sampling), will also be processed, in selected regions of the flame, to give cross-correlations or cross-power spectra. Clasically averaged single and multipoint data will be used, as far as possible, to derive values of individual terms in the partial differential equations for continuity, momentum and energy. For example, simultaneously acquired LDA and thermocouple data, measured with the thermocouple close to the LDA measurement volume, will enable a good approximation to Favre averaged velocity data, $\tilde{u^2}$. Ionization probe and thermocouple data will be processed to provide information on local reaction rates.

3.3. *Conditional Sampling for the Study of Flame Structure*

Conditional sampling techniques are being developed for the study of combustion flows, using single and multipoint measurements. The expression 'Conditional Sampling' is used in a general sense to distinguish from the classical statistical averaging procedures noted in 3.2, those techniques of data analysis which use ensemble averaging to examine flow features of interest, with the averaging conditioned either by a feature of the signal itself or by an event or quality of another signal acquired simultaneously elsewhere in the flow. A wide range of conditional sampling techniques has been applied to cold turbulent

flows. Some of these techniques have been outlined by Davies and Yule[14], Van Atta[15] and Laufer[16]. Yule[17] has attempted to bring some unification to the conditional sampling/coherent structures field by including a systematic description of the interpretation of various conditioned data analysis techniques.

There are two principal 'coherent structures' of interest for the present investigation:

(i) Interface burning regions The structures and coherence of such regions, where they exist, are of extreme importance from the point of view of overall flame structure, pollutant emissions and mixedness. Physical models, such as the 'wrinkled' flame front and Spalding's[18] ESCIMO concept, have been used in the past to describe premixed flames.

(ii) Large Eddies including the 'birth', structure and interactions of these eddies and, in particular, their interactions with the interface burning regions.

Many cold-flow conditional sampling techniques are not useable in reacting flows until further advances are made in flame measurement techniques. For example, LDA techniques cannot currently be used to detect the highest frequencies occurring in the turbulence so that velocity signals cannot be reliably processed to obtain intermittency information. On the other hand, the many additional dependent variables occuring in reacting flows compared with cold flows, vastly increases the permutations of conditioning criteria and conditioned signals, which could be used. It is, thus, necessary to be selective, and concentrate on designing techniques to provide direct information on large eddy structures and the interface burning region.

Some of these procedures are noted here:

(i) Conditioned Single Point Data The ionization probe provides, perhaps, the most useful signal for the application of ensemble averaging techniques. The sharp 'spikes' typically found in ionization density signals are produced by reaction zones and provide a clear and distinct signal of reaction occurring at interface layers moving through the flow. By fixing triggering levels in signal time histories, information can be derived on the frequency of occurrence of these layers, on the thickness of the layers and on variations found in the structures of reacting interface layers at a fixed position.

The temperature and velocity time histories from single point measurements are examined by using 'pattern recognition' techniques. The objective of using these techniques is to determine the proportion of a signal that can be attributed to structures which have a high degree of local repetitiveness. Such single point data cannot, however, provide information on the coherence of such structures. Examination of time histories in this manner is an essential prerequisite of multiprobe conditional sampling experiments, as information can be deduced concerning the triggering criteria which are likely to be most usefully applied. Yule[3] proposed that the simultaneous acquisition of single point signals, together with flow visualization films, provides the optimum method of designing conditional sampling techniques.

(ii) Multiprobe Conditional Sampling of Local Structures Signals acquired simultaneously by two, or more, probes with variable spatial separation, are processable to obtain averaged local structures of the eddies of interest. Figure 15 shows an example of a situation in which a fixed ionization probe is used to detect

the passing of a reacting interface layer. The signals from the LDA or thermocouple are ensemble averaged, at different positions, when the ionization signal peaks occur, so that the average temperature and velocity fields are measured relative to the interfaces. Variations and elaborations of this configuration are envisaged; for example, two adjacent ionization probes can be used to trigger the sampling, with the 'condition' that passing interfaces are at a specific angle to the axis. Signals from the LDA or thermocouple can also be used for the triggering criteria. In cold jets[3], conditional sampling, relative to potential core velocity peaks, reveals averaged large eddy structures. Figure 15 shows a situation where the burning interface encircles the eddy, as is found to be the case, for the first 10 D, of Flame I. The eddies have vortex-ring shapes and the flow is similar to the transitional flow in cold round jets.

A related technique utilizes an array, or rake, of probes stretched radially across the flow. A rake of 8 thermocouples, spaced at 10 mm intervals, has been constructed for this purpose. This arrangement allows conditional averaging of the radial temperature distribution, and also provides a means for searching for repetitive patterns in the instantaneous radial temperature distribution.

(iii) Measurement of Structure Coherence and Convection by Multiprobe Conditional Sampling The techniques described in the previous section, for measuring local structure, can be extended to measure the changes, coherence and convection downstream of the structures. The signal recovery probes are positioned at different positions downstream of the triggering

probe, and the signals are averaged with a time delay sufficient to permit the convection of the sampled structures to the recovery position.

Figure 16 shows a situation in which two ionization probes are used to measure the convection and changes in dimensions of reacting interface layers. Results obtained from these measurements will be compared with the equivalent space-time cross-correlations and indications will be sought of the extent to which these correlations can conceal, or 'smear', the true coherence of convected structures. Extraction of information concerning the true coherence and structure of an event from the signal properties introduced by 'phase scrambling' effects are discussed in Section 3.5. When, for example, coalescence of the structures of interest is known to occur, the triggering and conditioning procedures require to be specifically designed to educe this information from the recovered signals.

3.4. *Flow Visualization: Quantitative Applications*

The colour Schlieren and direct photography high-speed cine films of the flames are processed to provide quantitative data on flame characteristics. Such quantitative analyses are possible for at least the first 20 D of the flow in 'Jet Flame I', where repetitive structures and interfaces are very clearly visible. It is not yet known how far this quantitative analysis can be extended downstream. Vortex, or instability wave, passing frequencies can be measured from films in the transitional flow near the nozzle. Both in this region and further downstream, the properties of very clear interface burning regions are derived by measuring the changes in shapes and separations of these

interfaces as they are convected downstream. Analysis of films provides probability distributions of the shapes of interfaces at different positions and, as shown in Section 5, this information provides data on, and great insight into, the smearing, or phase scrambling, inherent in multiprobe point measurements.

3.5. *Data Interpretation in Terms of the Coherence of Structures and Phase Scrambling Effects*

In transitional and turbulent flows, there is evidence that structures, either eddies or interfaces, retain a high degree of spatial coherence, or identity, as they are convected downstream. The major problem in space-time cross-correlations and in conditional sampling experiments is to recognize this coherence. This coherence must be recognized and established in individual structures undergoing some degree of change in dimensions, geometry and trajectory as they move downstream. Other possible phenomena, such as three-dimensionality in structures and their movements and the coalescing of structures, combine to produce low levels of recovered signal, or cross-correlation, in spite of the coherence of individual structures. This 'smearing' of multipoint data will be referred to as 'phase scrambling', since the major contributor to the loss of recovered signals is produced by variations of the phases of individual sampled signals resulting from combinations of the various phenomena.

Figure 17 illustrates the phenomenon for the case when a characteristic signal $\alpha_2(\tau)$ is measured at times relative to the passage of the structure past the trigger probe (signal $\alpha_1(t)$) further upstream. For the flame, the signal can represent signals from ionization probes or thermocouples when reacting

interface layers are present. The conditionally sampled ensemble average $< \alpha_2(\tau) >$ has a low amplitude compared with the amplitudes of individual signals, so that an average convection velocity $<U_c>$ is the only useful quantity that can be extracted from the ensemble average. Various alternative more complex methods of ensemble averaging can be employed. Figure 17 illustrates one such procedure, where the phase scrambling effects are 'unscrambled' by ensemble averaging the recovered signal at times relative to the signal peaks, which occur at τ_n for the nth sampled structure. This procedure provides a more representative ensemble averaged structure, with a high amplitude and width more truly representative of the individual structures. Additional information such as, for example, the probability distribution of the arrival times, is also provided. Such a procedure is only possible for signals with sharp peaks which are clearly recognizable. Thus, this approximates to the convection of one-dimensional structures. More complex situations require more complex conditioning techniques. For example, rather than using signal peaks, the phase differences between individual recovered signals can be derived by phase shifting each individual signal to obtain the best fit with the predetermined ensemble average $< \alpha_2(\tau) >$. A new 'unscrambled' ensemble average can then be derived by taking these phase shifts into account.

Particular problems are encountered when velocity signals are used for conditional sampling. If an eddy retains coherence with distance downstream, this should be most clearly recognizable in scalar fields associated with the eddy or in the vorticity distribution in the eddy. The local fluctuations, in say the

U velocity component, will not necessarily be as recognizably repetitive with increasing distance downstream because of their interdependence with the vorticity and potential flow fields surrounding them.

Figure 18 illustrates the more general situation regarding coherent structures. Here the nth structure is identifiable (indeed it is defined by) a three-dimensional distribution of some scalar or vector quantity $\alpha(x'', y'', z'')$. The 'quasi-Lagrangian' coordinate system is based upon a reference position embedded in the structure. This coordinate system need not necessarily be identified with the same 'fluid element' throughout the structure's lifetime; it is more likely to be either the equivalent of a centroid of the structure or, alternatively, a position in the structure which produces the point signal which is recognized by the signal conditioning technique. In the same way, there is no reason why a coherent structure should be identified with the same packet of fluid throughout its existence. In fact, it can be argued that this is manifestly not the case for most coherent structures. Thus, the larger scales in the early transitional regions of shear flows can be considered as waves moving through the fluid and the large eddies in the turbulent flow continually entrain new fluid, and also shed old fluid. For coherent interfaces, one can also expect a flow of fluid across the interface. For example, reacting interface layers require a continual supply of fresh mixture for reaction to persist; also turbulent/irrotational interfaces diffuse into the irrotational flow.

As shown in Fig. 18, the structure moves downstream until

at some time τ, it can be identified in a certain position and with a certain change in the shape and distribution, with $\alpha = \alpha(x'', y'', z'', \tau)$. There may also be some loss of coherence. Such a loss may involve a breakdown in the structure so that it is no longer identifiable as such. A rather different type of breakdown occurs if the structure amalgamates with a neighbouring structure. The precise definition and concept which describe the coherence of individual eddies are somewhat arbitrary and even subjective. This is opposed to the coherence functions in statistical time averaged analyses, although these, and the equivalent cross-correlations, can give a very poor indication of the true physical coherence of individual structures. An important objective of current coherent structure studies is the identification, specification and definition of 'coherence' as applied to individual structures. A step towards this understanding will be made when the phase scrambling effects can be quantified. If the structures, shown in Fig. 18, are ensemble averaged over many realizations, at time τ, an ensemble averaged structure is obtained. $\langle \alpha(x', y', z', \tau) \rangle$, where the coordinate system, (x', y', z'), is an Eulerian system based upon P, the most probable position of the reference point P_n averaged over many structures at time $\tau = \tau_1$. The ensemble averaged structure will be smeared because of the variations is individual structures. Thus, the nth structure, shown in Fig. 18, is at a position $(x'_{P_n}, y'_{P_n}, z'_{P_n})$ relative to P. There will, thus, be a probability density function describing the probability of the reference point of a structure being at a position (x'_P, y'_P, z'_P) at τ_1 which can be written $P_{STRUCTURE}(x'_P, y'_P, z'_P \tau_1)$.

If all structures at time τ_1 are identical so that signals at $\tau = \tau_1$ are scrambled only due to shifting in the positions of structures from one to the next, phase scrambling is a function of P_{STRUCT} only, so that the ensemble averaged structure at $\tau = \tau_1$ is related to the α field of an individual structure by:

$$< \alpha(x', y', z', \tau_1)> = \iiint_{TURE} P_{STRUC} (x_p', y_p', z_p', \tau_1) \alpha(x'' = x'-x_p', y'' = y'-y_p', z'' = z'-z_p', \tau_1)\, dx_p'\, dy_p'\, dz_p' \quad (2)$$

where the integral is taken over the total volume in which the reference point, P_n, of structures can be found at the time delay $\tau = \tau_1$.

Further contributions to the loss of signal can be expected due to a lack of repetition in the triggering criterion relative to the structures and a lack of repetitiveness in the individual structures. Further forms of Equation (2) can be formulated to describe these effects. It is then necessary[17] to design experimental systems to quantify these contributions and, thus, attempt to extract information on the true coherence and structures of individual eddies from the data. These concepts are equally applicable to the quantitative analysis of flow visualizations and data on phase scrambling, derived from Schlieren films, as discussed in Section 5.

4 Preliminary Results

The initial experiments have concentrated on the first 20 D of Jet Flame I and the equivalent nonburning flow, Cold Jet I. The independent variables for these flows are specified in Table 1.

4.1. *Flow Visualization of Jet Flame I*

Figure 19 shows still photographs of the complete flame. From visual observations, the flame appears to be 'turbulent' beyond x = 5 D. High-speed photography, with close-up views, reveals, however, that the basic flow (at least in the first 20 D which have been analysed so far) consists of distinct flow regimes which contain coherent structures. A qualitative description of this flow is given here, while Section 5 discusses quantitative data derived from the films.

Figure 20 is a single frame from a high-speed film of the flame, showing the region 8 D $\leq$ x $\leq$ 16 D. Figure 21 gives a sequence of four frames, at 8 ms intervals, showing the region 16 D $\leq$ x $\leq$ 24 D. Both of these films were obtained by directly filming the flame so that light areas represent regions of high flame luminosity. Figure 20 shows the appearance of azimuthally distributed streaks of luminous burning. These streaks are themselves distributed fairly periodically with longitudinal distance along the jet flame. These streaks are considered to be formed by the azimuthal wave instability of the vortex rings in the first part of the jet flame. It is, thus, deduced that similar three-dimensional instability mechanisms can be found in both the jet flame and in the cold round jet. The overall structure of a cold jet is sketched in Fig. 2. In spite of the general similarity, quantitative differences must be expected between the cold and burning cases, and this will be shown to be the case.

The sequence of frames in Fig. 21 shows, on the left hand side of the jet flame, bulges of luminous burning which appear

to combine and produce an outward moving tongue of flame. This is evidence of the coalescing of structures in the jet flame. This phenomenon could be seen often in this region but the event is far from repetitive when examined using flame luminosity. It is found that flow visualization, by simple use of flame luminosity, is not the most useful technique for deriving qualitative and quantitative information on flame structure. There are two main reasons for this: (i) structures in three-dimensional flows are hidden by luminous areas on the outside of the flow; (ii) the occurrence of flame luminosity is sensitive to fluid mechanical and chemical kinetic criteria. Such criteria may only be met in certain regions of structures, so that a flow visualized by flame luminosity may appear relatively disorderly while, fluid mechanically, quite orderly structures are present. The use of colour Schlieren flow visualization with high-speed cine films, indicated a substantial orderliness, in the first 20 D of flow at least. Figure 22, showing the region $0<x<10D$ using colour Schlieren, indicates this orderliness. The reaction zone, up to approximately x = 1 D, appears to be completely laminar and almost cylindrical, but with a larger diameter than that of the nozzle. Further downstream, beyond x = 2 D, periodic waves develop in the reacting interface. These waves are believed to be caused by the entrainment action of the developing ring vortices. The cores of these vortices are found on the 'high' velocity part of the mixing layer (see Section 5). The high temperature interfaces can be seen to stretch around each vortex; discrete, individual interfaces break away and separate from the initially continuous interface. Beyond x = 6 D,

an array of 'S' shaped hot reacting can be seen in the central part of the mixing layer. These interfaces and their associated vortices or eddies are seen to coalesce in the region 4 D < x < 8 D. Similar 'S' shaped interfaces persist beyond the region of coalescence, in the high-shear region of the jet flame; they have been found at least up to x = 20 D, which is the furthest distance downstream which has been examined so far. Beyond the vortex coalescing region (x > 8 D), the shape, changes in shape and movements of the interfaces are visually less-repetitive than further upstream. Some individual interfaces can be seen to undergo extinction of reaction, while others coalesce with neighbours, but with less organized repetition than in the region x < 8 D.

The cine films show two fairly distinct regimes co-existing in the first 20 D of the flame. There is the inner, fast moving flow, which is in the central region of the jet flame, 0 < r < 0.4 D, and an outer slower moving flow which contains significant reacting regions. Observations[3,4] in cold jets have shown that the interacting vortices and eddies in the mixing layer shed fluid outwards to form a relatively disorganized sheath of slow-moving fluid. It seems likely that this same mechanism is also present in the jet flame and is responsible for the outer, slower moving component of the flow.

All the phenomena which have previously been observed in the mixing layers of cold jets have now also been identified in the jet flame. Furthermore, these phenomena have distinct and clear effects on the dynamics of coherent interface burning regions which appear to be the dominating components of the reacting flow. Reaction also affects the shape and dynamics of

the vortices and eddies, through dilatation and increased viscosity effects. In the cine films, vortex-like eddies were indentifiable up to at least x = 20 D, with considerably more clarity than for cold jets. It will be shown that there are important differences in the rates of spread of the mixing layer, the vortex frequencies and the transition distance between the jet flame and the cold jet.

4.2. *Cold Jet I Investigation*

Measurements have been made in Cold Jet I with a hot wire anemometer and laser anemometer (LDA) to establish very definitively the initial conditions for the mixing layer in the plane of the jet exit. It has been assumed, but will subsequently be verified by LDA measurements, that the initial conditions for Jet Flame I are the same as for Cold Jet I. Velocity measurements have also been made within the cold mixing layer and jet so that data can be compared directly with LDA data from Jet Flame I. This comparison provides information on the interaction between combustion and fluid dynamics in the transitional and turbulent flow.

Figure 23 shows velocity profiles measured near the inner nozzle lip at the nozzle exit plane (x/D = 0.04) for the flow conditions of Cold Jet I and also at a lower Reynolds number. Measurements of $(\overline{u^2})^{\frac{1}{2}}$ show very low values, with $(\overline{u^2})^{\frac{1}{2}}/U_J$ no more than 0.005. Thus, the initial jet flow was essentially laminar. The laminar inner boundary layer was found to be thicker than in most jets that have previously been investigated. Figure 24 shows that data for the 'maximum shear' thickness of the boundary layer fit the equation

$$\delta_J/D = 9.5\ Re_D^{-\frac{1}{2}} \qquad (3)$$

In previous studies, a typical value for the proportionality constant in the equation is 3. The explanation for this relatively thick boundary layer is found in the special requirements in the design of the unusually long nozzle and entry pipe to provide low turbulence levels without the insertion of screens or gauzes and, at the same time, to prevent separation of the low velocity secondary flow on the outside of the nozzle. It can be argued that the inner nozzle boundary layer may not be the only factor determining the initial jet instability when there is a secondary stream. The boundary layer on the outside of the nozzle, and also the wake caused by the nozzle lip, could contribute towards the instability, but these effects should be small when $U_S << U_J$, as is the case for Cold Jet I. In an idealized situation, if the initial velocity deficit at the lip is quickly filled by entrainment from the secondary stream, an initial shear layer thickness b_o can be defined such that $b_o = (1 - U_S/U_J)\ \delta_J$. The expected variation of b_o with Re_D, when U_S is kept constant, is included in Fig. 24.

Figure 25 shows radial traverses at x = 2 D in Cold Jet I, with (U_S/U_J = 0.11) and without (U_S/U_J = 0) the secondary flow. It is seen that the velocity gradient is the central part of the mixing layer is unaffected by the presence of the secondary flow. Small differences are, however, found between the two cases, in the potential core flow of the jet. It is thought that these small differences can be attributed to changes in the vortex dynamics in the initial transitional flow. Figure 25 also shows the good agreement found between the LDA and hot wire data. The

differences between the cases $U_S/U_J = 0$ and 0.11 are also seen in the centreline values of U and $(\overline{u^2})^{\frac{1}{2}}$ shown in Fig. 26. The rate of increase of fluctuations in the potential core is significantly lower for the case $U_S/U_J = 0.11$. This damping effect may be considered as being caused by a 'stretching' of the transitional flow by the secondary stream. Measurements show, however, that the secondary stream does not affect the initial instability frequency; nor does it affect the frequency spectra peaks throughout the transitional jet. A full description of the effect of a secondary stream on the transitional flow in round jets requires further study.

At this stage of the investigation, evidence suggests that the presence of the low velocity secondary stream does not drastically affect the overall physical structure of the jet; a number of recognizable, small effects have been detected. All subsequent data refer to jets and jet flames, with the secondary flow.

Comprehensive mapping of amplitude spectra of u in Cold Jet I has been made to derive detailed knowledge of the transitional flow. Figures 27 and 28 show spectra at the centreline for $0 < x/D < 6$. The fundamental instability frequency occurs at 215 Hz; the amplitude increases to reach a maximum at $x/D = 3.5$. This 'growth' corresponds to the rolling up of the initial shear layer instability to form near-periodic vortex rings.

The subharmonic of the fundamental frequency, peaking at 104 Hz, is just discernable at $x/D = 1$; it is caused by the pairing or coalescing of vortices as they move downstream. After $x/D = 3.5$, the fundamental frequency peak decays until, beyond

x/D = 5, it is lost in the typical turbulent spectrum. However, the subharmonic peak increases to a maximum value at x/D = 4 and it is still discernable at x/D = 6.

The spectra at r/D = 0.5, shown in Figs. 29 and 30 are strikingly different from those on the centreline (r/D = 0). The fundamental and subharmonic frequencies are the same as those found in the potential core, although there is a small, but noticeable, decrease in the subharmonic peak frequency, with increasing x. In the transitional mixing layer, the fundamental frequency peak is greater in amplitude than the subharmonic amplitude until both peaks disappear at x/D = 5. Between x/D = 1.5 and x/D = 3, there is a very rapid increase in the amplitude of the subharmonic; this coincides with the region of coalescing of initial vortices. The mixing layer spectra, in Figs. 29 and 30, also display first and higher order harmonics of the fundamental frequency. These higher harmonics are associated with the viscous core of the vortices.

Figures 31 and 32 show spectra at different radial positions at x/D = 4 and x/D = 6. The peaks that are evident across the complete mixing layer at x/D = 4, disappear at x/D = 6, apart from the subharmonic peak which is discernable at r/D = 0. On the basis of the establishment of turbulent forms for spectra inside the mixing layer, the transition length of Cold Jet I is deduced to be x_T = 5 D. By coincidence, this roughly corresponds with the end of the potential core.

4.3. *Measurements in Jet Flame I*

Comprehensive measurements of velocity, temperature, ionization current and other quantities in flames are continuing to be made and periodic reports of this information will be made.

In this report, a selection of data is presented with the aim of providing clear definitions and descriptions of the initial and boundary conditions. The data and flow visualization from the flame and cold jet presented in this report also provide insight into the combustion-flow interaction in the initial part of the flame.

Figure 33 shows LDA velocity profiles in the initial part of Jet Flame I. In general terms, the flow in the flame is similar to that in the cold jet. There is a central, uniform velocity, potential core with an outer 'cylindrical' mixing layer. The mean temperature distribution at x/D = 2, which is also included in Fig. 33, has a peak at the outer part of the mixing layer. The location of this temperature peak within the mixing layer is determined by the location of the stoichiometric fuel/air mixture ratio. In Fig. 34, the velocity distributions at x/D = 4 are compared for cold and burning jets. The potential core has ended for the cold jet while, for the burning jet, the core still extends out to r/D = 0.4. The rate of spread of the mixing layer into the potential core of the flame is very much slower than in the cold jet. These differences can be attributed primarily to the increased viscosity and dilatation effects on the initial transitional vortex flow in the flame.

Flow visualization indicated that the flame was stabilized in a steady, laminar, cylindrical interface which was attached to the nozzle lip. This laminar flame appeared to be steady up to x/D = 2 and had a diameter greater than the nozzle diameter. Figure 35 shows temperature and velocity profiles at x = 2 mm

in the flame stabilization region. It is seen that the peak temperature, corresponding the the centre of this initial laminar diffusion flame, occurs 0.2 D outside the high shear region of the velocity distribution. The temperature increase in this high shear region is no more than 300 K, but the viscosity changes due to this increase might be expected to be sufficient to affect the initial shear layer instability growth. The low velocity region between 0.5 r/D and 0.65 r/D, where flame stabilization actually occurs, will be investigated in detail using a newly acquired Bragg cell frequency shift unit for the LDA.

The spread of the mixing layer into the potential core region of the flame is greatly reduced compared to the cold jet. However, on the outer, low velocity, section of the mixing layer, where high temperatures are found, velocities are higher than those found in the cold jet mixing layer. These increased velocities are primarily due to dilatation, although buoyancy forces will also provide contributions to the acceleration of the outer flow. For example, at x/D = 2, in the high temperature region at r/D = 0.6, the velocity in the flame is $U/U_J = 0.38$, while, at the same position, in the cold jet, $U/U_J = 0.2$. The rate of increase of the peak 'turbulence' intensity $(\overline{u^2})^{\frac{1}{2}}$ is much less in the jet flame than in the cold jet (Fig. 34).

In the first 10 D of flow, the ionization probe was found to give significant signals, only on the inner side of the mixing layer of the jet flame, i.e. for r/D < 0.5. Figure 36 shows a typical spectrum of the ionization current signal at x/D = 8; r/D = 0.5. Various distinct peaks can be seen in the spectrum. Some of these peaks can be identified with frequencies derived

by analysing high-speed cine films. It can be seen from Fig. 36, that the fundamental instability frequency of the cold jet cannot be identified in the spectrum for the flame.

5. Discussion and Concluding Remarks

The initial conditions of the cold and burning jets, including the initial shear layer instability and flame stabilization, will first be discussed. Michalke's[19] theory predicts the most amplified shear layer instability frequency as a function of the initial shear layer thickness. Figure 37 shows the predictions from this theory in the form of the Strouhal number St_δ. It is seen that the measured fundamental frequency of Cold Jet I is in good agreement with the prediction of Michalke. It is, thus, reasonable to assume that both the cold and burning jets become unstable naturally, so that there is no influence from the low initial turbulence levels nor from external sound sources. Most of the initial turbulence at the nozzle, where $\overline{(u^2)}^{1/2}/U_J < 0.4\%$, is concentrated near the 30 Hz frequency, as can be seen in Fig. 27. The small fluctuations are thought to be the result of an 'organ-type' resonance of the nozzle and inlet pipe. This resonance does not affect the natural shear layer instability which occurs at 215 Hz.

The transition distance of the cold jet, deduced from the spectra measurements described in Section 4.2, is included in Fig. 38. Figure 38 also includes measurements of the transition distance, as a function of Reynolds number Re_δ made by Yule[3] in a 50.8 mm diameter cold round jet. For the latter jet, the nozzle boundary layer thickness obeyed the proportionality $\delta_J/D = 3\ Re_D^{-1/2}$. Thus, for a given value of Re_D, the 50.8 mm diameter jet had a much thinner nozzle boundary layer than the

present 25.4 mm diameter jet. It is seen from Fig. 38 that the data do not satisfy the proportionality $x_T \sim \delta_J$ which has been proposed by several authors[20]. In addition, no reasonable agreement can be found with the alternative suggestion that the transition Reynolds number, $x_T U_J/\nu$, is approximately constant. It is clear that round jet transition is still far from being understood and further work is required to elucidate the relative importance of viscous damping (including the role of the initial nozzle boundary layer), coalescence and the growth of three-dimensionality. It seems reasonable to assume that, when a transitional mixing layer flow extends towards the end of the potential core, interaction across the jet will enhance the growth of three-dimensionality, and thus the development of turbulent flow. Thus, for example, if Re_D is fixed and δ_J is gradually increased by some means, x_T may indeed initially increase almost linearly with δ_J. However, when x_T becomes comparable with the potential core length, transition is accelerated and x_T then increases less quickly with increasing δ_J.

A further important consideration is the role of vortex coalescence in transition. A feature of transitional jet flow is the near-periodic vortex ring formation and coalescence which occurs in well-defined regions. These vortex rings, and their coalescence, are recognized by single, double or triple spectra peaks. The present Cold Jet I has only one recognizable vortex coalescence prior to turbulent flow. The large eddies, after transition, appear to coalesce, but they lack the repetitativeness required for the production of spectra peaks and subharmonics. Up to three transitional coalescence regions have

been observed in various jets[3,4]. It appears[3] that the latter stage of transition involves the coalescence of vortex rings which have developed core waves greater than some critical size. It can be surmised that, if the end of transition is identified with a particular coalescence, a sufficiently detailed investigation of x_T as a function of Re_D for a given jet, might reveal 'ripples' in the distribution corresponding to transition occurring after one, two, three or perhaps more coalescings.

Figure 39 includes the axial distributions of Strouhal numbers corresponding to spectra peaks, and thus vortex passing frequencies, in the cold jet. Data have only been included for regions where peaks can be identified in the spectra. For the jet flame, spectra, such as those shown in Fig. 36, cannot yet be unambiguously interpreted in terms of vortex passing frequencies. However, in the first 20 D of the jet flame, at least, the vortices, eddies and interfaces associated with them can be identified sufficiently clearly in Schlieren cine films for passing frequencies to be measured accurately. Figure 39 includes Strouhal number distributions derived from eddy passing frequencies measured from the Schlieren film. The differences between the cold and burning jets are large and their nature was rather unexpected. The initial frequency, identified at $x/D = 2$, was more than twice the initial frequency found in the cold jet. The coalescence of these initial vortices in the flame occurred in the region $4\ D < x < 8\ D$ as opposed to $2\ D < x < 4\ D$ in the cold jet. This 'stretching' of the initial part of the flame transition can be attributed to both the effect of dilatation in accelerating the vortices and also the temperature-related viscosity increases which decrease the rate of growth of the

vortices.

Measurement of 100 consecutive vortices between 3 D < x < 5 D yielded an average vortex convection velocity, $U_c = 0.92\ U_J$ in this region of the flame. This contrasts with $U_c = 0.6\ U_J$ for the cold jet. Individual vortices in the flame had convection velocities in the range $0.86\ U_J < U_c < 0.98\ U_J$. Further downstream, the vortices, or eddies, were found to accelerate so that between 12 D < x < 16 D the average convection velocity is $U_c = 1.06\ U_J$. In this same region, individual convection velocities were measured in the range $0.94\ U_J < U_c < 1.22\ U_J$.

Using Schlieren and direct visualization techniques, the appearance of the initial part of the jet flame is shown in Fig. 40. The visualization by flame luminosity indicates predominantly fuel-rich burning regions, which are, initially, associated with specific three-dimensional features of the flame. In the first two diameters of flow, the cylindrical laminar flame is separated from the inner, high shear flow, as is shown by the LDA and thermocouple data in Fig. 35. The velocity profile at x = 2 mm in the high shear region, resulting from the detached nozzle boundary layer, differed insignificantly from that measured in the initial cold flow by the hot wire anemometer. It cannot, therefore, be argued that an altered initial velocity profile is responsible for the higher initial instability frequency in the burning jet. Other factors that could influence the initial frequencies are, feed-back pressure or sound fields set up downstream of the nozzle by combustion/flow interaction. In addition, the high temperature at the outside of the initial shear layer could cause damping of instabilities,

resulting in a reduced 'effective thickness' of the shear layer compared to that found in the cold jet. Further, more detailed, measurements require to be made in the initial flow region in order to explain fully these differences. Further insight is being sought by carrying out a mathematical analysis using a finite difference, time-stepping model to investigate the effects of combustion on shear layer instability and vortex roll-up.

Between 2 D < x < 4 D Schlieren films show the outer reacting interface being entrained by the inner periodic vortices. Significant flame luminosity is only found after x = 6 D in the region of coalescence of the initial vortices. This luminosity occurs as axial streaks around pairs of coalescent vortices. These streaks correspond to the development of three-dimensionality in the vortices, similar to that previously observed in cold round jets.[3] After x = 8 D, continuous interface burning regions begin to break up into detached 'S' shaped interfaces associated with the leading edge of each eddy. In this region, although there is some noticeable circumferential symmetry across the flame, it is debatable whether the observed structures can be labelled 'vortex rings'. Beyond x = 12 D the movements of these reacting interfaces become noticably less repetitive although, individually, they generally remain coherent up to at least x = 20 D.

A striking feature of the jet flame downstream of approximately x = 10 D was the appearance of an outer, slow moving component of the flow. Tongues of reacting or hot gas detached themselves from the main, inner flow, containing the eddies and interfaces. This outer flow moved downstream at a velocity of approximately

0.3 U_J, while the inner eddies moved with $U_c \simeq U_J$. These outer tongues of flow have a similar appearance to the three-dimensional 'jets' of relatively disorderly fluid which have been observed to be ejected from cold jets.

The experiments have shown that reaction, in the first 20 D of the jet flame, at least, is concentrated largely in interfaces. An individual region of reacting interface can generally be followed from its formation near the nozzle, through coalescence, up to x = 20 D. These interfaces, therefore, can reasonable be termed 'coherent structures' in the flame, and they are also associated with coherent vortex-like eddies. One objective of this study is to measure the structures and histories of these coherent structures. As a first approach to this end, a conditional sampling technique has been applied to the analysis of high-speed cine films. The shapes of fifty interfaces were recorded at the times when the passed through a 'trigger' position, x/D = 12, r/D = 0.5, as shown in Fig. 40. The shapes and positions of each interface were also recorded at intervals of 16 ms after passing through the trigger position. Results obtained by using this procedure are shown in Fig. 41. The averaged shapes of the interfaces, at τ = 0 are similar to the potential/irrotational flow interfaces found in cold jets. The probability distribution of interface positions, at r/D = 0.5; τ = 16 ms, has a totalled measured range of positions of plus or minus 12% about the mean. It is expected that this variation, coupled with variation in interface structures, will contribute to an appreciable phase scrambling effect on multi-probe measurements. The double ionization probe measurements

which have been described will provide a comparison with the film analysis data.

It has been found that coherent structures are at least as important in jet flames as they are in cold jets. The experiments now in progress will provide quantitative information and descriptions of these structures in jet flames. Furthermore, the experiments will be extended downstream to investigate the full length of the flame. An important question which still remains unanswered is the extent to which these flames can be considered to be turbulent. At x = 8 D the flame is undoubtedly transitional, containing periodic, essentially axisymmetric, vortex rings. Beyond x = 14 D, the flame has all the appearances of turbulent three-dimensional flow, although coherent structures are still present.

Acknowledgements

The following members of the research team of the Combustion Aerodynamics Research Laboratory are making major contributions to the research project: Dr. D. S. Taylor and R. Boulderstone - Signal processing and digital analysis by computer; S. J. Ralph - laser anemometry; J. Ventura - ionization probe; J. Newton and M. Wilde - High-speed Schlieren and cine photography; R. Pattie - Mathematical analysis; G. Fletcher - Technician and Mrs. D. Sayliss - preparation of report and typing.

Funding for this research project is provided by ONR (Project SQUID), AFOSR and the Science Research Council (UK).

References

1. Roshko, A., Progress and problems in understanding turbulent shear flows. Turbulent Mixing in Nonreactive and Reactive Flows (ed. S. N. B. Murthy), pp 295-311, Plenum, 1975.

2. Browand, F. K. and Weidman, P. D., Large scales in the developing mixing-layer. J. Fluid Mech. 76, 127-144, 1976.

3. Yule, A. J., Large-scale structure in the mixing layer of a round jet. J. Fluid Mech. 89, 413-432, 1978.

4. Browand, F. K. and Laufer, J., The role of large scale structures in the initial development of circular jets, Proc. 4th Biennial Symp. Turbulence in Liquids, Univ. Missouri-Rolla, pp 333-344, Science Press, 1975.

5. Winant, C. D. and Browand, F. K., Vortex pairing: the mechanism of turbulent mixing-layer growth at moderate Reynolds number. J. Fluid Mech. 63, 237-255, 1974.

6. Tyndall, J., On the action of sonarous vibrations on gaseous and liquid jets, Phil. Mag., 4, 33, 375-391, 1867.

7. Grant, A. J., Jones, J. M. and Rosenfeld, J. L. J., Orderly structure and unmixedness in lifted jet diffusion flames, Proc. 1st Comb. Inst. European Symposium, pp 548-552, Academic Press, 1973.

8. Ballantyne, A. and Bray, K. N. C., Investigations into the structure of jet diffusion flames, 16th Symp. (Int.) on Combustion, Combustion Institute, pp 777-785, 1977.

9. Kent, J. H. and Bilger, R. W., Measurements in turbulent jet diffusion flames, Charles Kolling Res. Lab., Tech. Note F-41, Dept. Mech. Eng., Univ. of Sydney, 1972.

10. Yule, A. J., Taylor, D. S. and Chigier, N. A., Thermocouple signal processing and on-line digital compensation, AIAA, J. Energy, 2, 223-231, 1978.

11. Lockwood, F. C. and Odidi, A. O. O., Measurement of mean and fluctuating temperature and of ion concentration in round free jet turbulent diffusion and premixed flames, 15th Symp. (Int.) on Combustion, The Combustion Institute, 561-571, 1975.

12. Clements, R. M. and Smy, P. R., Electrostatic-probe studies in a flame plasma, J. of Appl. Physics, 40, 11, Oct. 1969.

13. Kennedy, I. M. and Kent, J. H., Measurements of a conserved scalar in turbulent jet diffusion flames, Charles Koling Research Lab., Tech. Note F-86, Univ. of Sydney, Dept. Mech. Eng., 1978.

14. Davies, P. O. A. L. and Yule, A. J., Coherent structures in turbulence, J. Fluid Mech., 69, 3, 513-537, 1975.

15. Van Atta, C. W., Sampling techniques in turbulence measurements, Annual Review of Fluid Mechanics, 6, pp 75-91, Annual Reviews Inc., Palo Alto, Ca., 1974.

16. Laufer, J., New trends in experimental turbulence research, Annual Review of Fluid Mechanics, 7, pp 307-326, Annual Reviews Inc., Palo Alto, Ca., 1975.

17. Yule, A. J., Phase scrambling effects and turbulence data analysis, 2nd Symposium on Turbulent Shear Flow, Imp. Col., London, July 1979.

18. Spalding, D. B., The theory of turbulent reacting flows - A Review, Paper 79-0213, AIAA 17th Aerospace Sciences Meeting, New Orleans, January 1979.

19. Michalke, A., Vortex formation in a free boundary layer according to stability theory, J. Fluid Mech., 22, 2, 371-383, 1965.

20. Bradshaw, P., The effect of initial conditions on the development of a free shear layer, J. Fluid Mech., 26, 225-236, 1966.

TABLE 1

Jet Flame I Parameters	
Primary (diluting) air flow rate	120 l/min
Primary propane flow rate	44 l/min
Equivalence ratio	10.4
U_J, primary jet velocity	6.4 m/s
U_S, secondary flow velocity	0.74 m/s
Cold Jet I Parameters	
Primary air flow rate	164 l/min
Primary propane flow rate	0
U_J	6.4 m/s
U_S	0.74 m/s
δ_J, Nozzle boundary layer (shear) thickness	2.36 mm
Nozzle Geometry	
D, nozzle internal diameter	25.4 mm
Secondary flow diameter (square cross-section)	400 mm
Nozzle lip thickness	1 mm
Physical Gas Properties at 20°C and 1 atms.	
Propane (C_3H_8) density	2.13 kg/m^3
Propane viscosity	80.29 μ poise
Air density	1.205 kg/m^3
Air viscosity	183 μ poise

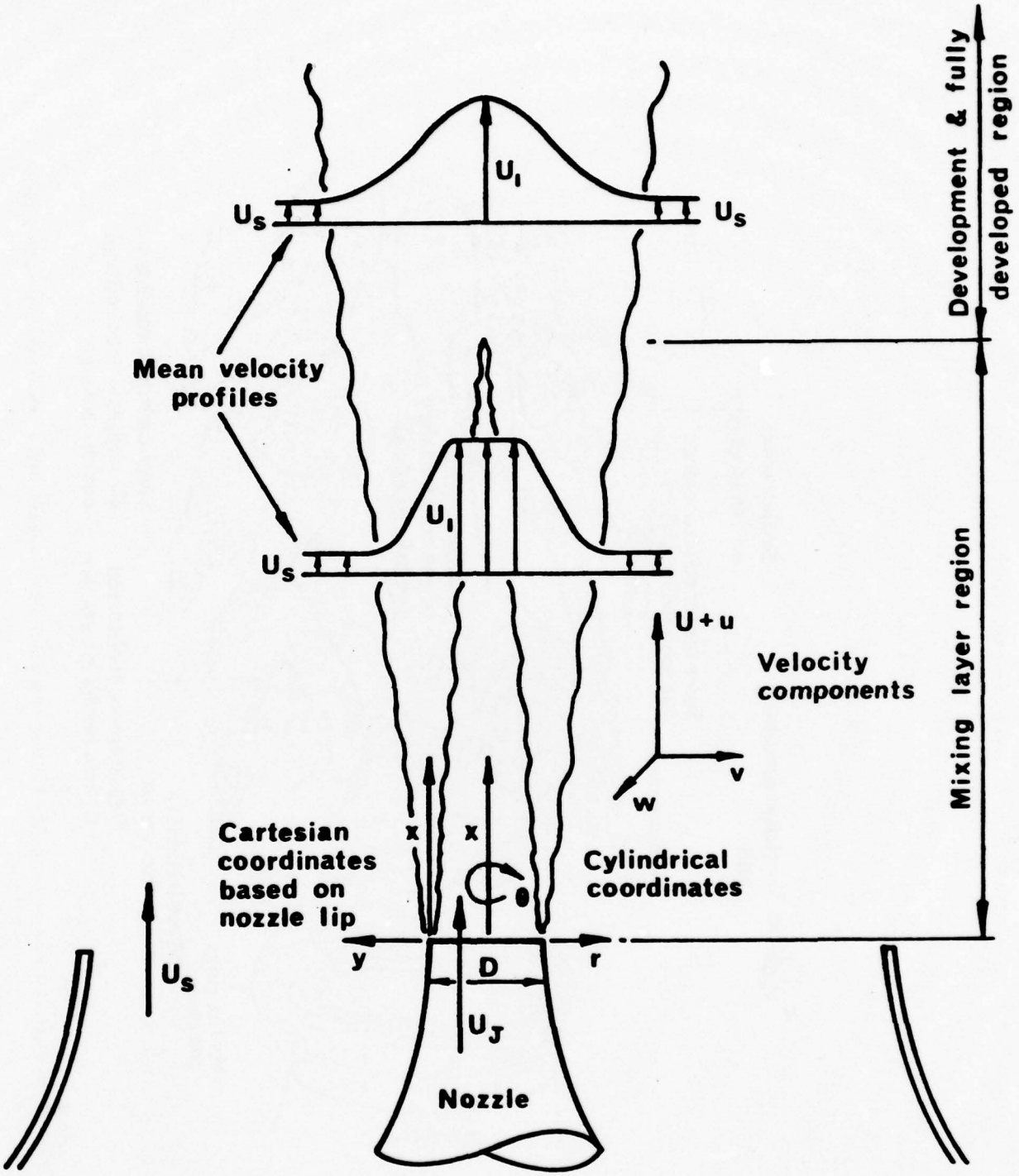

Fig. 1 Notation for axisymmetric jet flame

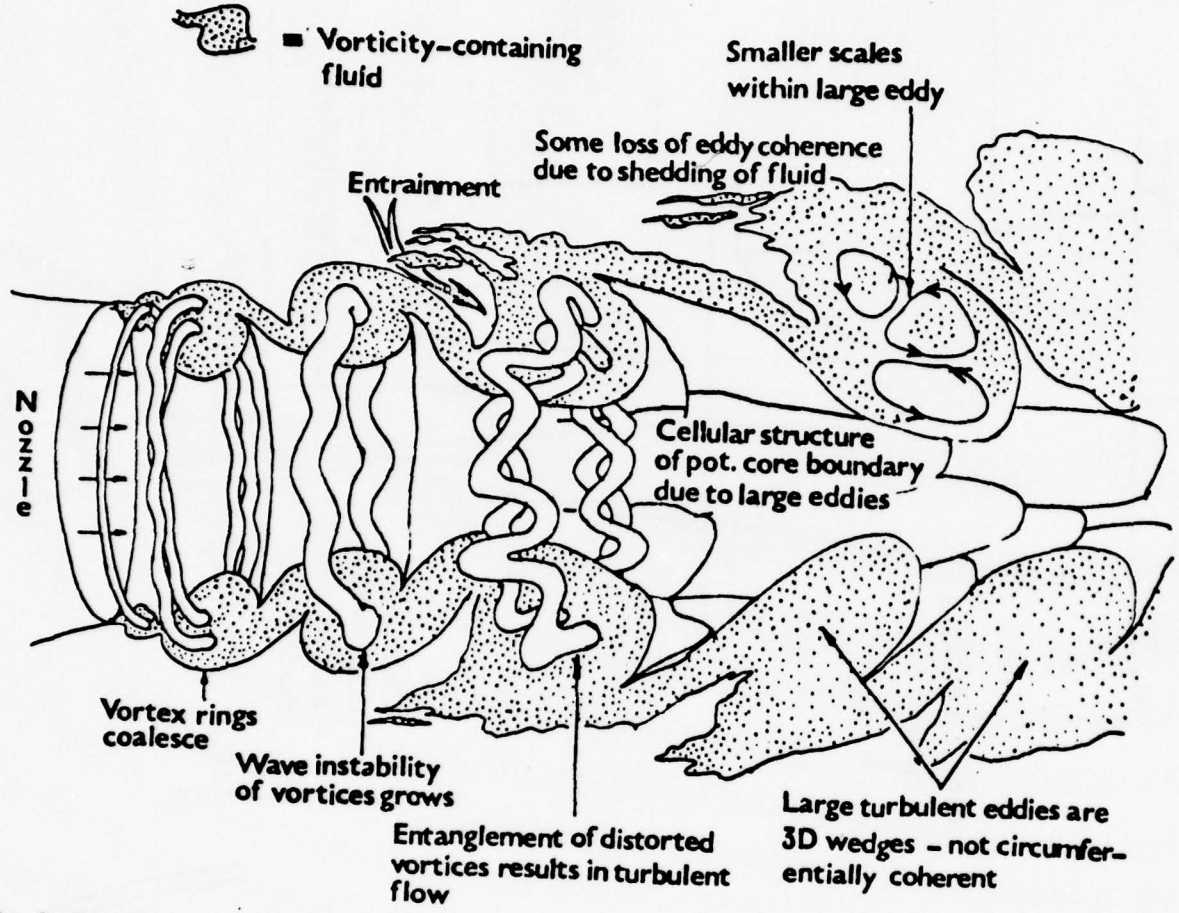

Fig. 2 The physical structure in the mixing layer of a round jet developing from a laminar nozzle boundary layer

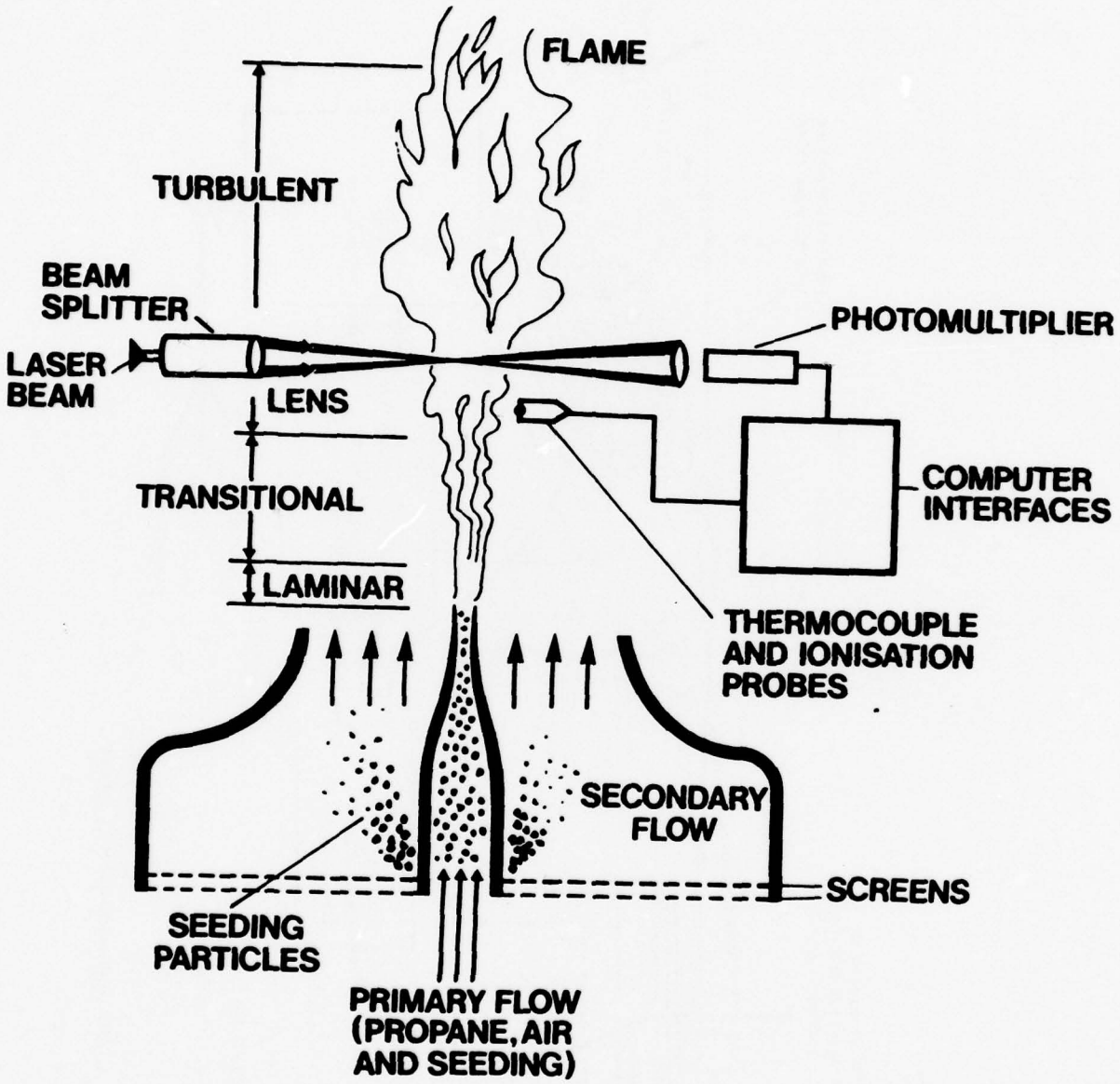

Fig. 3 Apparatus for the investigation of axisymmetric jet flame

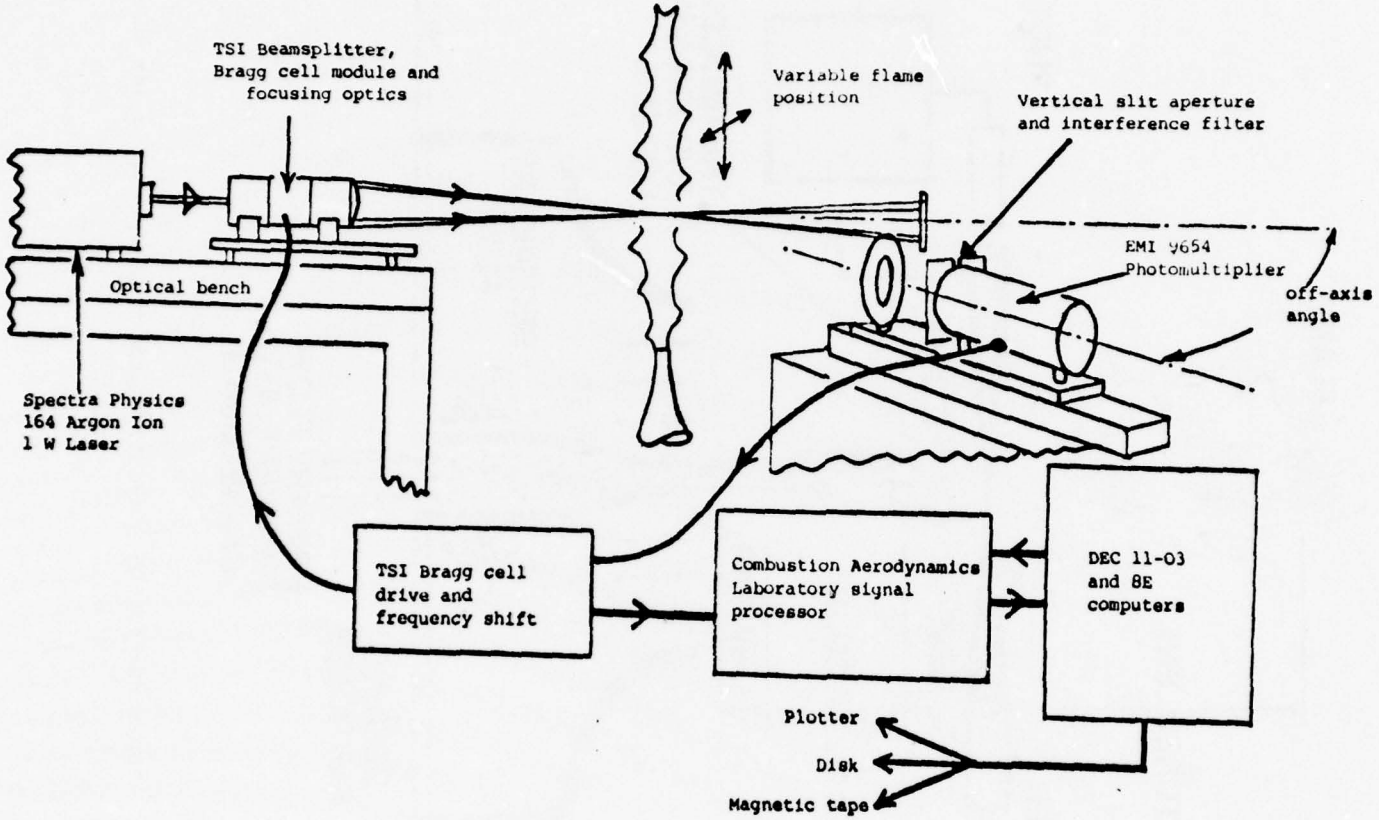

Fig. 4 Laser Doppler Anemometer System

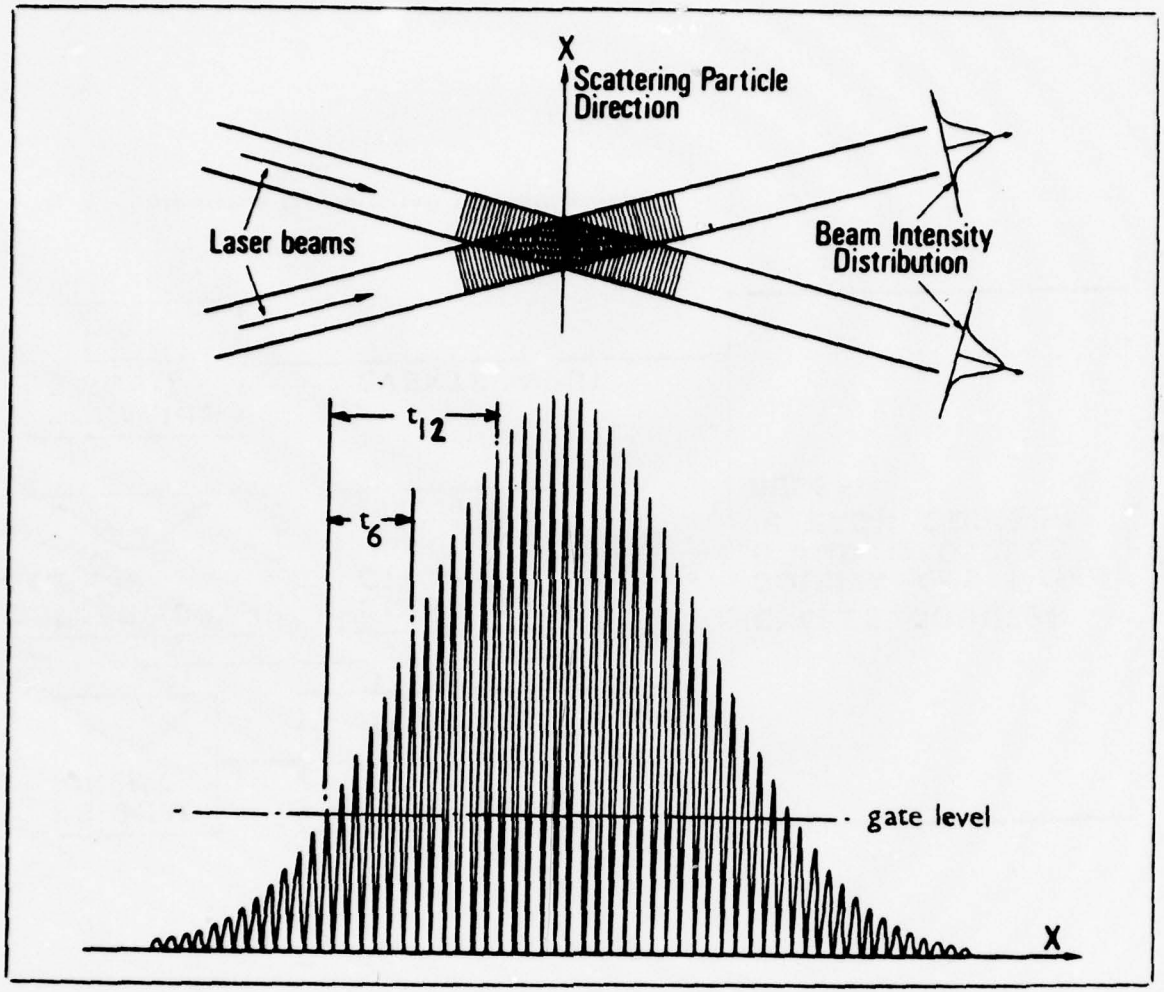

Fig. 5 **Doppler signal – single scattering particle**

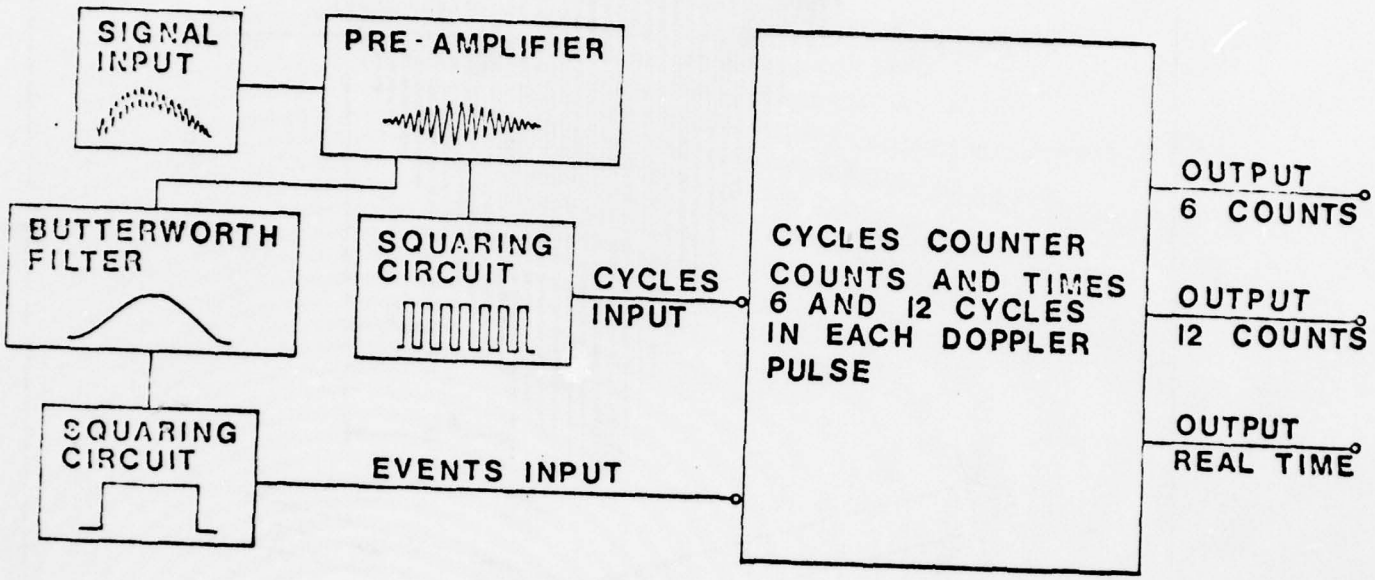

Fig. 6 Logic diagram for two channel LDA counting system

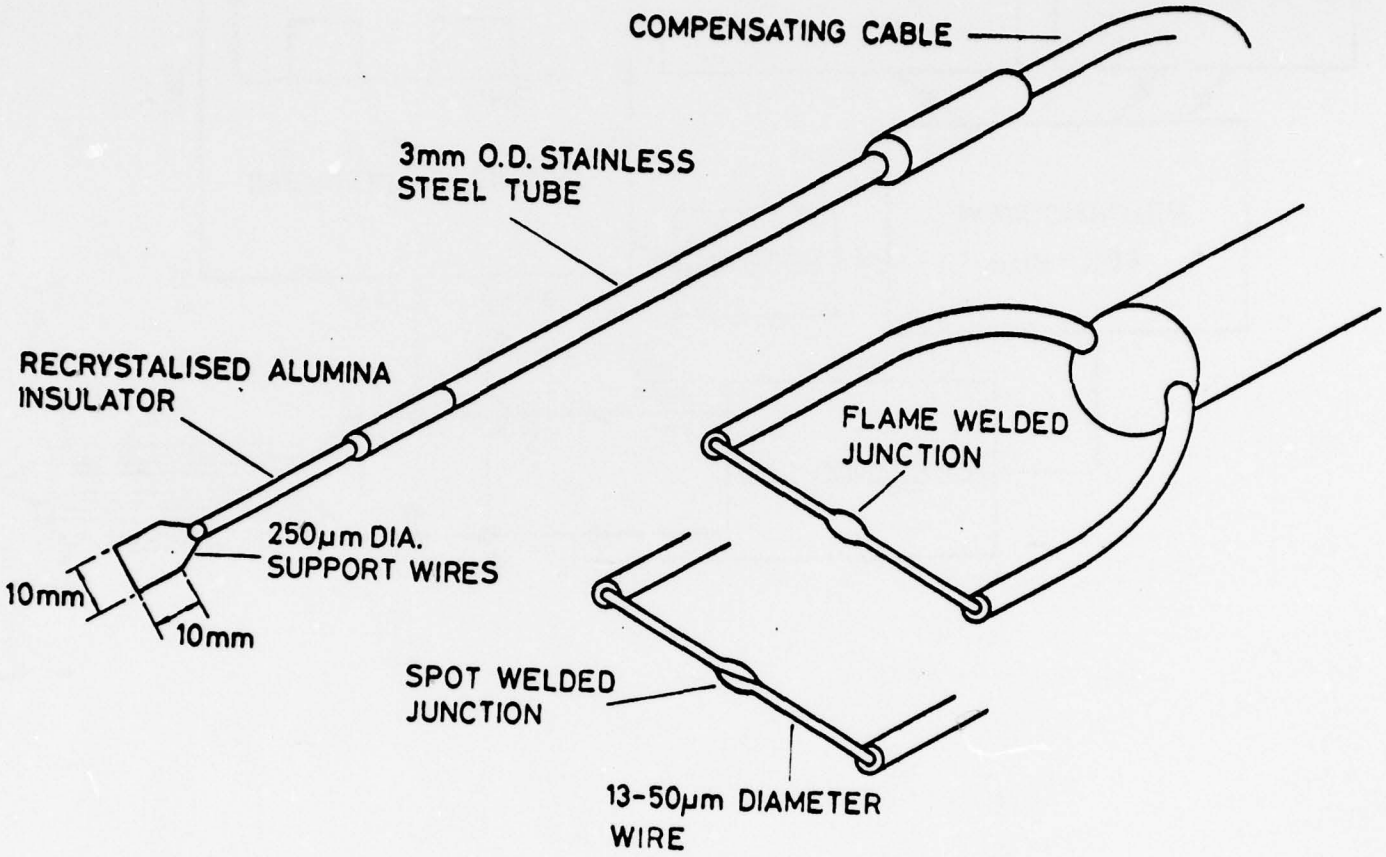

Fig. 7 Designs of fine wire thermocouples

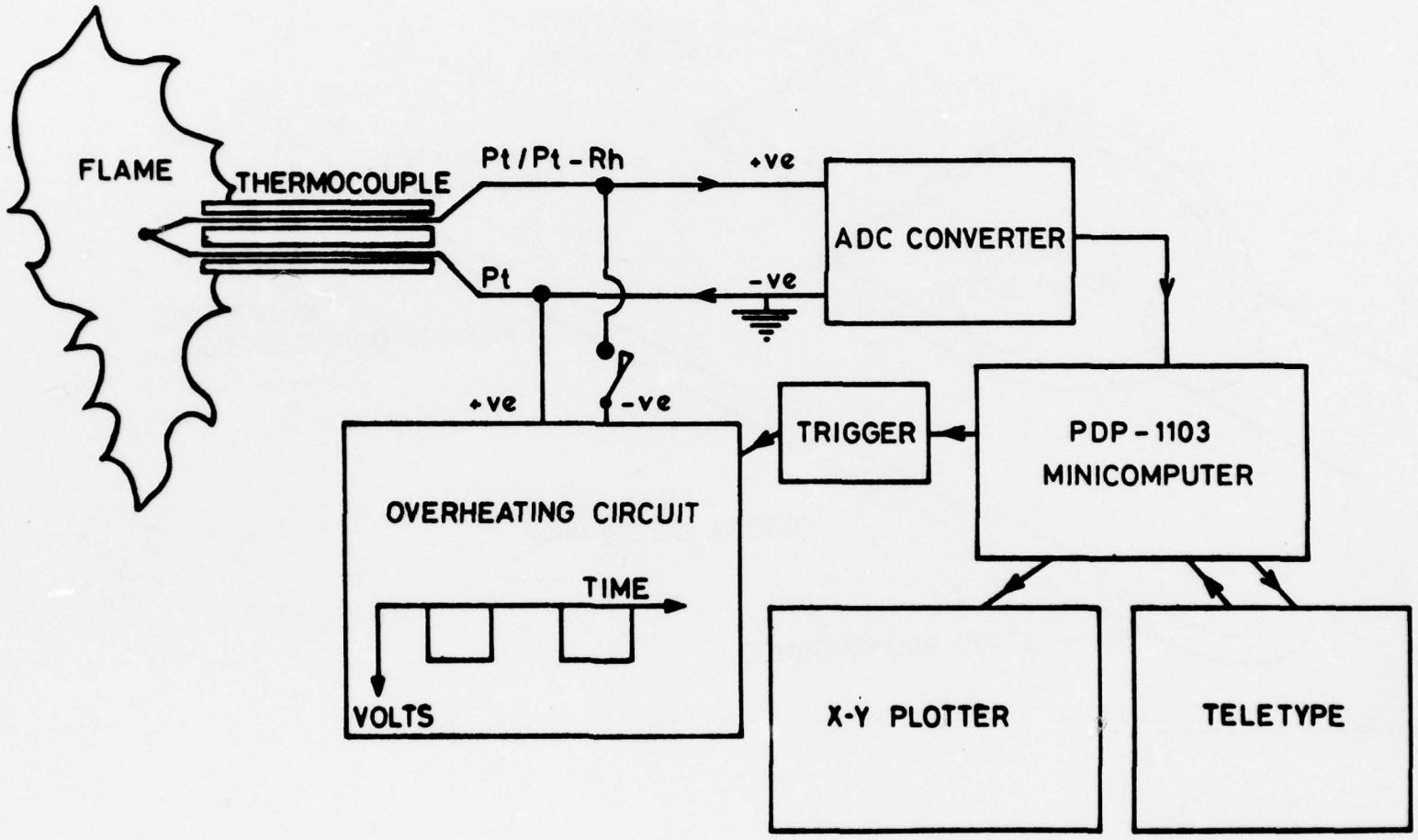

Fig. 8 System for measuremment of thermocouple time constant

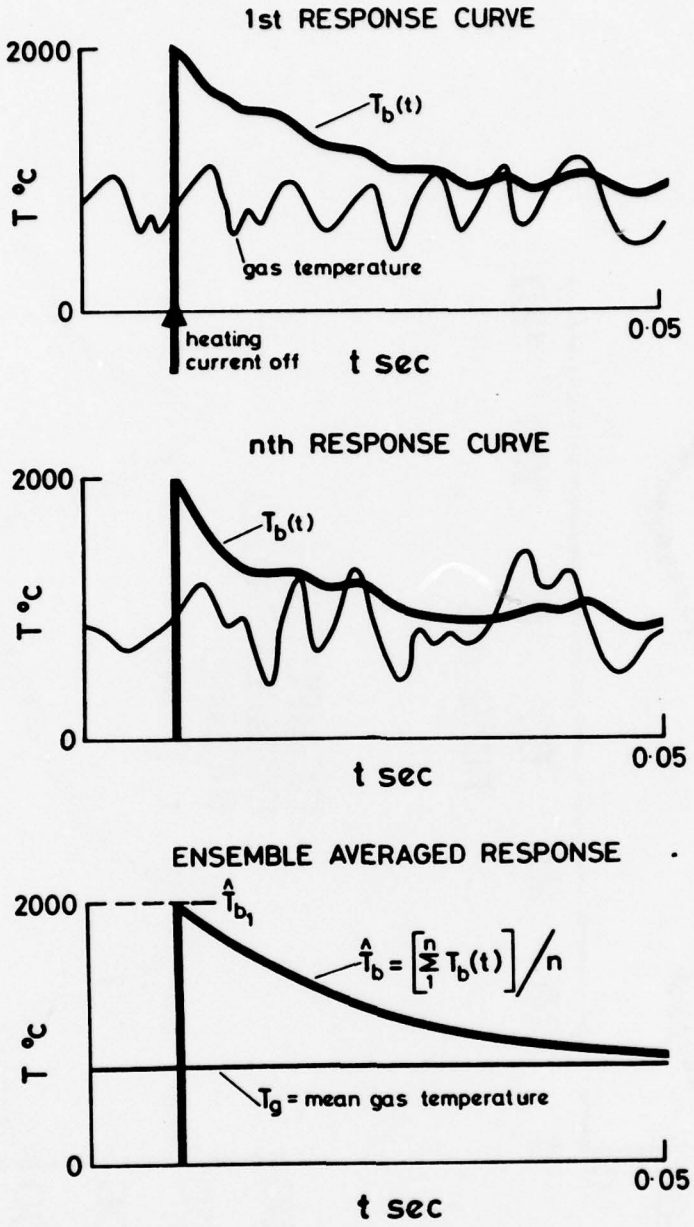

Fig. 9 Ensemble averaging of temperature decay curves for in situ measurement of thermocouple time constant

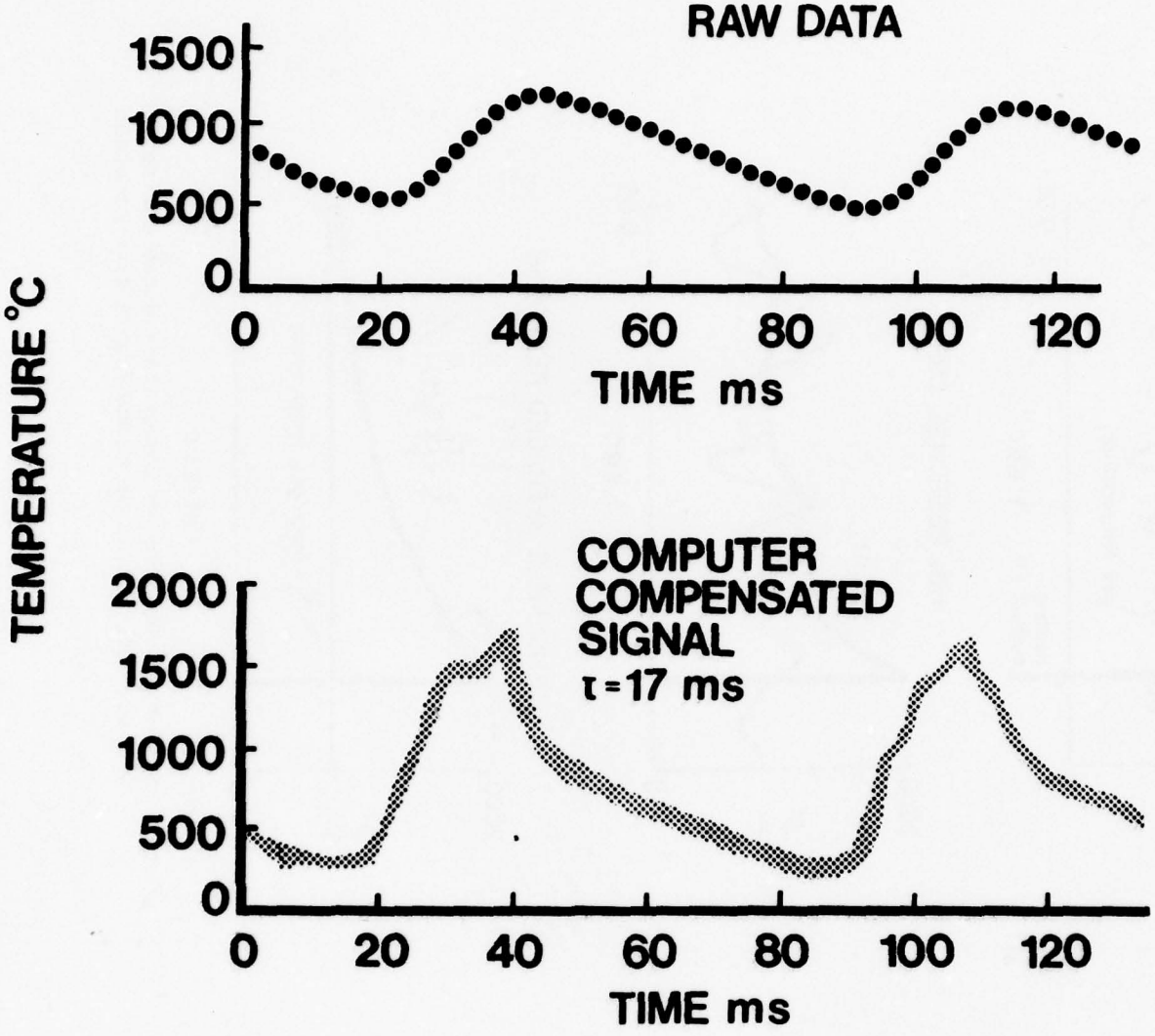

Fig. 10 Temperature time histories before and after compensation

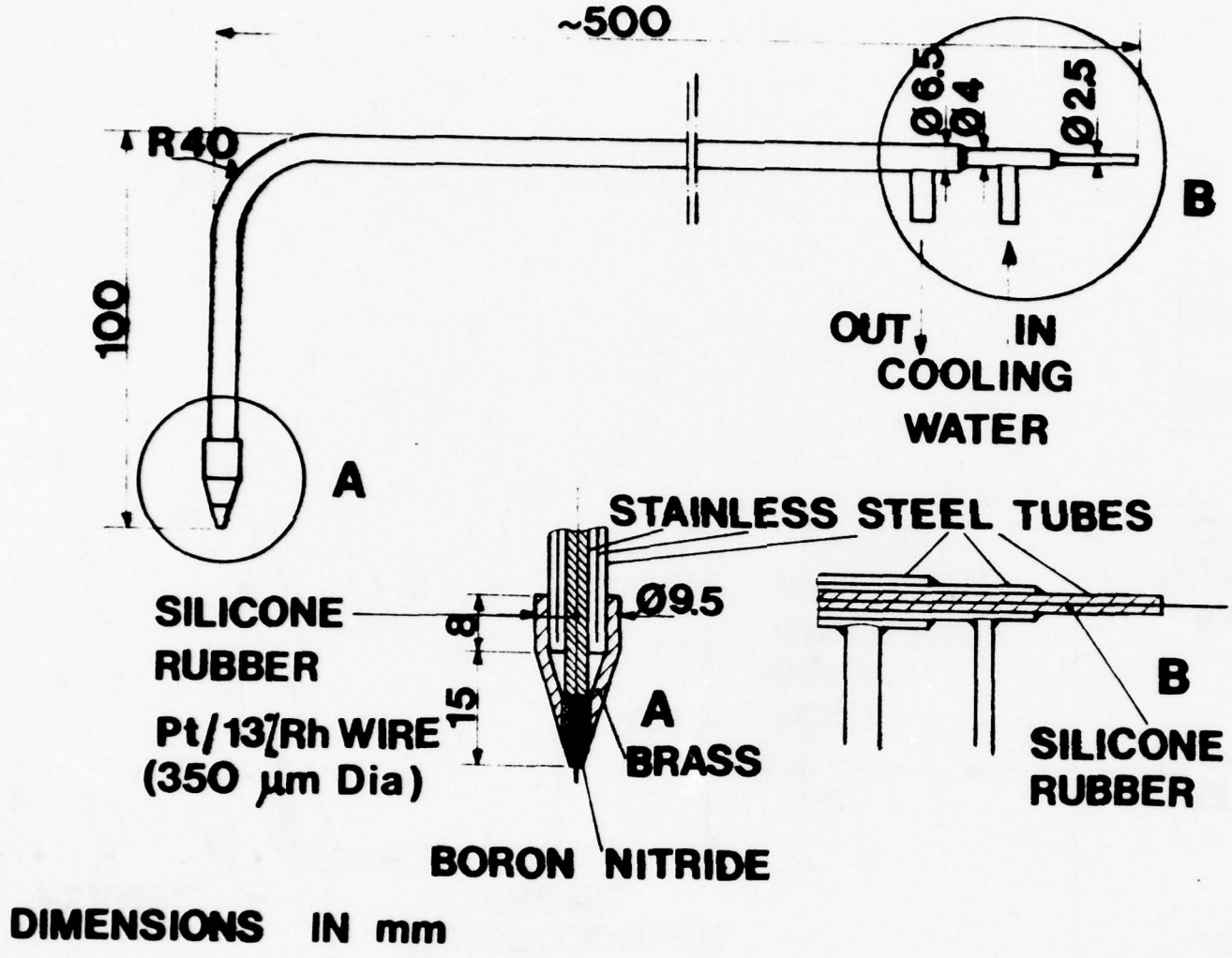

Fig. 11 Ionization probe design

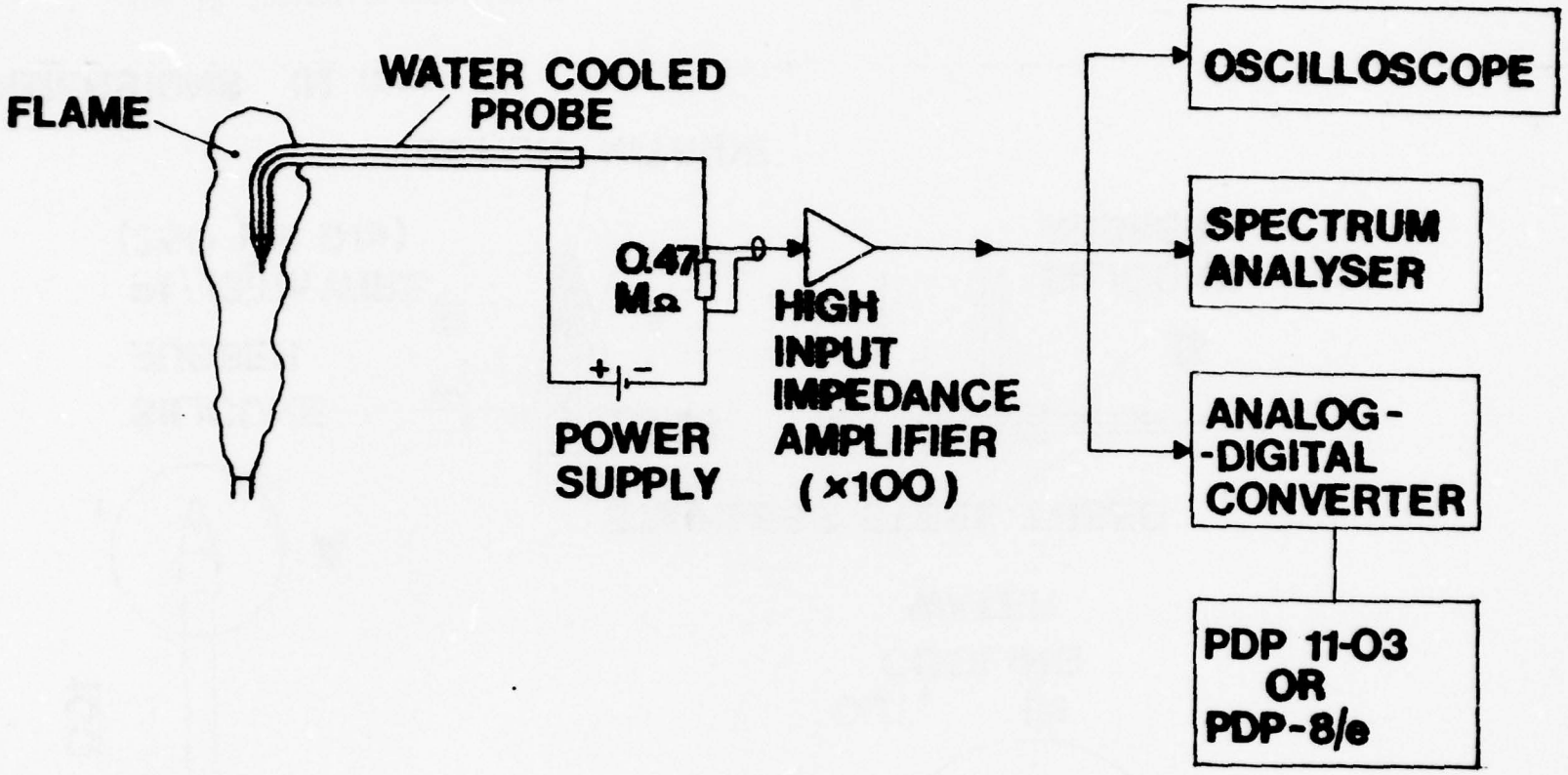

Fig. 12 Ionization probe circuit

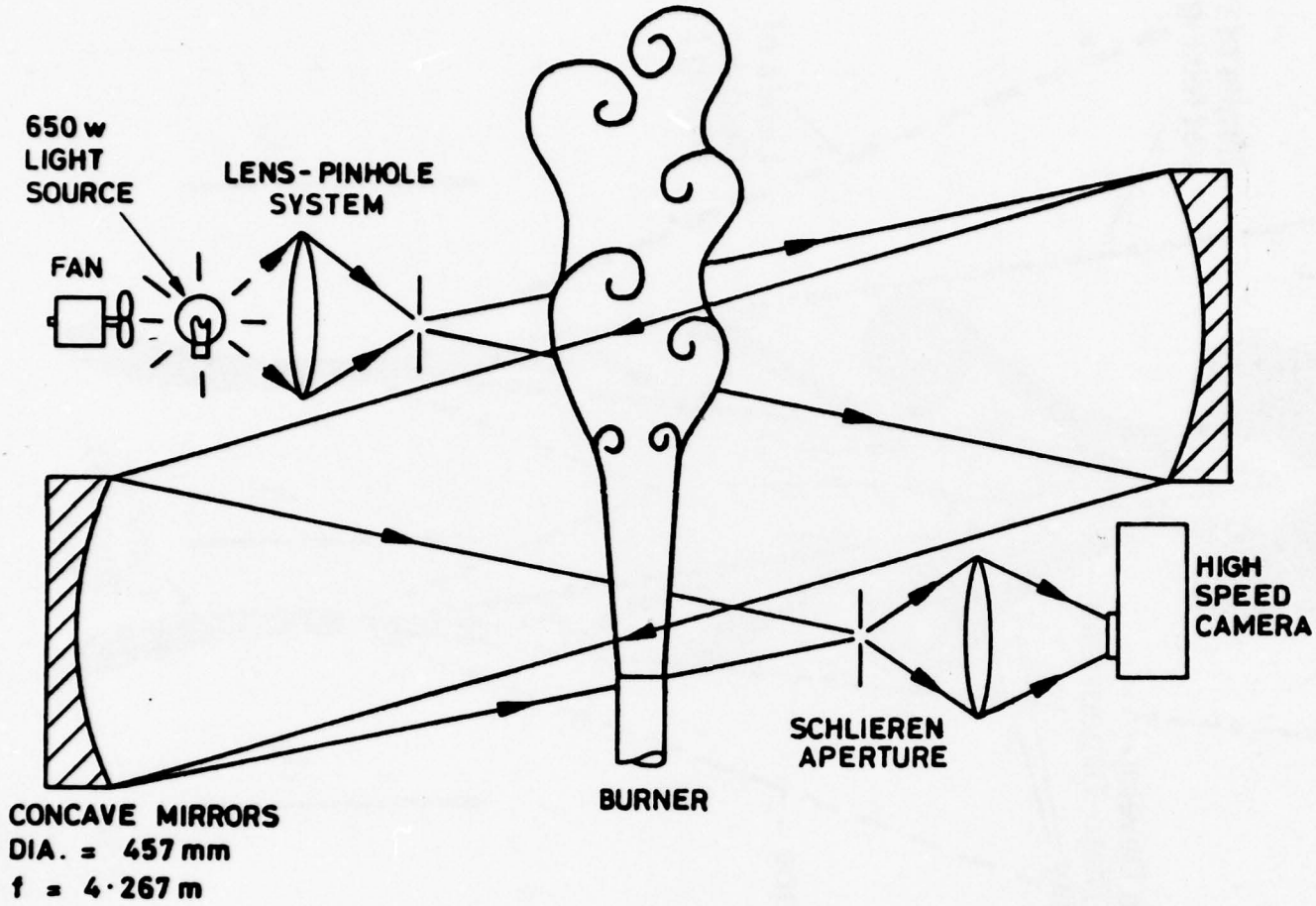

Fig. 13 Colour Schlieren system

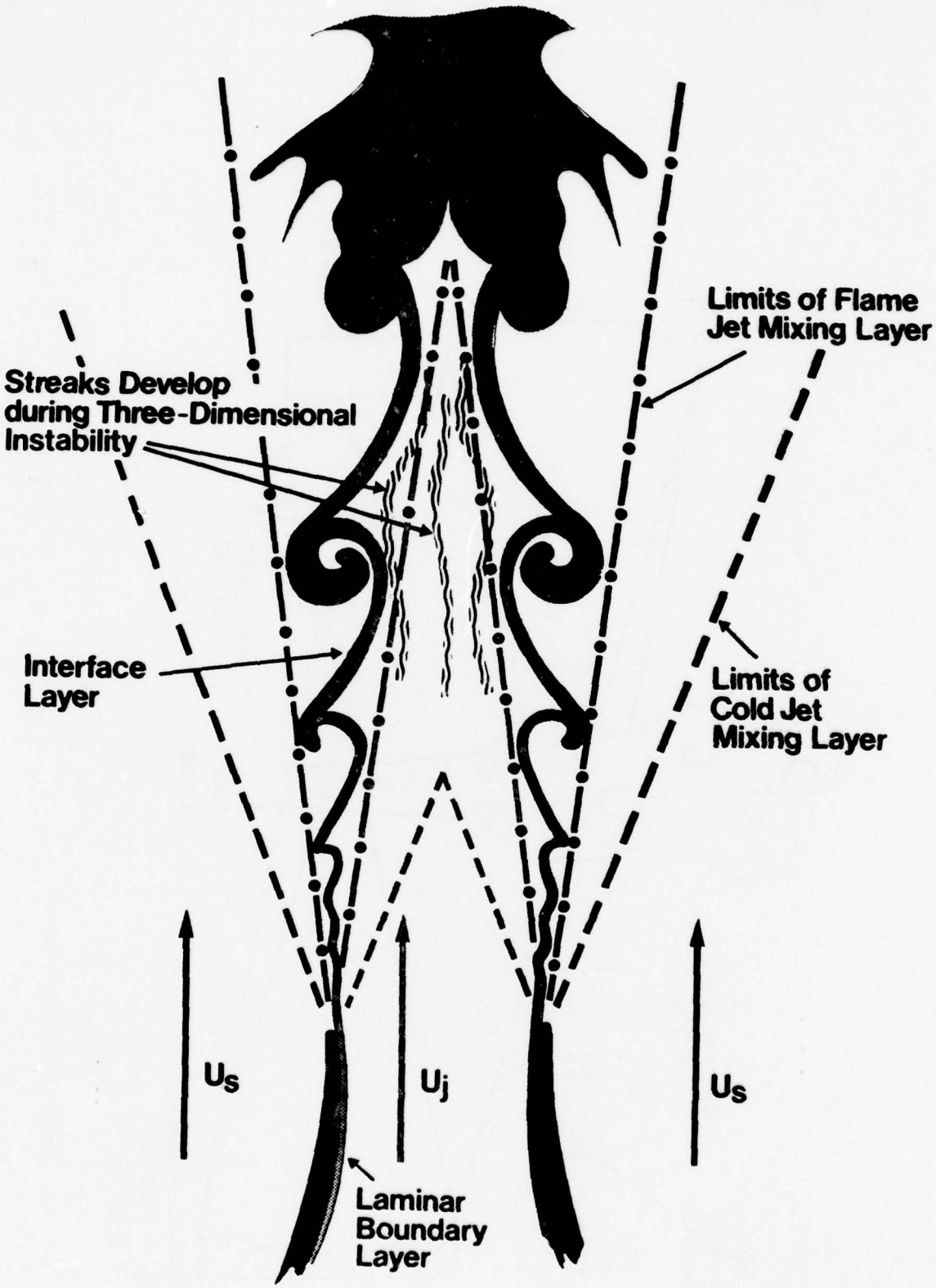

Fig. 14 Schematic view of transitional flame

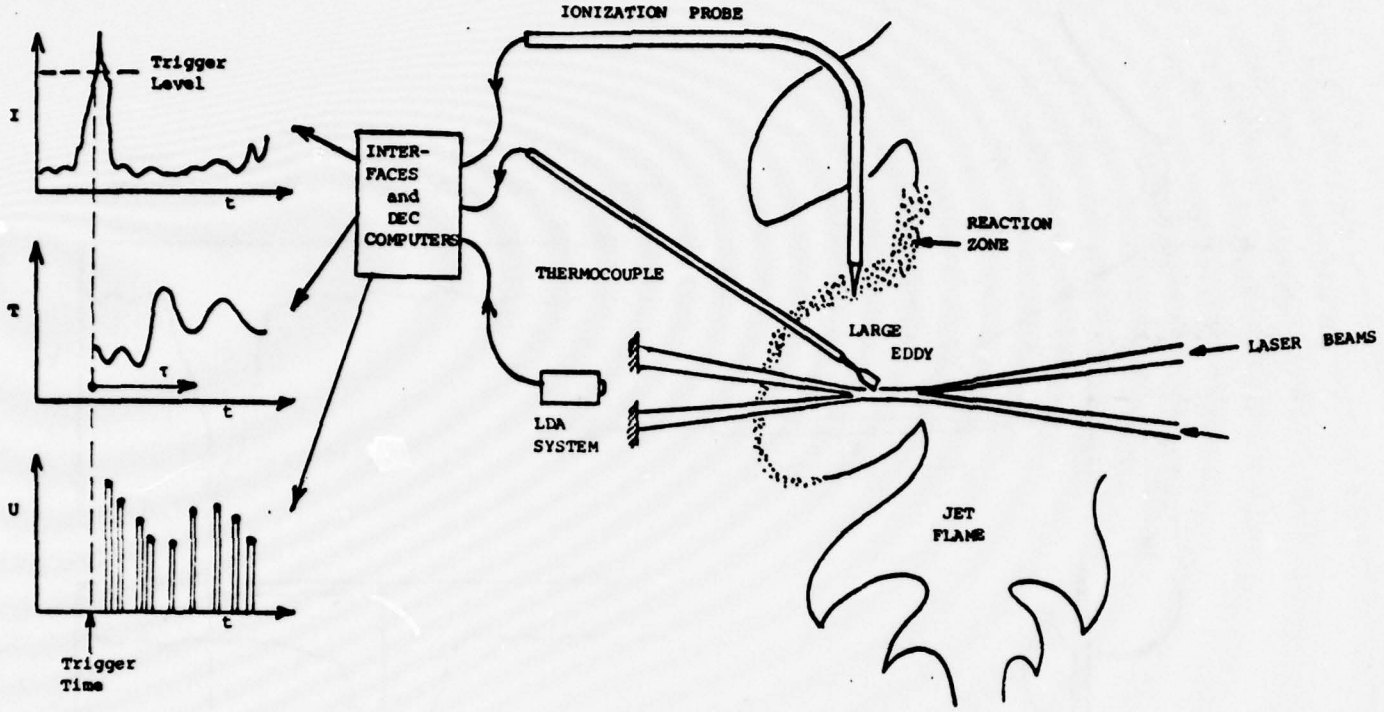

Fig. 15 Conditional Sampling to Measure Local Average Eddy and Reaction Zone Structure

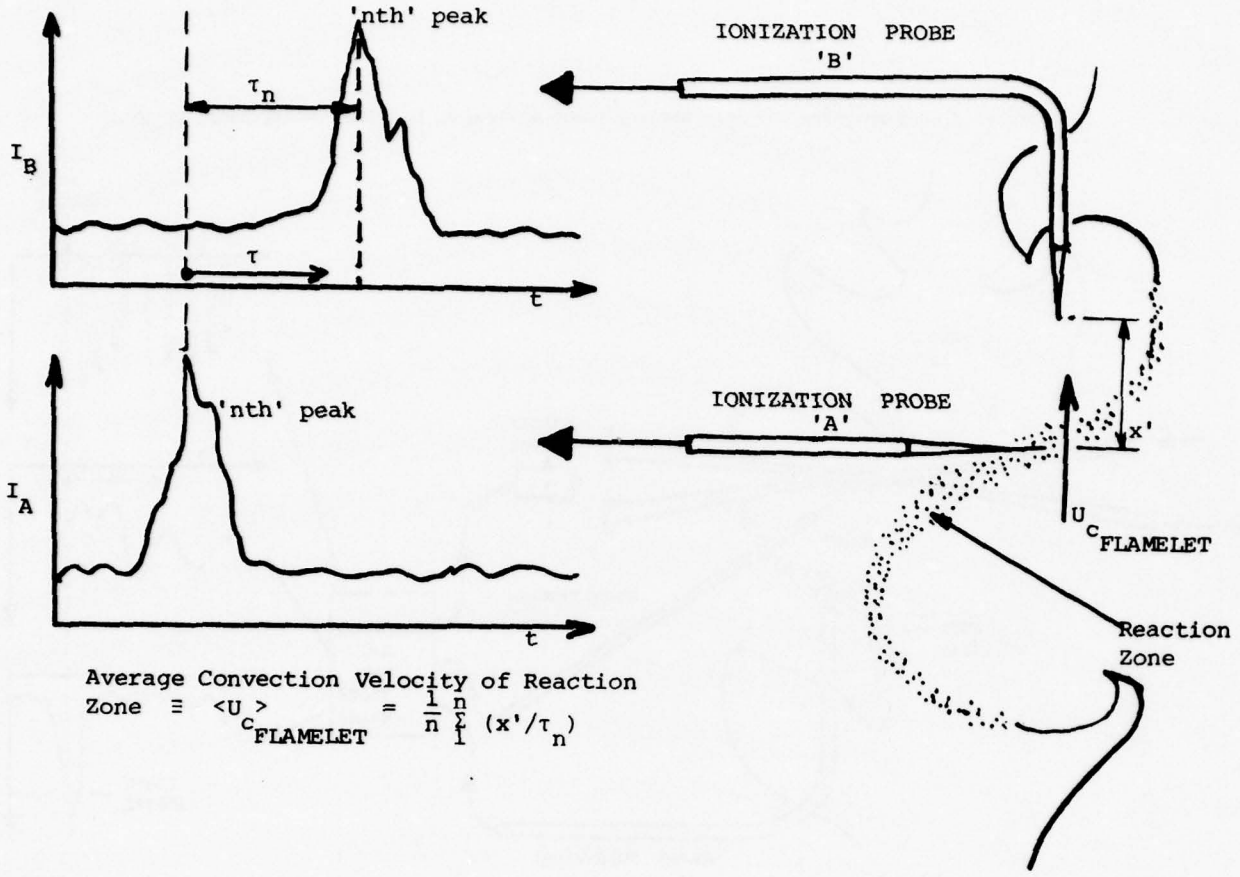

Average Convection Velocity of Reaction Zone $\equiv \langle U_{C_{FLAMELET}} \rangle = \frac{1}{n} \sum_{1}^{n} (x'/\tau_n)$

Fig. 16 Convective Properties of Coherent Structures: Measurement of Reaction Zone Convection using Two Ionization Probes

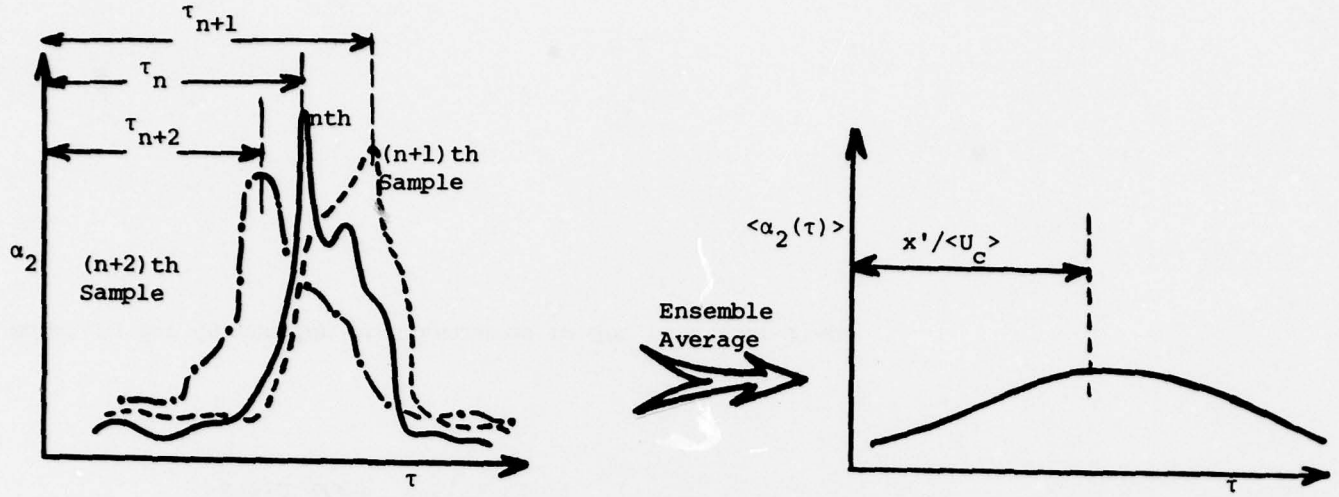

Normal Ensemble Average of Conditionally Sampled Signal

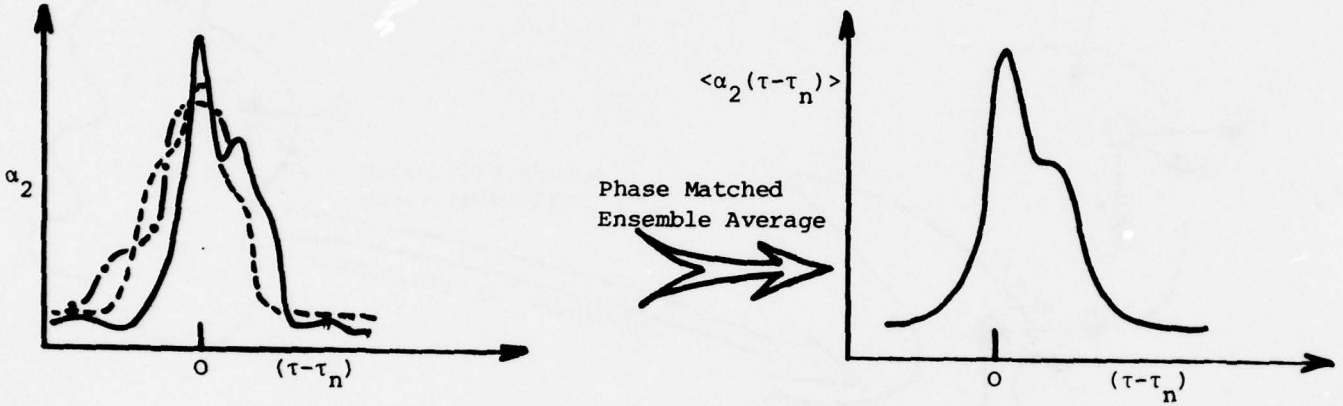

Enhanced Ensemble Averaging by Phase Matching Peaks

Fig. 17 Phase Scrambling Effects on Signal Recovery in Conditional Sampling

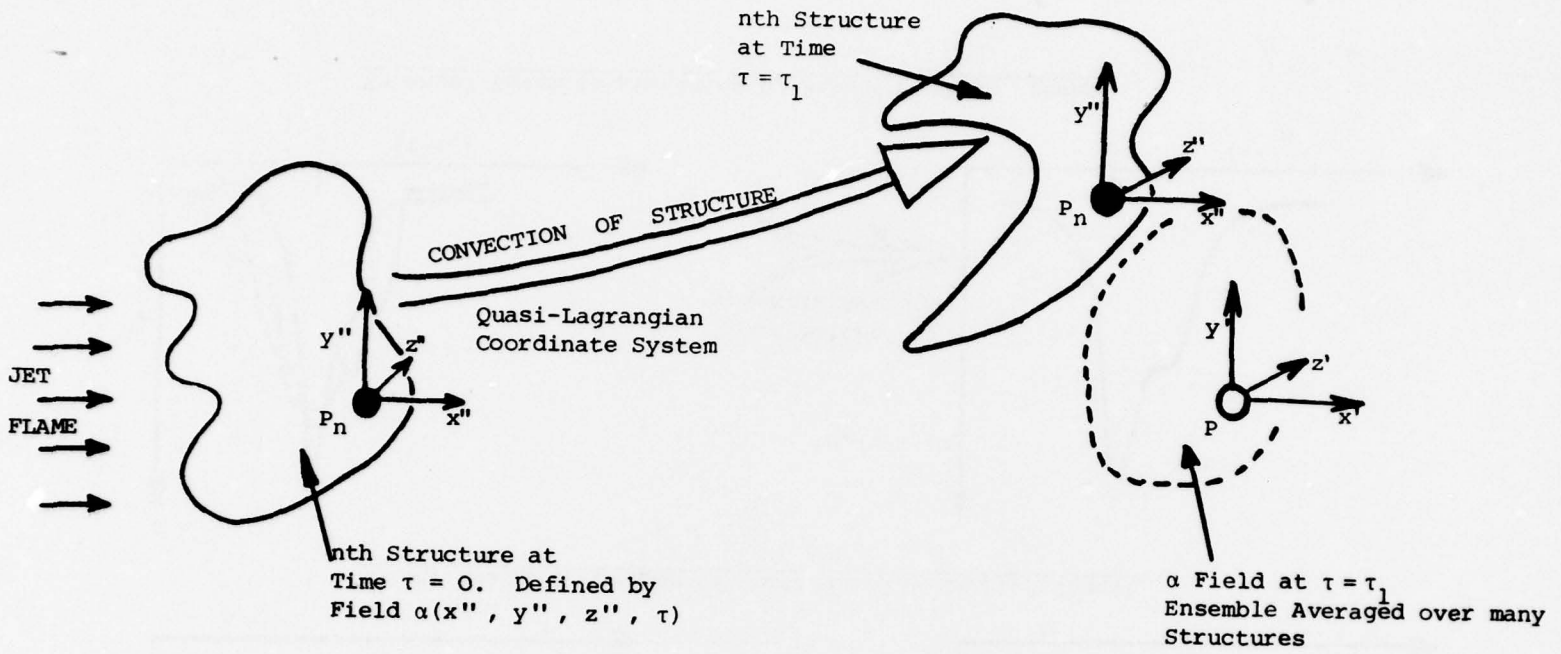

Fig. 18 Notation for Convection of Structures in Jet Diffusion Flame

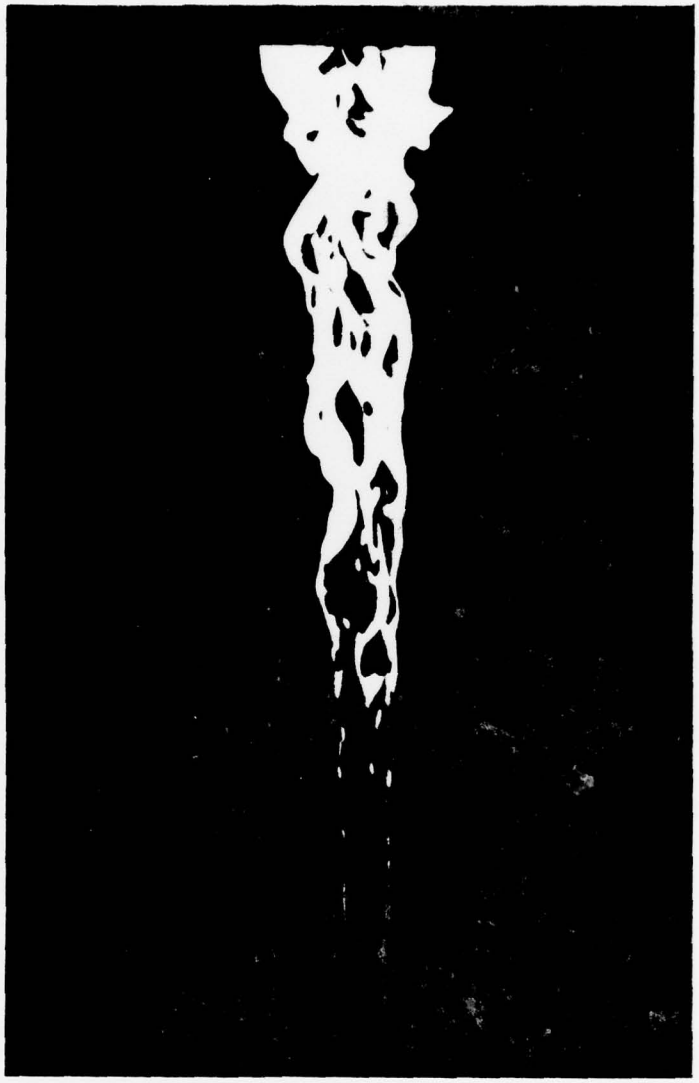

Fig. 19a Photograph of Flame I $0 < x < 24\ D$

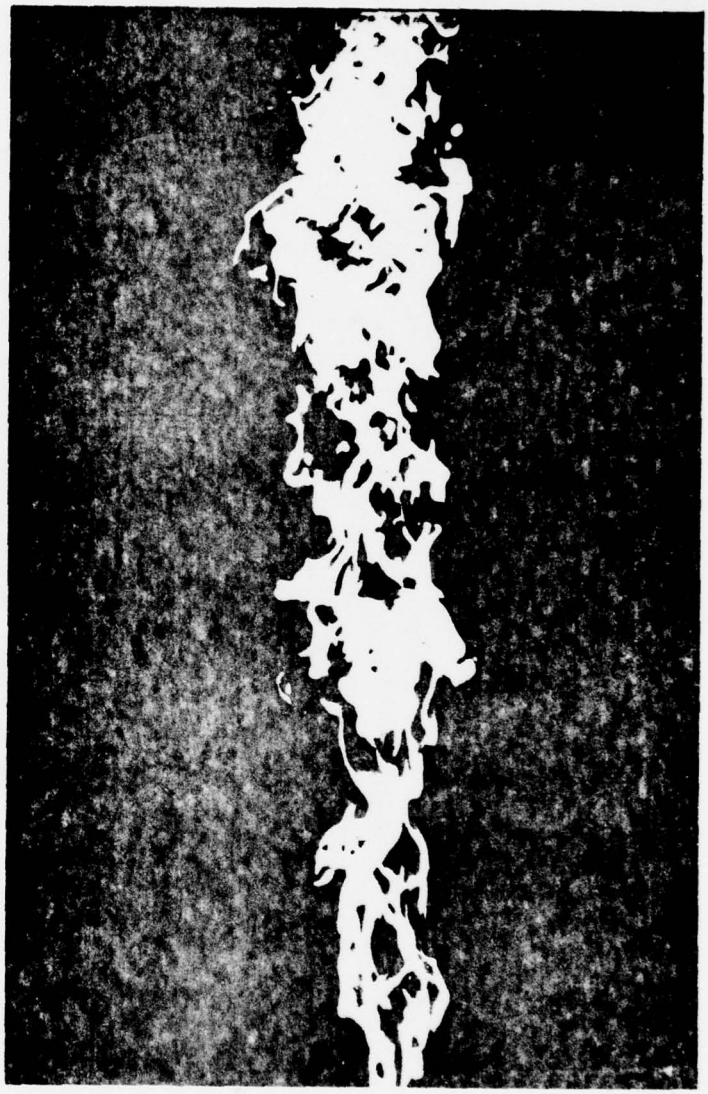

Fig. 19b Photograph of Flame I 24 D < x < 80 D

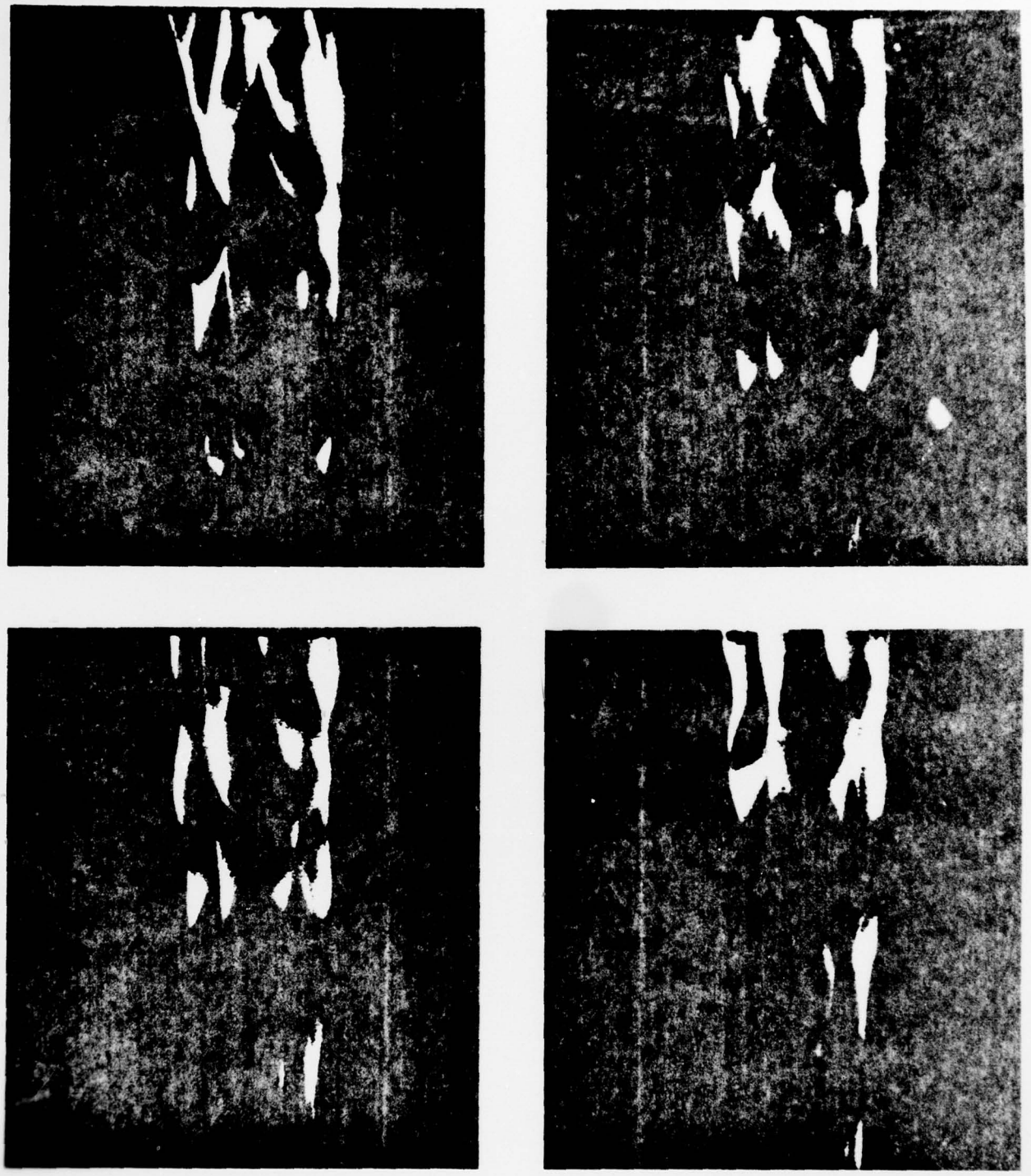

Fig. 20 Single frames from cine film of Flame I, visualization by flame luminosity, interval of 4 ms between frames, 8 D < x < 16 D

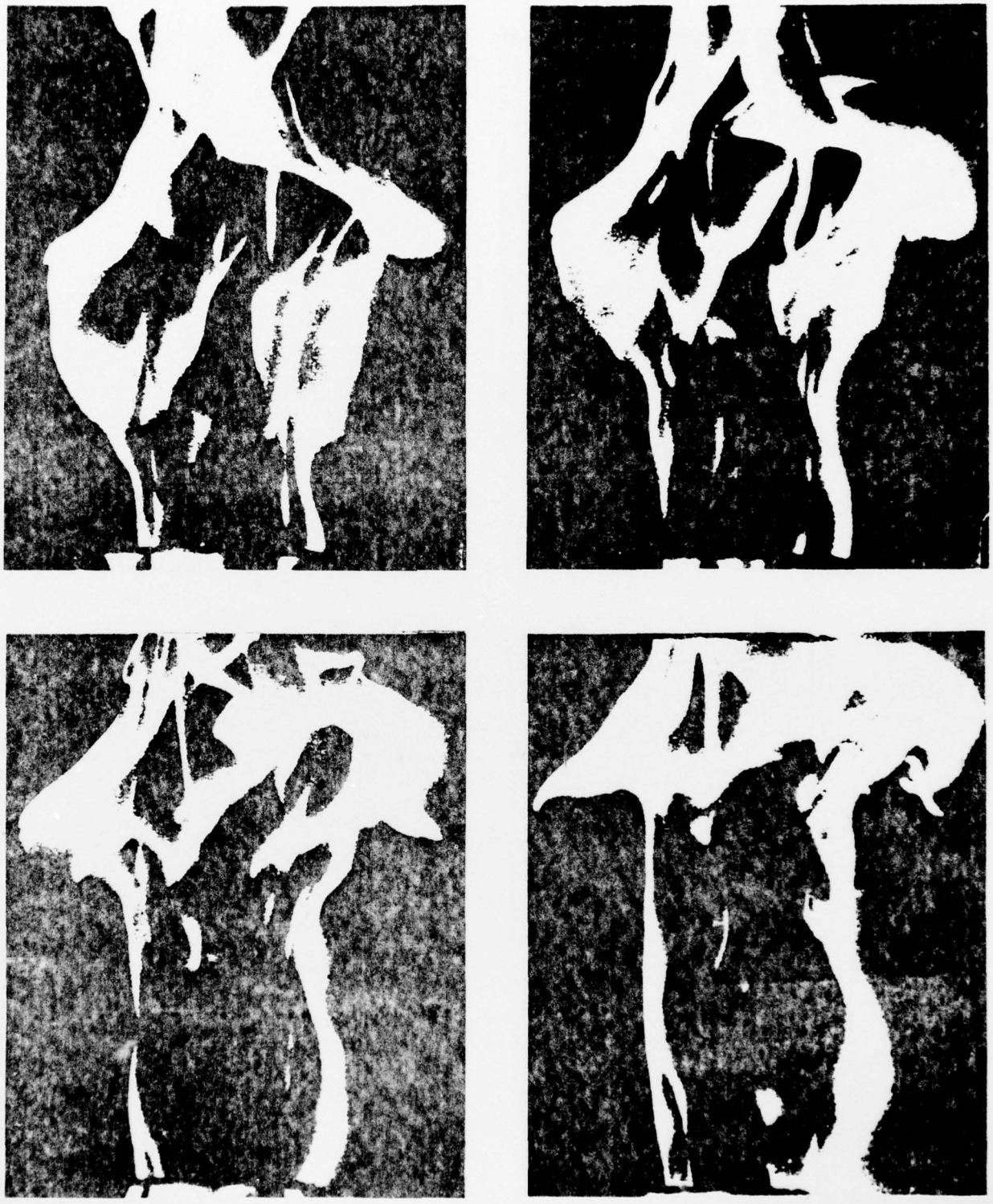

Fig. 21 Sequence of frames at 8 ms intervals, visualization by flame luminosity, 16 D < x < 24 D

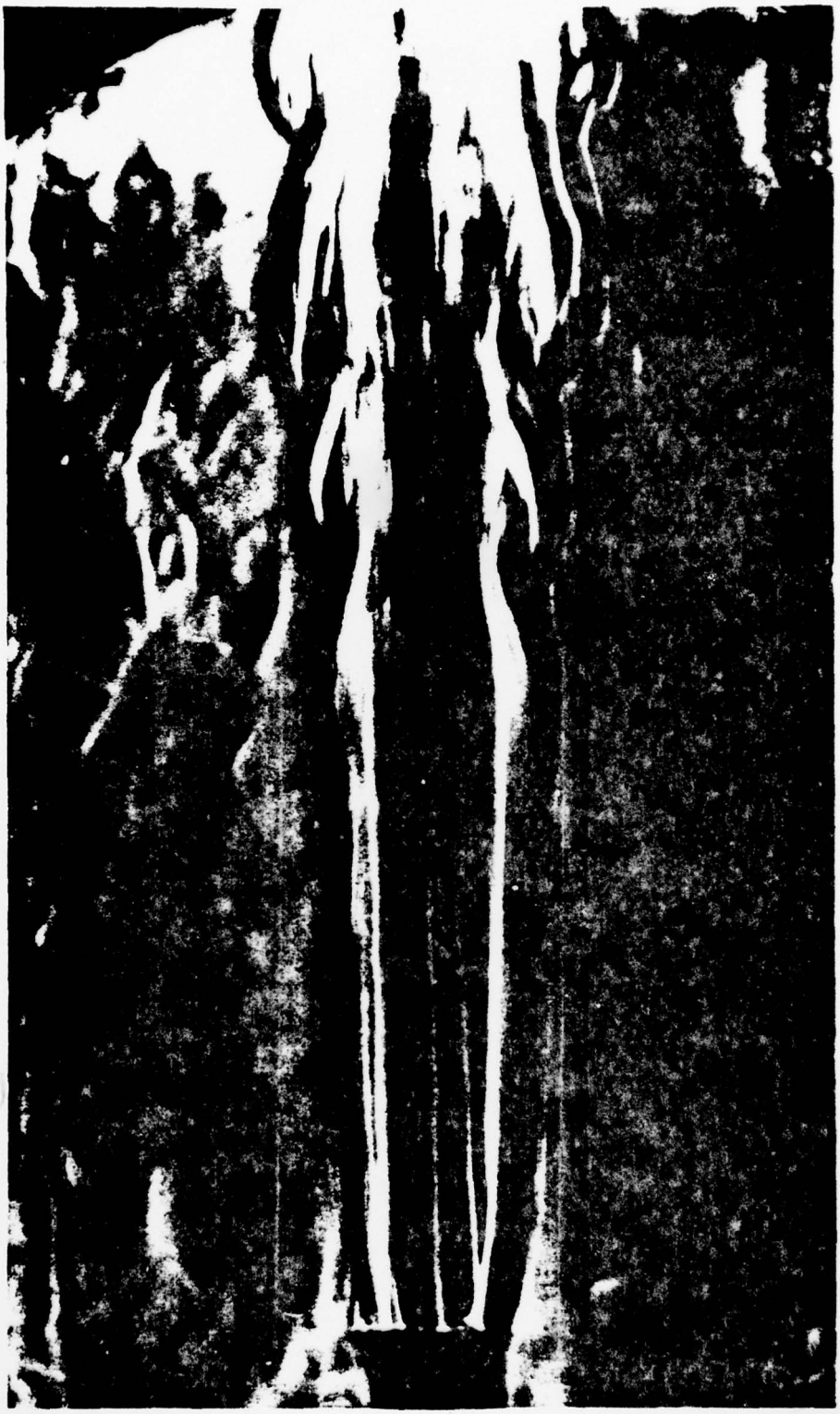

Fig. 22 Schlieren photograph of Flame I, exposure time 1 ms, $0 < x < 10$ D

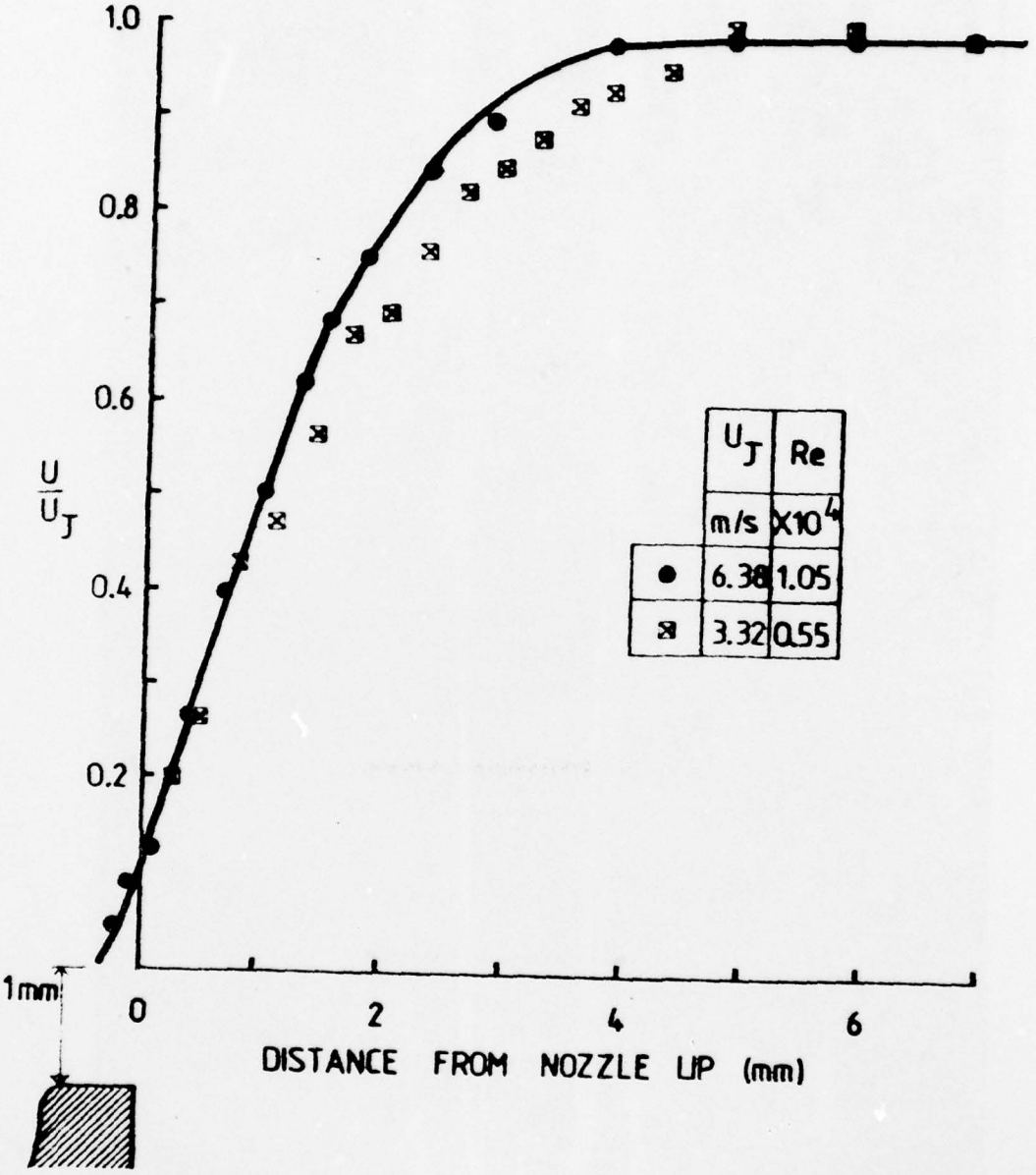

Fig. 23 Velocity distribution near nozzle lip, Cold Jet I, x/D = 0.04; hot wire data for two Reynolds numbers

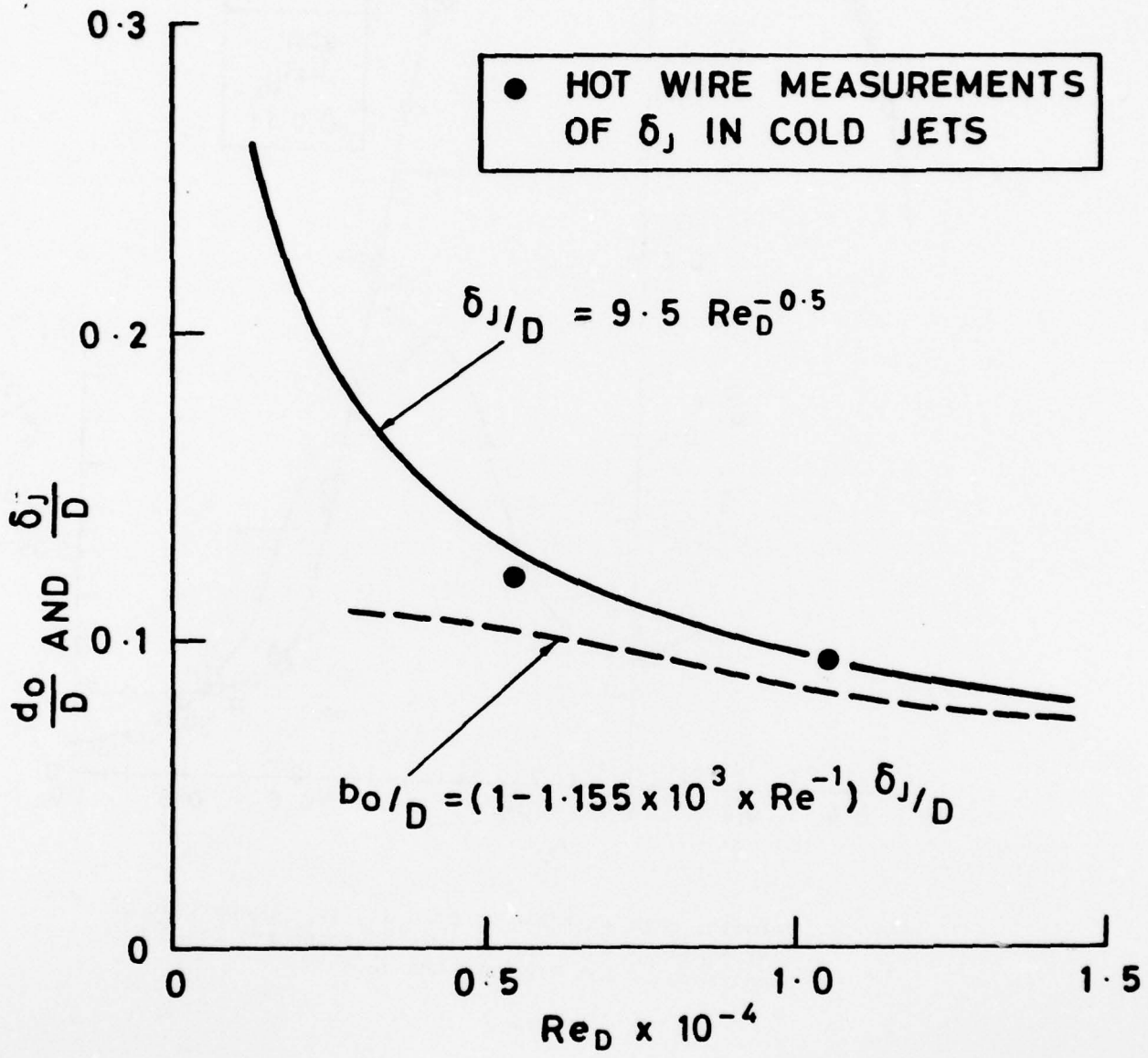

Fig. 24 Nozzle boundary layer thickness versus Reynolds number

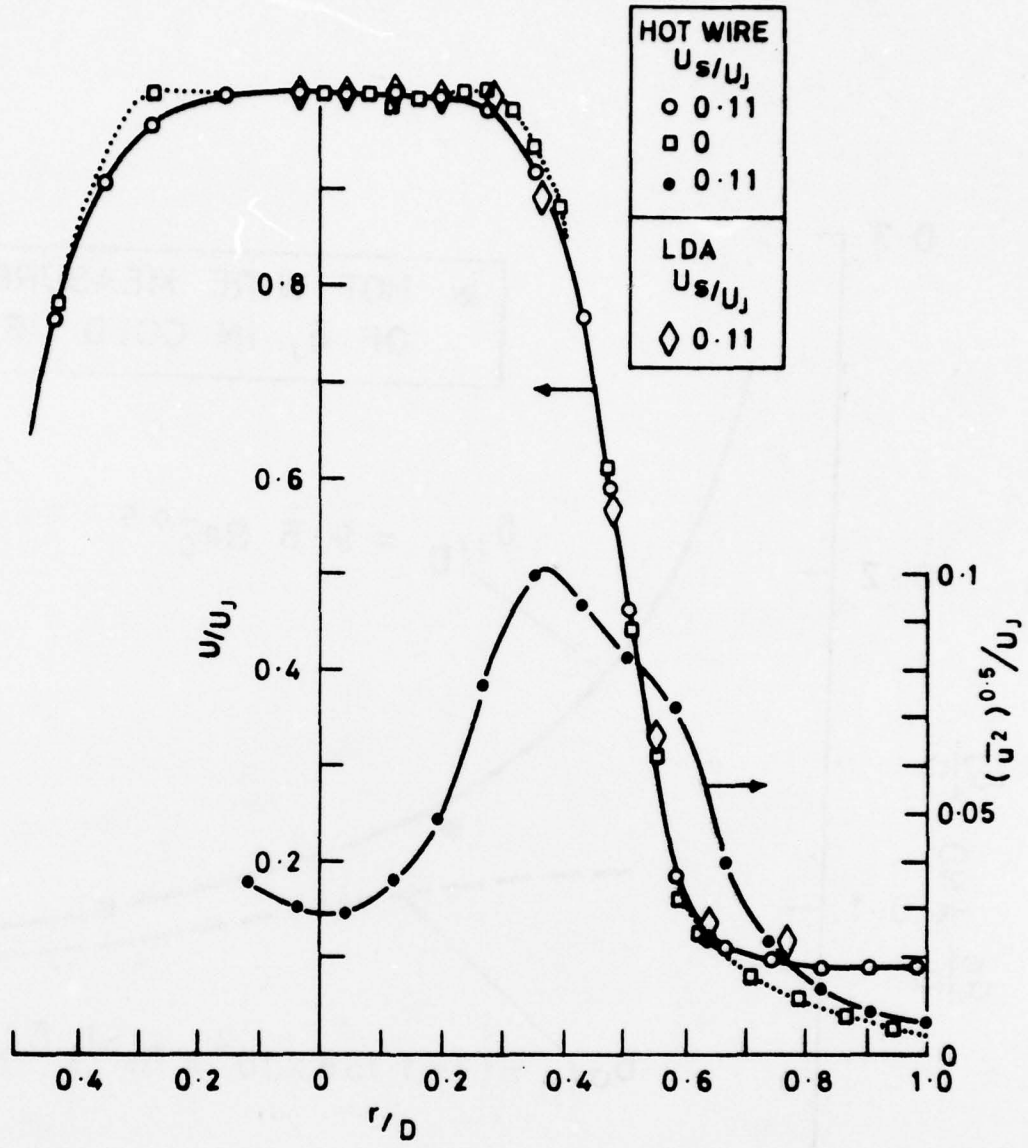

Fig. 25 Velocity data at x/D = 2, Cold Jet I. Comparison of distributions with and without a secondary flow and comparison of hot wire and LDA data

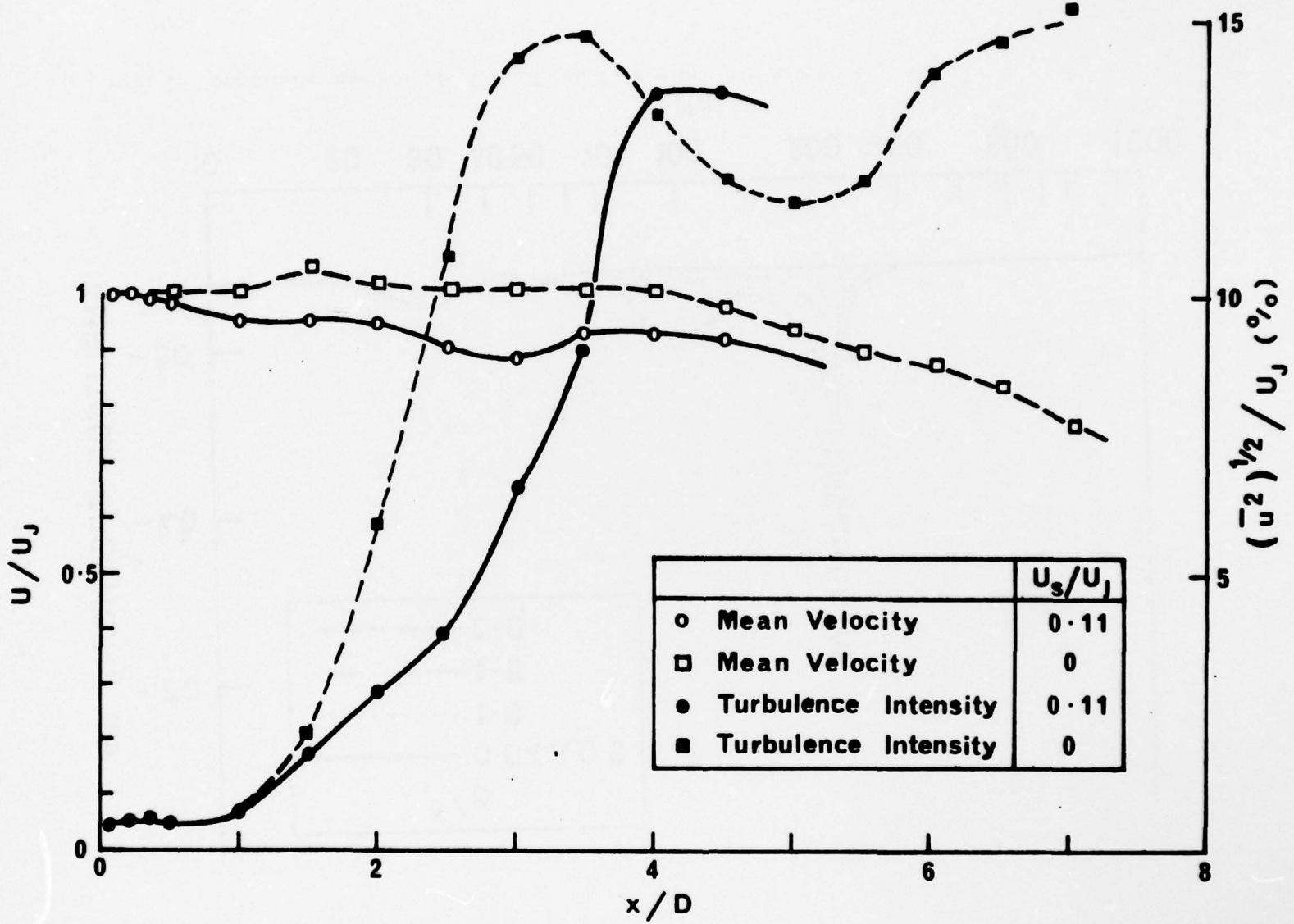

Fig. 26 Centreline distributions of mean velocity and turbulence intensity in Cold Jet I with and without a secondary flow

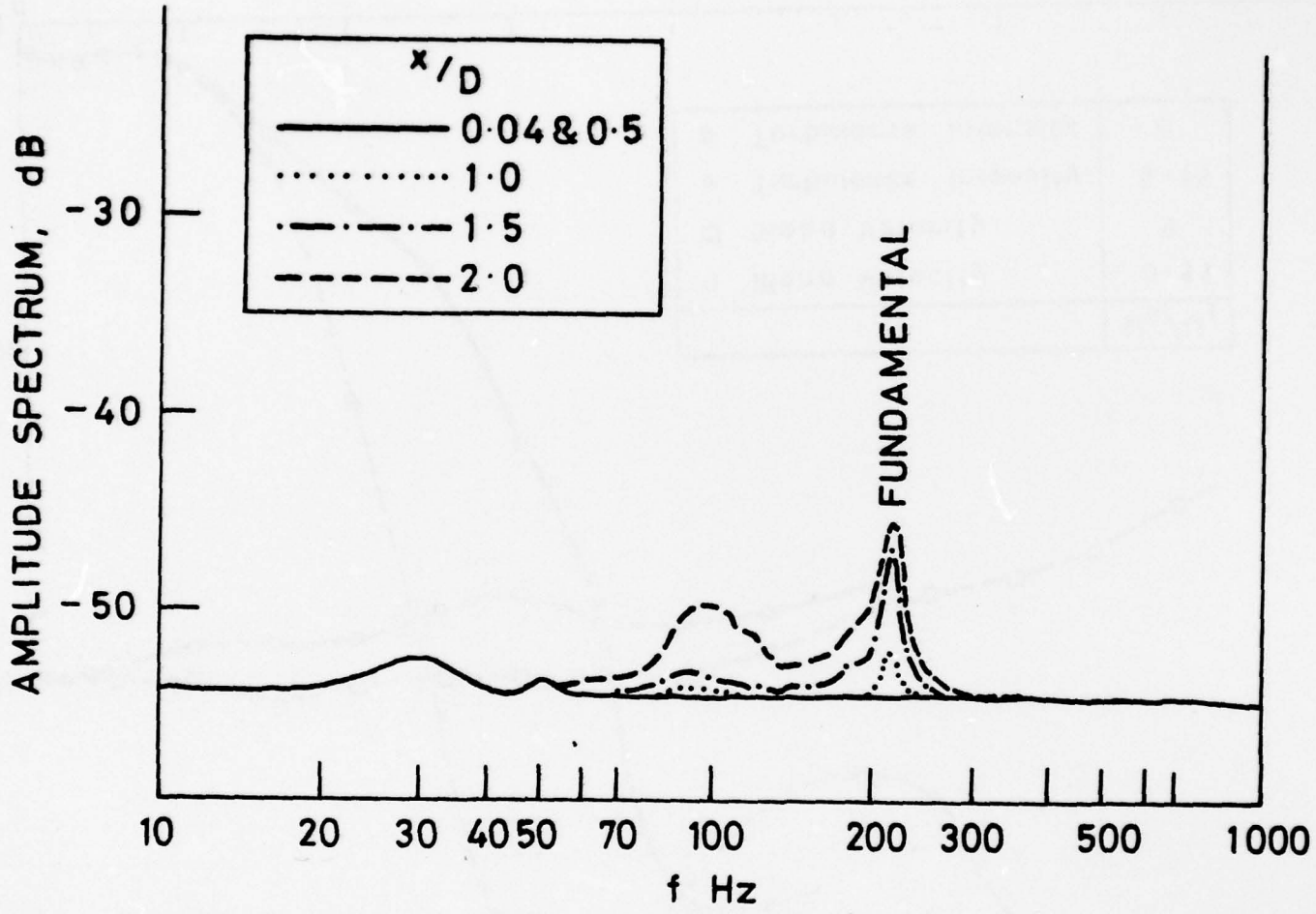

Fig. 27 Amplitude spectra of u, Cold Jet I, r = 0; 0 < x/D < 2

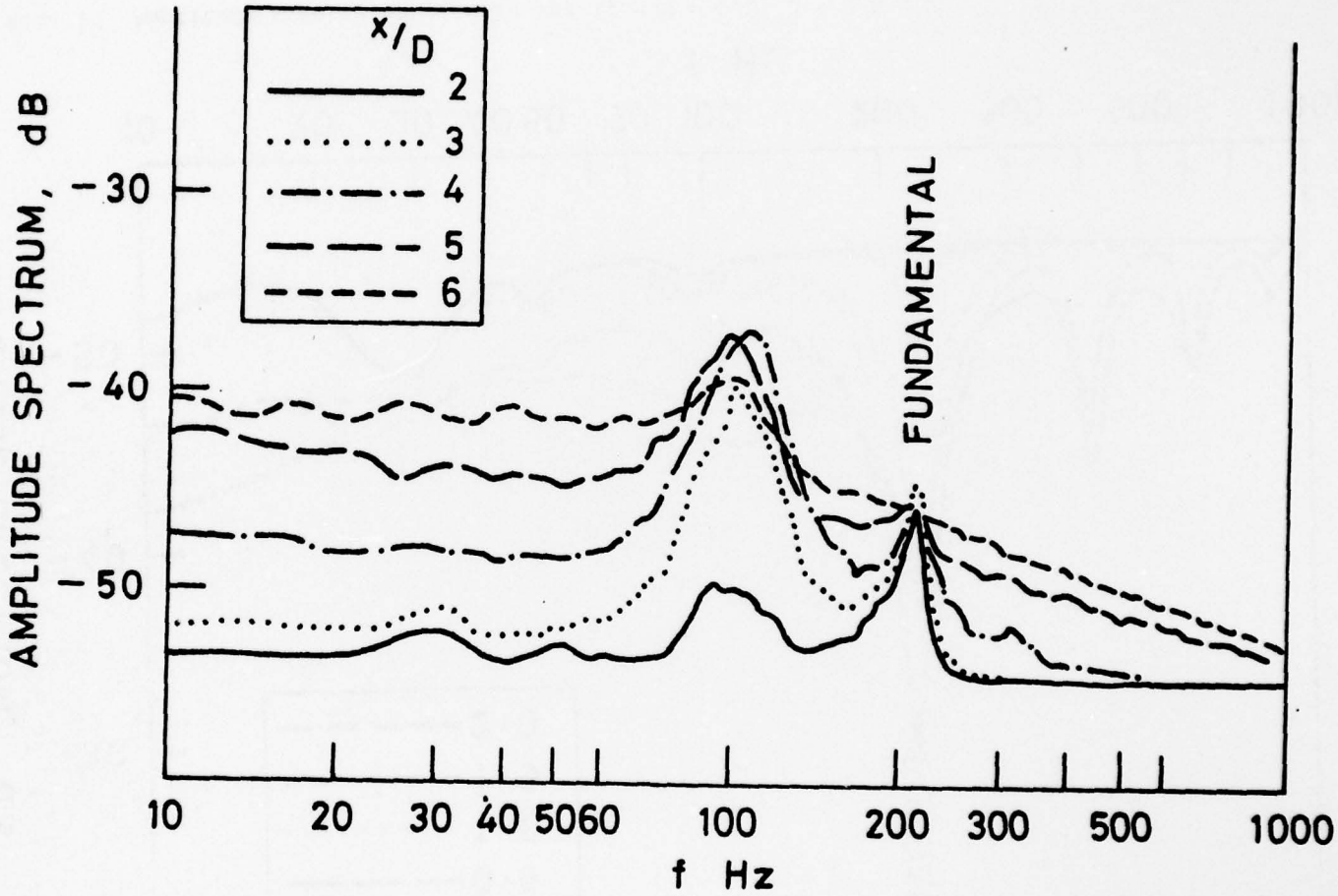

Fig. 28 Amplitude spectra of u, Cold Jet I, r = 0; 2 < x/D < 6

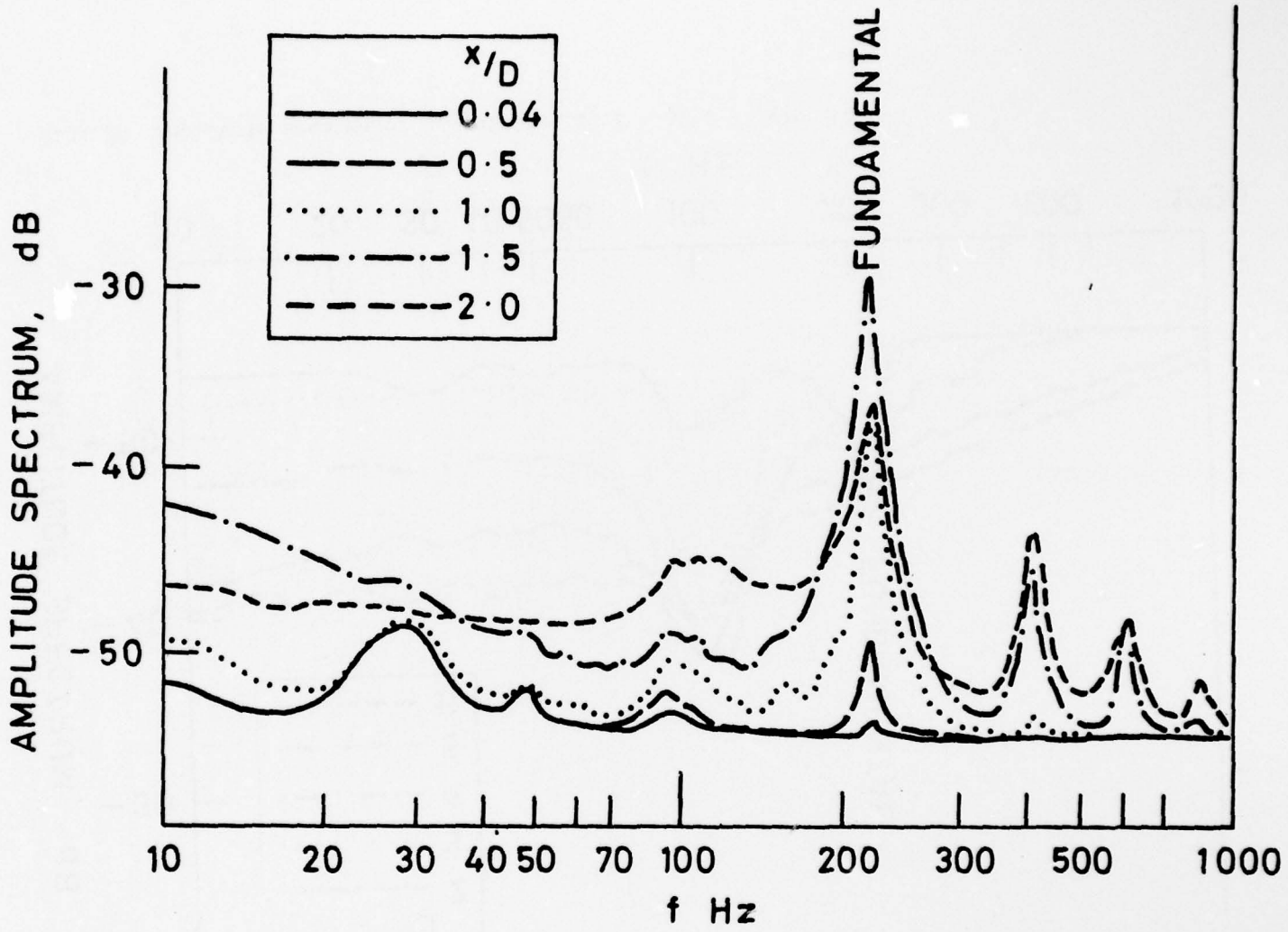

Fig. 29 Amplitude spectra of u, Cold Jet I, r/D = 0.5, 0 < x/D < 2

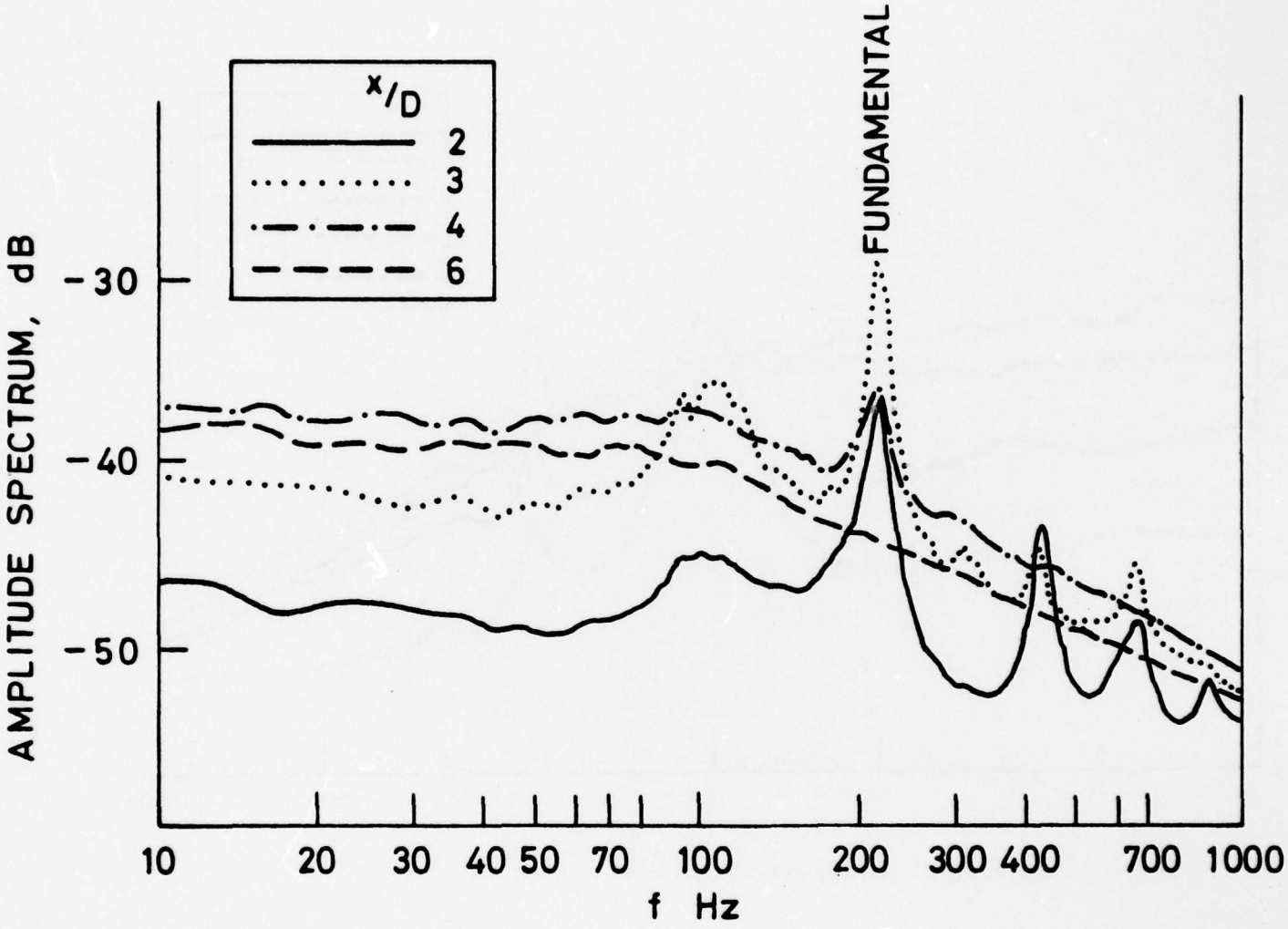

Fig. 30 Amplitude spectra of u, Cold Jet I, r/D = 0.5; $2 < x/D < 6$

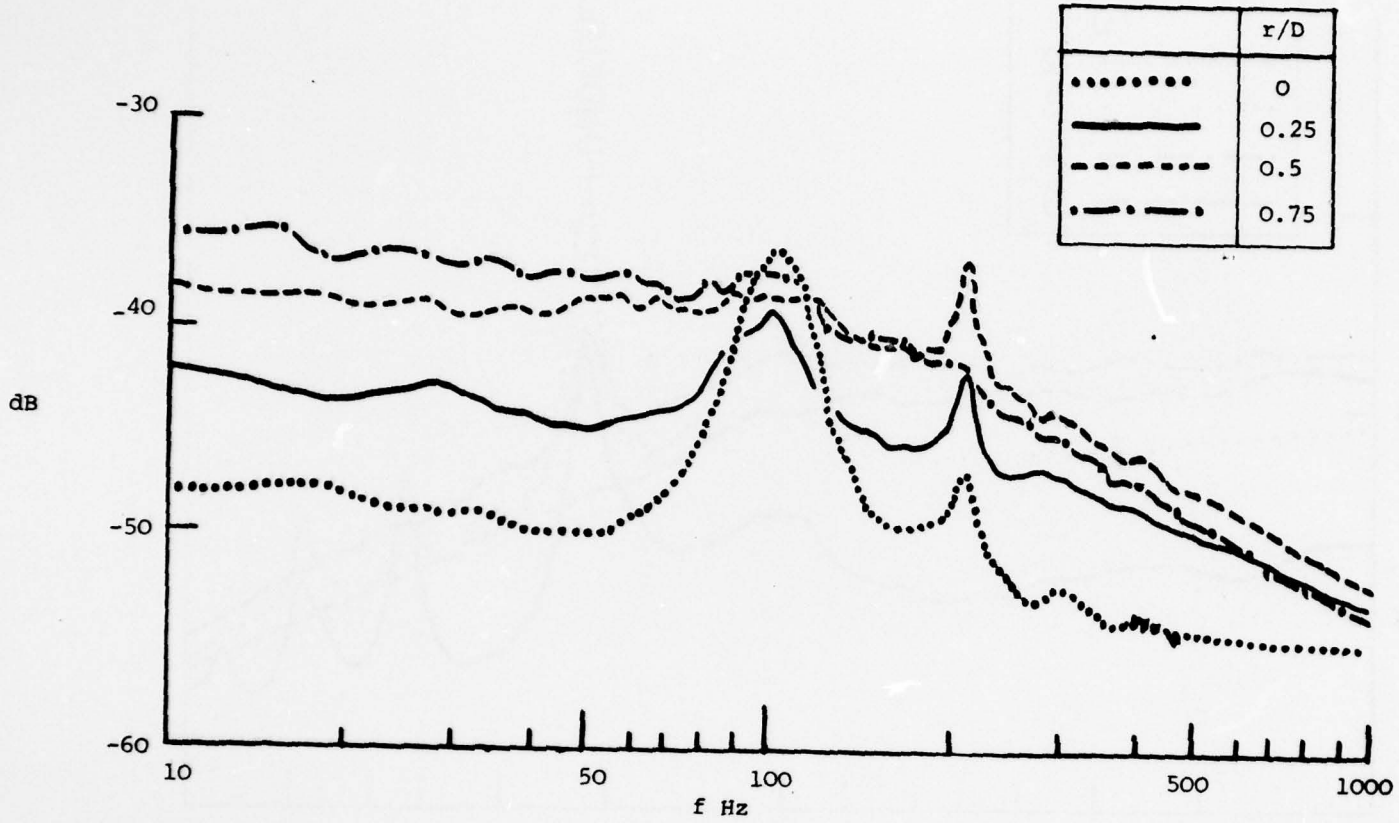

Fig. 31 Amplitude spectra of u, Cold Jet I, x/D = 4

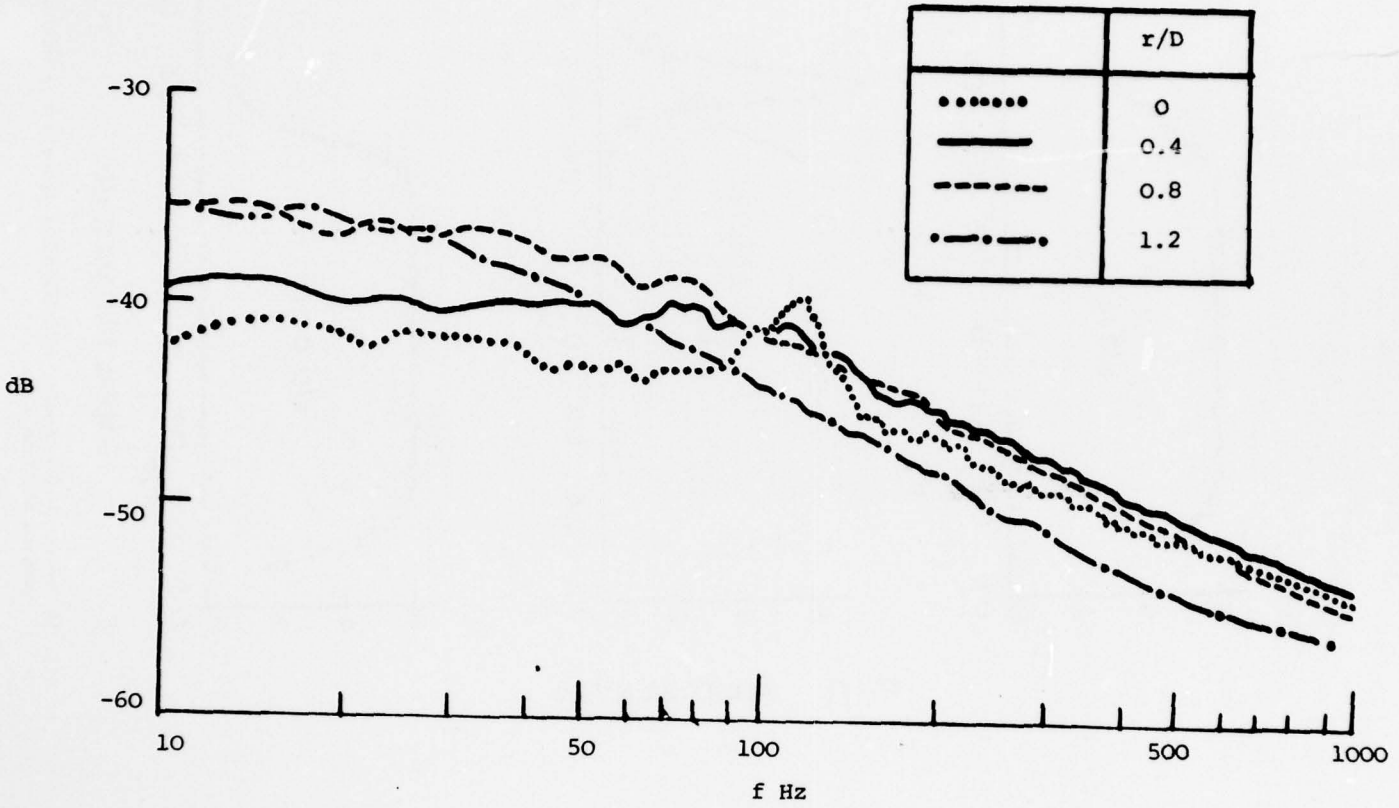

Fig. 32 Amplitude spectra of u, Cold Jet I, x/D = 6

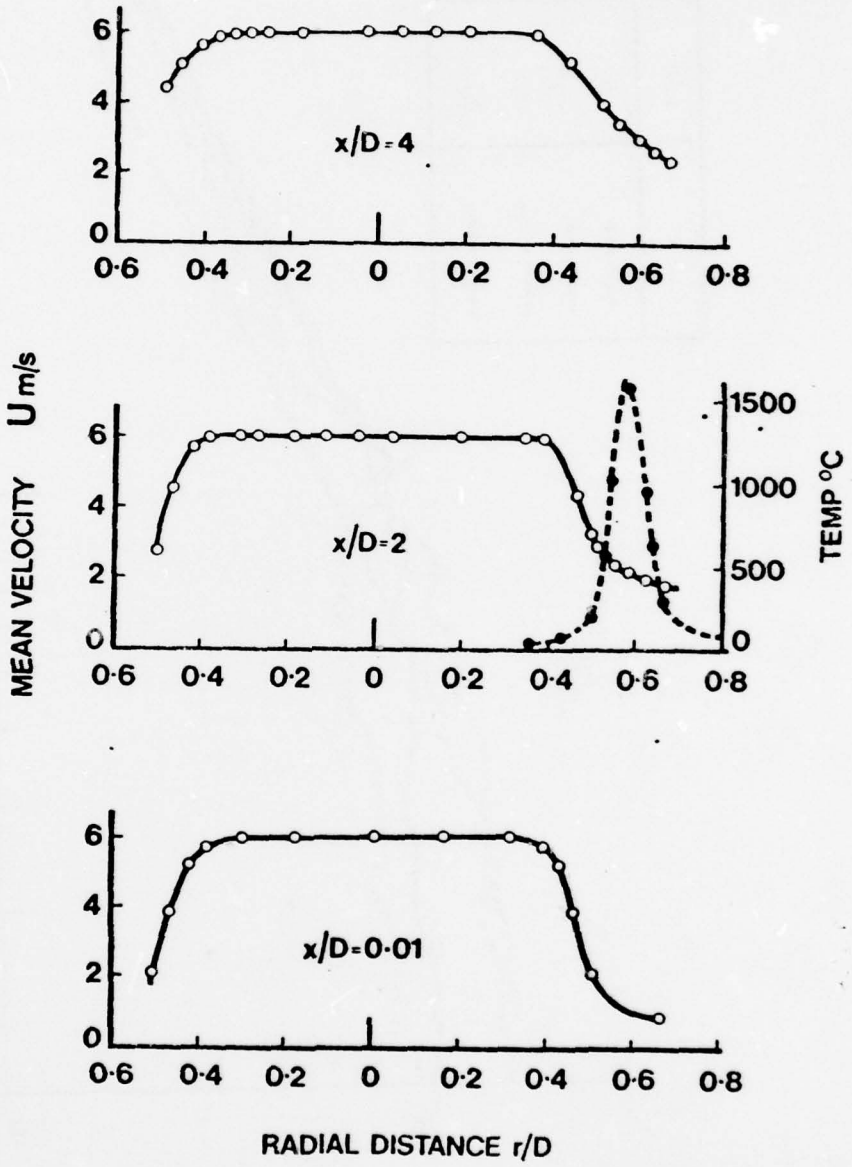

Fig. 33 Measurements of mean velocity and temperature in mixing layer region of Flame I

AD-A078 625 PURDUE UNIV LAFAYETTE IND PROJECT SQUID HEADQUARTERS F/G 21/2
THE STRUCTURE OF EDDIES IN TURBULENT FLAMES - I.(U)
MAR 79 N A CHIGIER , A J YULE N00014-75-C-1143
UNCLASSIFIED SQUID-US-1-PU NL

2 OF 2
AD
A078625

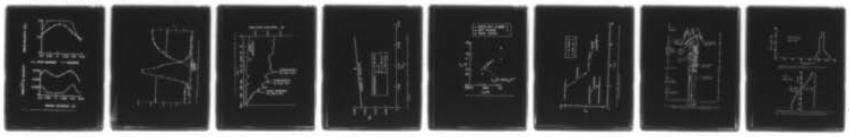

END
DATE
FILMED
1-80
DDC

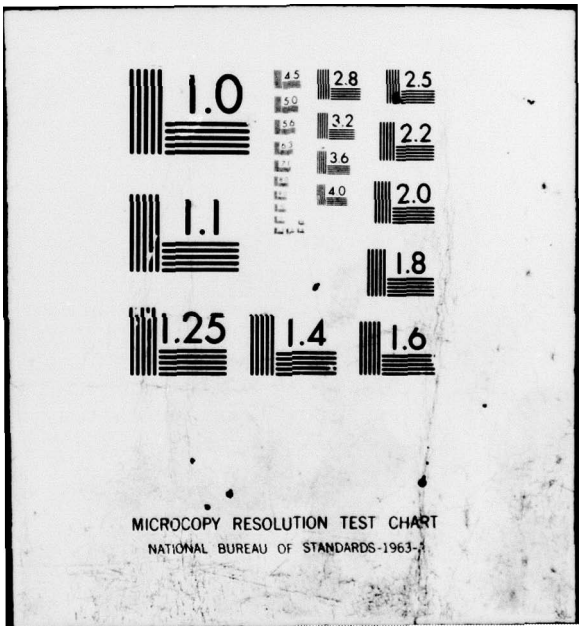
1.0
1.1
1.25
1.4
1.6
1.8
2.0
2.2
2.5
2.8
3.2
3.6
4.0
4.5
5.0
5.6
MICROCOPY RESOLUTION TEST CHART
NATIONAL BUREAU OF STANDARDS-1963-A

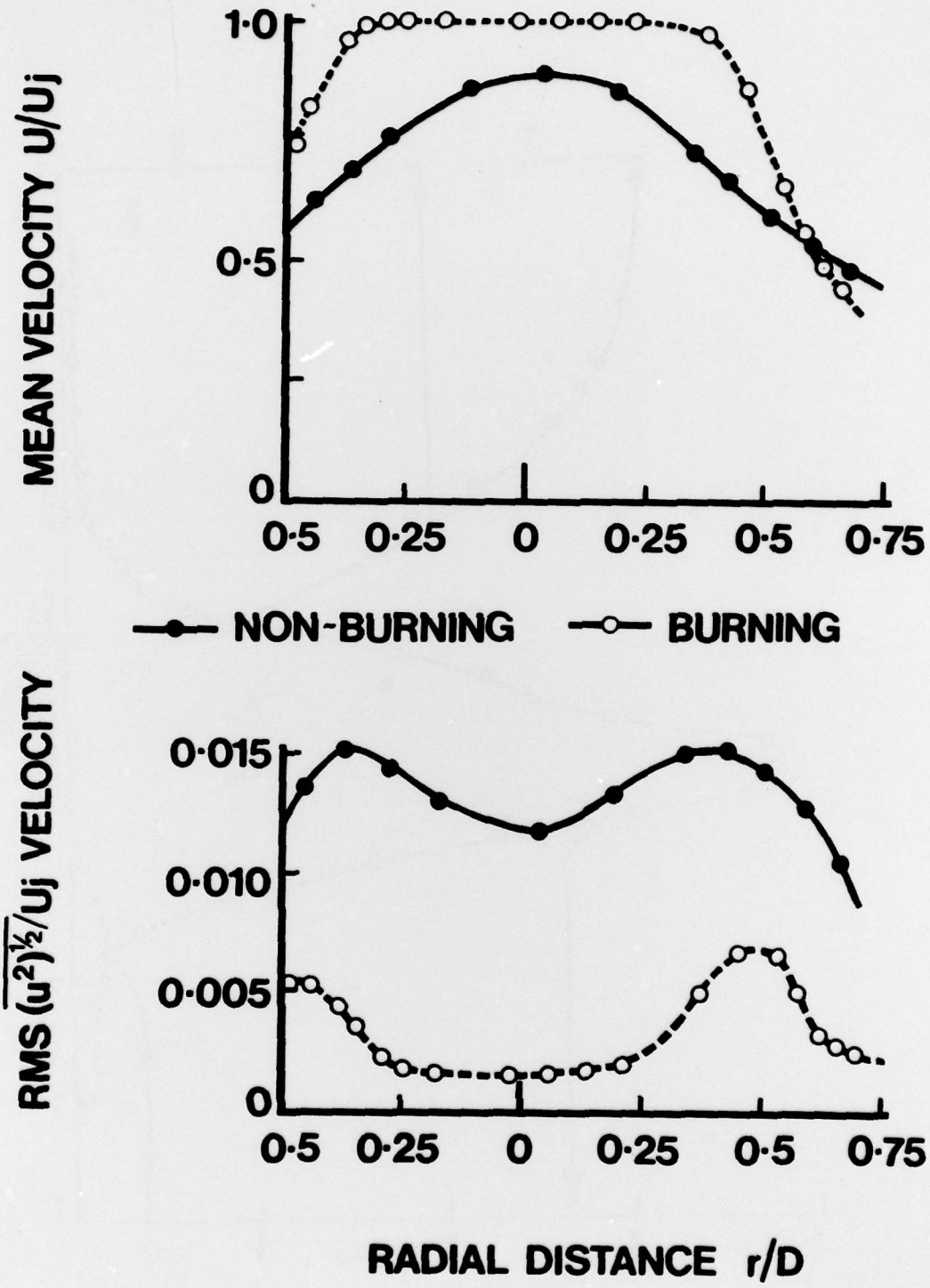

Fig. 34 Comparison of burning and nonburning jets at x/d = 4

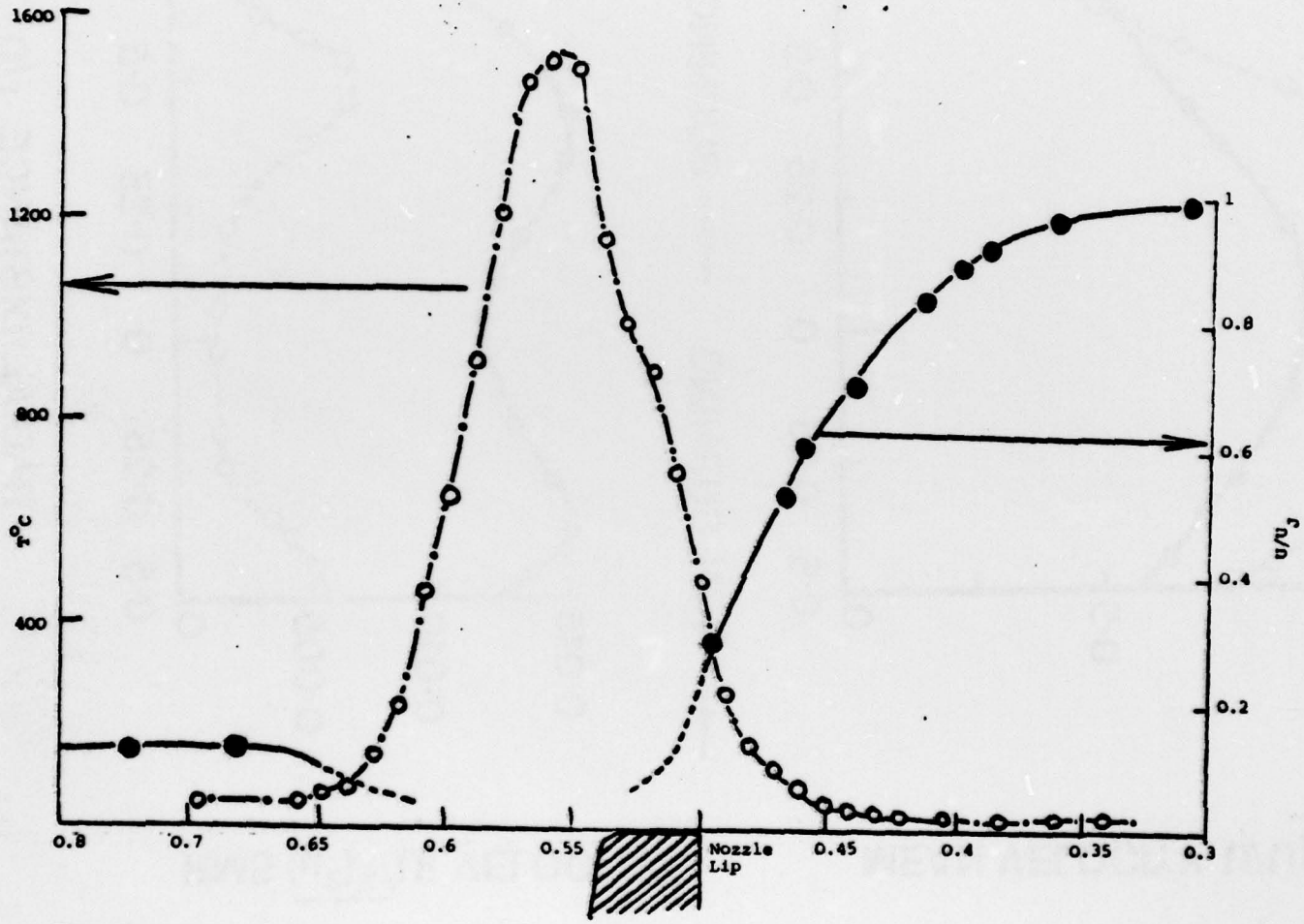

Fig. 35 Temperature and velocity distributions in stabilization region of Flame I, x/D = 0.04

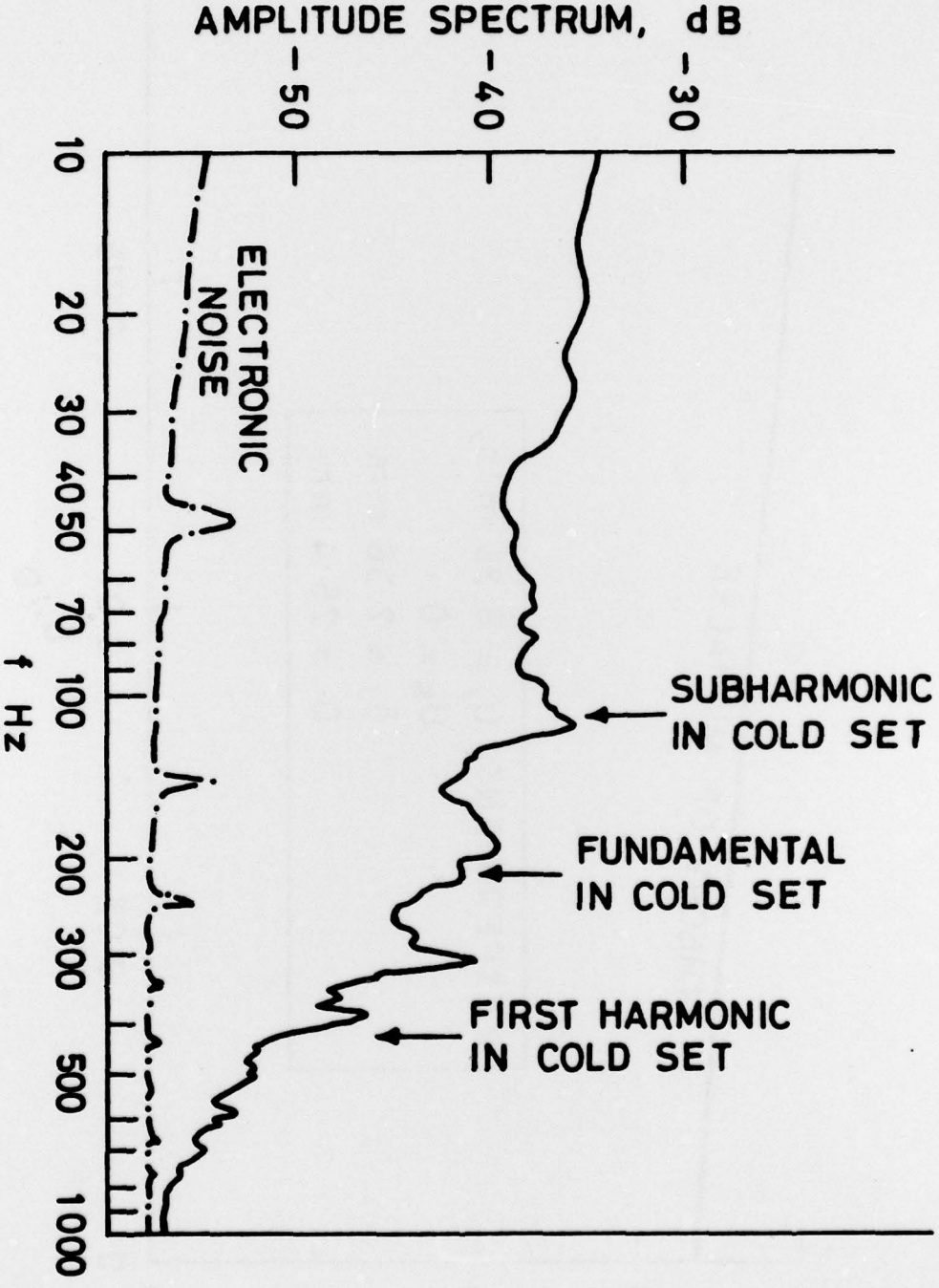

Fig. 36 Amplitude spectrum from ionization probe, x/D = 8; r/D = 0.5

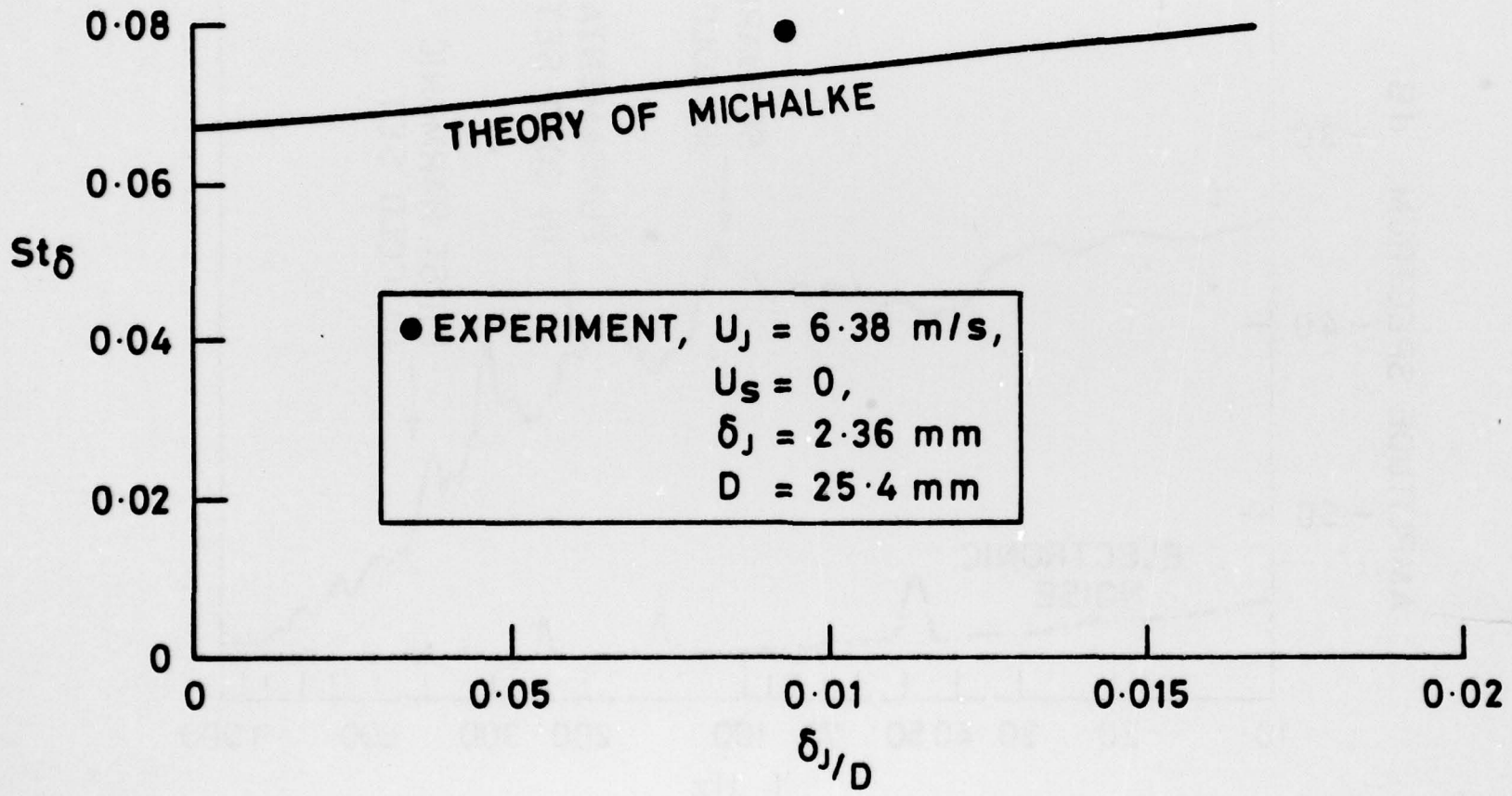

Fig. 37 Comparison of fundamental instability frequency in Cold Jet I with theory of Michalke

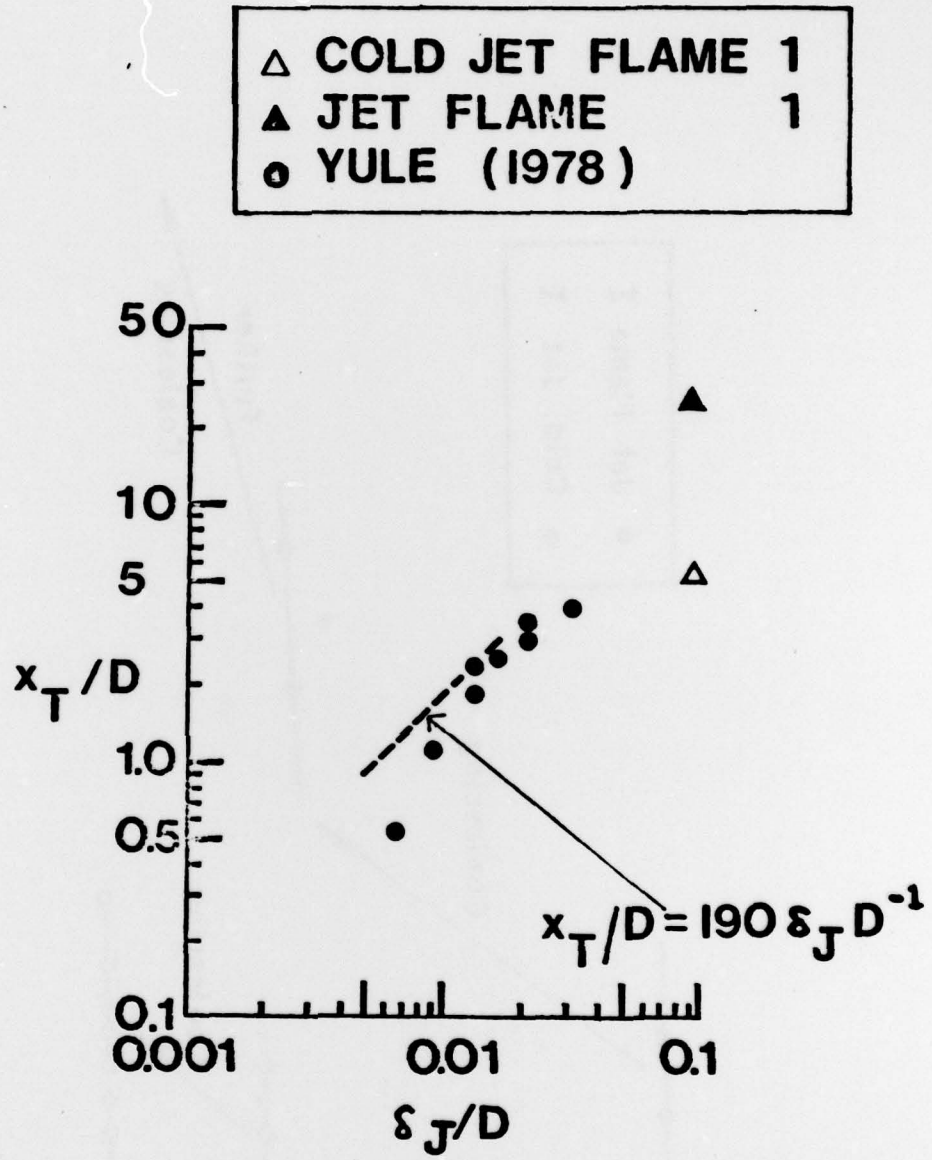

Fig. 38 Jet transition distance versus Reynolds number

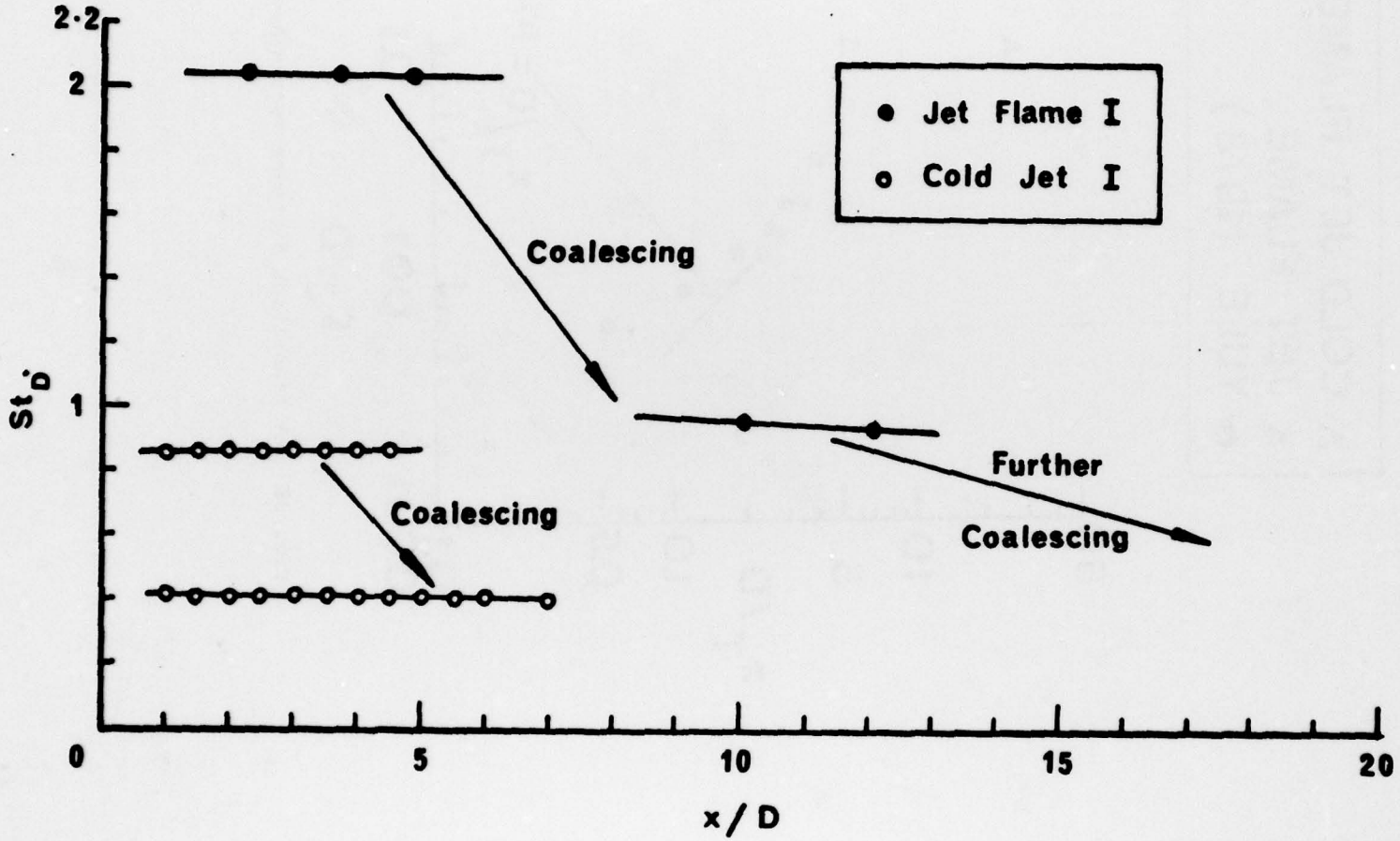

Fig. 39 Axial Strouhal number variations in cold and burning jets derived from spectra peaks and eddy passing frequencies

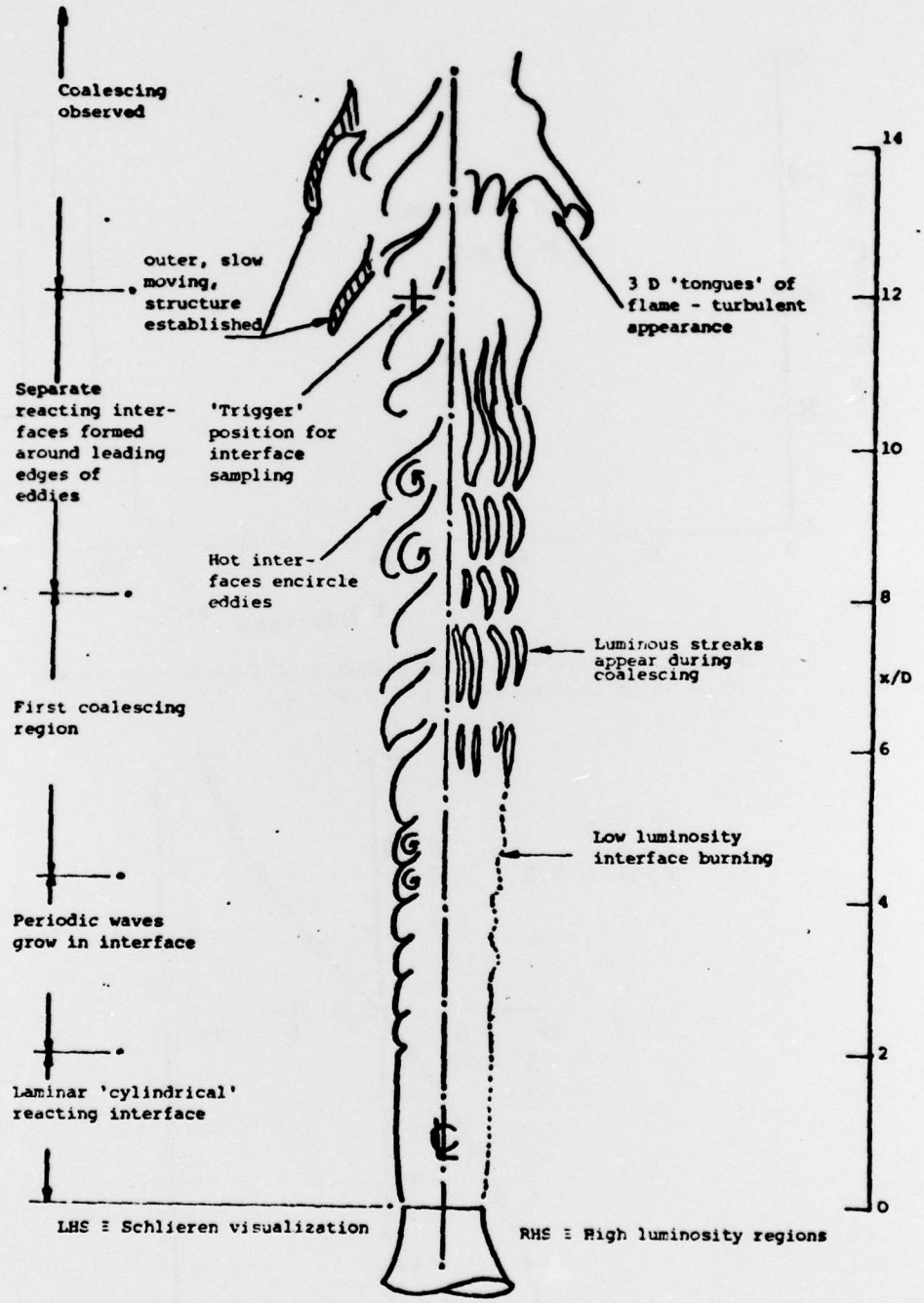

Fig. 40 Schematic view of jet flame showing visual appearance of high-temperature interfaces and the method for ensemble averaging from films

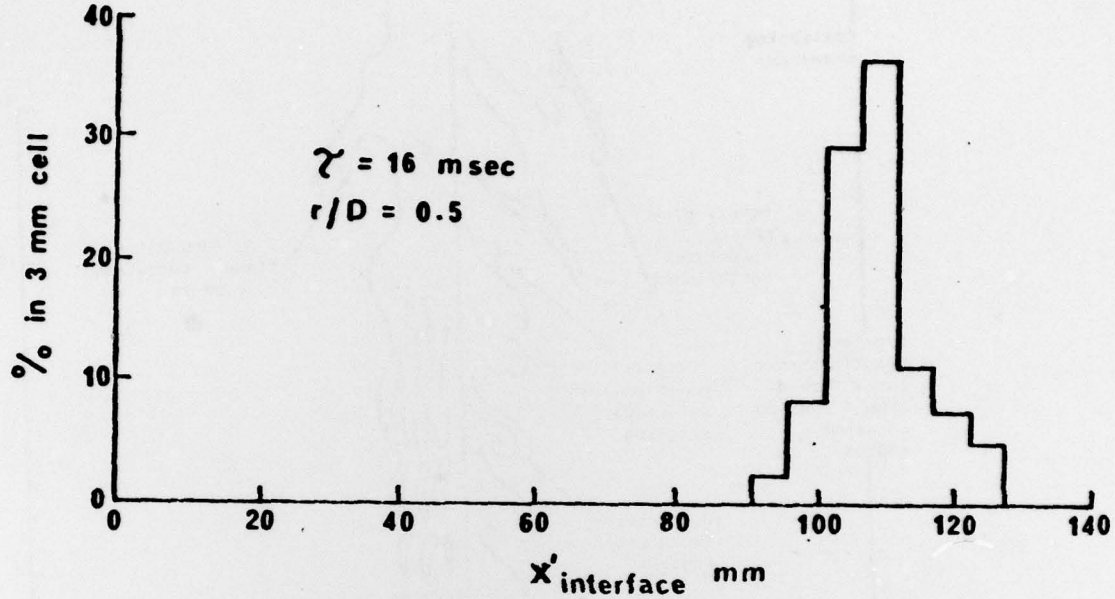

Probability distribution of distance of interfaces from x/D = 12, 16 ms after passing x/D = 12; r/D = 0.5

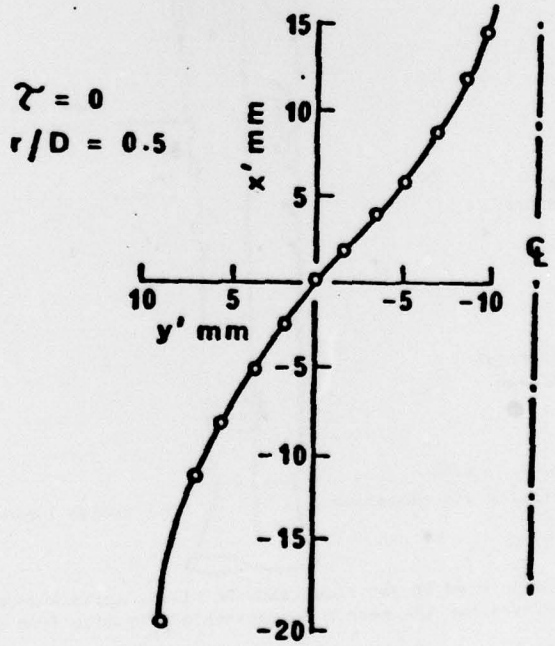

Ensemble averaged interface shape when passing through x/D = 12; r/D = 0.5

Fig. 41 Ensemble averaged interfaces by analysis of Schlieren films